Utrecht University

MSc Thesis

Impacts of Mangrove Dieback and Recovery on Coastal Wetland: A Case Study in the Gulf of Carpentaria, Australia.

Author:
Sarah Dzimballa

Supervisors:
Danghan Xie
Maarten G. Kleinhans

A thesis submitted in fulfillment of the requirements for the degree of Master of Science

in the Masters

Marine Sciences

March 10, 2022

Statement of originality of the MSc thesis

I declare that:

1. this is an original report, which is entirely my own work,

2. where I have made use of the ideas of other writers, I have acknowledged the source in all instances,

3. where I have used any diagram or visuals, I have acknowledged the source in all instances,

4. this report has not and will not be submitted elsewhere for academic assessment in any other academic course.

Student data:

Name: Sarah Dzimballa

Registration number: 2012243

Date: 22.02.2022

Signature: S. Dzimballa

UTRECHT UNIVERSITY

Abstract

Impacts of Mangrove Dieback and Recovery on Coastal Wetland: A Case Study in the Gulf of Carpentaria, Australia.

by Sarah DZIMBALLA

Mangrove forests are valuable ecosystems, offering socioeconomic and ecological services and thereby supporting the livelihood of millions of people. However, mangrove areas are declining due to various threats. These include coastal development, increasing extreme weather events (e.g. droughts and cyclones) and sea level rise. One recent example of a mass mangrove area loss is the dieback event in the Gulf of Carpentaria, Queensland Australia. With the loss of the mangrove trees, their valuable ecosystem services such as coastal protection and carbon sequestration are lost. Therefore, a need to further understand these valuable ecosystems and their morpho- and hydrodynamic interactions becomes apparent. In order to mitigate such dieback events and identify recovery projections.

The aim of this study is to gain insights into the causes of the dieback event and project the possible recovery of the mangrove characteristics within an estuary, by conducting numerical simulations with a biomorphodynamic model. Thereby, the hydromorphodynamic model, Delft3D is coupled to a dynamic mangrove vegetation model. The model was used to simulate the development of mangrove trees within an estuary, dependent on inundation and competition. Thereby the effects of tides, river discharge and sediment availability are included. The model input parameter and boundary conditions were chosen to resemble the case study of the Leichhardt estuary in the Gulf of Carpentaria. In five phases, the estuary development, mangrove establishment (with and without fluvial mud supply), mangrove dieback due to sea level drop and river discharge decrease and mangrove recovery were modelled.

The results indicate that, during the mangrove colonization, the inclusion of fluvial mud supply lead to lower mangrove area coverage in the estuary. This was found to originate from sedimentation and mud accumulation on bars, elevating the bed to a level that no inundation can reach these areas. Therefore, not enough water is available in those areas for mangrove growth. During the mangrove dieback simulation, the results further show that mangrove dieback can be provoked within the model by a sea level drop and river discharge decrease. Thus, the hypothesis of sea level drop and drought conditions causing the large-scale dieback was validated within the model. But at the same time some differences in dieback pattern suggest that further factors could have potentially played a role in the dieback in certain areas. The mangrove dieback has effects on the morphology and hydrodynamics of the estuary. The absence of mangrove vegetation leads to an increased flow velocity in the area of mangrove loss and decreased flow velocity in the channels and thereby, channel infilling, channel shifting, and decreased sedimentation in the previously vegetated areas. This was found to be based on the reduced flow resistance in the dieback areas. While this leads to a decrease in flow velocities in the channels causing the channel infilling. Channel shifting is on the one hand caused by reduced vegetation bank stabilization

and vertical velocity increase due to the vegetation cover. During the simulation of the recovery it was found, that these hydromorphodynamic changes due to the decreased mangrove cover have effects on the mangrove recovery, leading to a hysteresis effect. It was seen in the different scenarios that mangrove recovery depends on the location where the dieback occurs, specifically the local hydro- and morphodynamic processes and changes. Furthermore, the recovery rates depend on the extend of morphological change which occurred during the dieback. Additionally, the simulations of the recovery suggest that the recovery of the mangrove tree characteristics (e.g., basal area, stem diameter, etc.) are slower, compared to the mangrove growth during the initial colonization. Therefore, the mangrove area dieback leads to morphological and hydrodynamic change within the estuary which in turn has a negative effect in the resettlement of mangroves in the dieback area. For the natural system, it was therefore concluded that considering the likelihood of further disturbance events (e.g., sea level rise, droughts, cyclones) during the recovery process a full recovery seems unlikely.

The coupled numerical model used in this study was found to give insights into the processes governing mangrove vegetation characteristics and their feedback with morpho- and hydrodynamic processes. The pattern of mangrove colonization and dieback seen in the case study were produced in the model. Therefore, the model provided valuable information on the interaction of mangrove vegetation and morphodynamics on an estuary scale, which understanding is crucial for mangrove conversation and restoration efforts. This stresses the importance of further studies to understand the processes in more detail and to mitigate future dieback events as well as support restoration. For that, models can represent a valuable tool to further understand the processes governing mangrove coverage in estuaries.

Acknowledgements

I would first like to thank my thesis supervisors Danghan Xie and Maarten G. Kleinhans at Utrecht University. Danghan Xie was always available whenever I ran into a trouble spot or had a question about my research or writing. His expertise was invaluable in formulating the research questions and methodology. Maarten Kleinhans, your insightful feedback pushed me to sharpen my thinking and brought my work to a higher level. You both provided me with me with valuable guidance throughout this research and with the tool I needed choose the right direction and successfully complete this thesis. I would also like to thank Barend van Maanen, who was involved as an expert providing valuable insights and discussions. I am gratefully indebted to his for his very valuable comments on this thesis.

Finally, I must express my very profound gratitude to my parents and family and especially to my boyfriend, Siddharth Seshan, for providing me with unfailing support and continuous encouragement throughout my years of study and through the process of researching and writing this thesis. I could not have completed this thesis without your support, providing stimulating discussions as well as happy distractions to rest my mind outside of my research. Thank you.

Sarah Dzimballa

Contents

Abstract ii

Acknowledgements iv

1 Introduction 1

2 Literature Review 4
2.1 Mangrove Habitat and Their Functions . . . 4
2.1.1 Mangroves Distribution and Economic and Ecological Functions 4
2.1.2 Threats to Mangrove Forests . . . 7
2.1.3 Mangrove Conservation and Recovery . . . 8
2.2 Estuary Morphology and Mangrove Interaction . . . 8
2.2.1 Morphology and Sediment in Estuarine Systems . . . 9
2.2.2 Interactions of Mangroves with Hydrodynamics and Morphology 10
Impacts on Hydrodynamic Processes . . . 11
Impacts on Morphological Processes . . . 12
Impacts of Environmental Factors on Mangroves . . . 12
2.3 Previous Modelling Approaches . . . 13
2.3.1 Morphological and Hydrodynamic Modelling . . . 14
2.3.2 Mangrove Modelling . . . 15
2.3.3 Coupling of Morphology and Vegetation . . . 18

3 Research Region and Background 20
3.1 The Leichhardt River Estuary in the Gulf of Carpentaria . . . 20
3.2 Mangroves in the Gulf of Carpentaria . . . 21
3.3 Climatic Conditions . . . 22
3.4 The Mangrove Dieback Event in the Gulf of Carpentaria . . . 24

4 Research Questions and Hypotheses 28
4.1 Objectives and Research Questions . . . 28
4.2 Hypothesis . . . 28

5 Methodology 30
5.1 Hydro-Morphodynamic Model . . . 30
5.1.1 Governing Equations . . . 30
5.1.2 Boundary Conditions and Initial Bed . . . 33
5.1.3 Model Design . . . 37
5.2 Vegetation Model . . . 39
5.2.1 Governing Equations . . . 39
5.3 Coupling between Delft3D and Vegetation Model . . . 44
5.4 Model Scenarios . . . 44

6 Results **49**
6.1 Impacts of Mud Supply on Mangrove Distribution 51
6.2 Mangrove Dieback 53
6.2.1 Dieback Induced by Model Boundary Conditions 53
6.2.2 Dieback by Manual Removal 58
6.3 Influences of Dieback on Morphology - Disturbed State 59
6.4 Mangrove Recovery 62
6.5 Overall Mangrove Growth 72

7 Discussion **74**
7.1 Impacts of Mud on Mangrove Colonization 74
7.2 Model Dieback and Differences to Case Study 75
7.3 Dieback Effects on Morphology and Hydrodynamics 77
7.4 Mangrove Recovery 78
7.5 Evaluation of the Modelling Approach 81

8 Conclusion **84**

A Appendix **86**
A.1 Model Design Runs 86

Bibliography **91**

List of Figures

2.1 Salt excretion of A. marina. a Salt secretion through the leaves of A. marina. b Salt crystals under electron microscope (Naskar and Palit, 2015) 5
2.2 Root systems of (1) A. marina, (2) Bruguiera, (3) Sonneratia and (4) Rhizophora (from: Marchand (2008)) 5
2.3 Concept of a Hydro-morphodynamic System 9
2.4 Longitudinal variation of the intensity of the three main physical processes, river currents, tidal currents and waves (Dalrymple and Choi, 2007). 10
2.5 Schematic of major factors influencing estuarine bathymetry (Prandle, 2009). 10
2.6 Interaction of hydrodynamic, morphological and ecological processes in mangroves (adopted from: Gijsman et al. (2021)). 11
2.7 Mangrove colonization due to hydroperiod in cross-shore direction (from: Mcivor et al. (2013)). 13

3.1 Map showing the location of the Gulf of Carpentaria, Queensland Australia (from Heap et al. (2006)). 21
3.2 Grey mangrove (*Avicennia marina*), Towra Point Nature Reserve. 22
3.3 The mangrove dieback in the southern Gulf of Carpentaria in five different locations (A-E) as indicated in the map (bottom right). (A) Roper River shoreline, (B) Limmen Bight River shoreline (images taken by Tony Griffiths, 9.06.2016), (C) Gangalidda shoreline (image taken by Roger Jaensch, 13–14.04.2016), (D) Leichhardt River mouth (on 17.11.2016), and (E) Karumba, Queensland, Norman River shoreline (on 27.10.2016) (images from surveys reported in Duke et al. (2021)). 24
3.4 The condition of climate and environmental factors up to and after the 2015/2016 mangrove dieback event (from: Duke et al. (2021)) 25
3.5 Leichhardt River Dieback Map (Accad et al., 2019). 26
3.6 Nicholson River Catchment Dieback Map (Accad et al., 2019). 27

5.1 Delft3D Model Structure (from: Duong et al. (2018)). 34
5.2 Leichhardt River Top View. 34
5.3 Delft3D Model Grid. 35
5.4 Initial bathymetry as input to the Delft3D model. 36
5.5 Depth profile of the initial domain. 36
5.6 Bathymetry of the model estuary after 400 years of spin-up period. 39
5.7 Growth Parameter for Mangrove Model over Stem Diameter. 40
5.8 Mangrove Stress Factors with a) inundation stress over relative hydroperiod and b) competition stress over mangrove biomass (from Xie et al., 2020). 41
5.9 Coupling of vegetation and hydromorphodynamics in the model. 44
5.10 Implementation of the sea level drop with an additional tidal component. 46

5.11 Overview of the conducted modelling phases (phase 1 - 4). 47

6.1 Overview of the bathymetry and vegetation distribution for the four different phases of model runs.[1] 50
6.2 Bathymetry and mangrove cover map after the 200 years of mangrove colonization for (A) the only sand scenario and (B) the scenario including fluvial mud supply. 51
6.3 Comparison of (A) total mangrove basal area, (B) average geometric density and (C) average numeric density for the scenario with (orange) and without (blue) fluvial mud supply. 52
6.4 Hydroperiod map after the 200 years of mangrove colonization for (A) the only sand scenario and (B) the scenario including mud supply, with the red circle indicating the area of interest mentioned in the text. 53
6.5 Comparison of (A) mud thickness, (B) bed level and (C) hydroperiod between mud and no mud scenario at the point x = 11 km and y = 0.8 km. 54
6.6 Bathymetry and mangrove coverage, including the dieback (in red), over the whole domain. The circles are upstream and downstream tidal flat locations discussed in the text. 54
6.7 Comparison of the hydroperiods over the whole domain (A) before the dieback (600 years), (B) after the dieback (610 years) and (C) the area where the hydroperiod drops from an initially suitable hydroperiod for mangrove growth to zero. 55
6.8 Comparison of the hydroperiods over time at two different dieback locations: (A) along the channel upstream and (B) at the upper delta platform. 56
6.9 Comparison of mangrove vegetation parameters: (A) total basal area, (B) average numeric density, (C) average geometric density and (D) hydraulic resistance, over the 10 year dieback event for the different dieback scenarios and the undisturbed reference. 56
6.10 Bed level, Mud thickness in top layer and flood/ebb velocity ratio over the whole domain of the reference run and relative bedlevel, mud thickness and flood/ebb velocity ratio of the SLD & RDD dieback scenario compared to the reference run. 58
6.11 Map of bathymetry and mangrove coverage (green) including the dieback area (red). 58
6.12 Basal area (blue) and geometric density (orange) of mangroves before (left) and after (right) the manual removal. 59
6.13 Bed level of the two dieback scenarios (top and middle) and the reference run (bottom). 59
6.14 Ebb and flood velocities (top and middle) of the two dieback scenarios and the reference run (bottom). 60
6.15 Average velocities over tidal cycle (A) in the channel and (B) on the platform. 61
6.16 Mud thickness (in top layer) of the two dieback scenarios (top and middle) and the reference run (bottom). 61
6.17 Comparison of the bed level, flood/ebb velocity ratio and mud thickness to the reference run after 100 years of recovery. 63
6.18 Cross section of channel bed elevation with locations of vegetation indicated over the 100 years recovery for (A) reference run, (B) 16 km seawards for manual removal and (C) SLD & RDD. 64

6.19 Flow velocities in x- and y-direction at x = 17 km in the deepest channel part of the reference run over a tidal cycle (A) after 50 years of recovery and (B) after 100 years of recovery. 65
6.20 Time series of the 100 years of recovery of the (A) channel depth represented by the 5th percentile of bed level, (B) tidal flat elevation represented by the 95th percentile of bed level, (C) flood/ebb velocity ratio within the channel area (5th percentile of bed level) and (D) flood/ebb velocity ratio on the tidal flat (95th percentile of bed level). 66
6.21 Bathymetry and mangrove cover map after 100 years of recovery for three scenarios: (A) 16 km seawards manual removal, (B) SLD & RDD model dieback and (C) undisturbed reference scenario. 67
6.22 Hydroperiod maps after 100 years recovery of the three scenarios: (A) 16 km seawards manual removal, (B) SLD and RDD model dieback and (C) the undisturbed reference run. 68
6.23 Mangrove characteristics over the 100 years of recovery over the whole domain including (A) Mangrove tree total basal area, (B) average numeric density, (C) average geometric density and (B) hydraulic resistance on the basis of lamda over the 100 years recovery of the three scenarios. 69
6.24 Mangrove stems hydraulic resistance over the 100 years of recovery. . . 70
6.25 Comparison of stem diameters from the to dieback scenarios to the reference run over the 100 years of recovery. 71
6.26 Mangrove total basal area for all simulations considered over the different phases of mangrove growth (year 400 - 600), mangrove dieback (year 600 - 610) and mangrove recovery (year 600/610 - 700/710). 72
6.27 Ratio of the actual growth rate/optimal growth rate based on the change in average stem diameter over the first 10 years of colonization and recovery. For the dieback scenario only the dieback area is included. 73

7.1 Cross - section of the Dieback characteristics observed in the Gulf of Carpentaria (Duke et al., 2017). 76
7.2 Overview of the interactions between mangrove cover, flow velocity and bed level elevation during mangrove colonization and mangrove dieback within an estuary. 78

A.1 Straight Q50 Y200 86
A.2 Straight Q50 IK A10 Y200 87
A.3 Straight Q50 IK A100 Y200 87
A.4 Sinus shallower Q50 Y200 87
A.5 Sinus Q50 shallower2 Y200 88
A.6 Sinus Q50 shallower IK A10 Y200 88
A.7 Q50 FK A0.1 Y400 diurnal 88
A.8 Q50 IK A100 diurnal Y400 89
A.9 Q50 IK A100 semidiurnal Y400 89
A.10 Q100 IK A100 diurnal Y400 89
A.11 Q100 IK A100 semidiurnal Y200 90
A.12 Q300 IK A100 semidiurnal Y400 90
A.13 Q400 IK A100 semidiurnal Y200 90

List of Tables

2.1 Summary of Mangrove Services (adopted from: FAO (2007)) 7
2.2 Mangrove Models Summary in Recent Decades 17

5.1 Delft3D Input Parameter 37
5.2 Mangrove Input Parameter 43

List of Abbreviations

DBH	**D**iameter at **B**reast **H**ight
NbS	**N**ature at **b**ased **S**olutions
RDD	**R**iver **D**ischarge **D**ecrease
SLD	**S**ea **L**evel **D**rop
SLR	**S**ea **L**evel **R**ise

Chapter 1

Introduction

Estuaries are water bodies located where the freshwater from rivers meets the ocean and thereby are defined by brackish water. The morphological development in an estuary is controlled by the intricate interplay of hydrodynamics and morphology. Hydrodynamic factors like tidal currents, wave processes, density currents, storms and river discharge and morphodynamic processes such as sediment transport, bed level changes, the presence and distribution of cohesive and non-cohesive sediment and their characteristics, interact with each other non-linearly on different time and spatial scales (van der Wegen & Roelvink, 2012). Determined by geomorphological settings estuarine systems are further influenced by climate events such as droughts or cyclones (Prandle, 2009).

Despite these dynamic conditions, estuaries are important ecosystems as many nutrients and detritus for their aquatic inhabitants accumulate in estuaries (National Geographic Society, 2012). Also humans have discovered the values offered by estuaries early on. Estuaries provide freshwater for different uses such as drinking water and it provides access to the river as well as the ocean, and thus it represents a perfect position for trading (Prandle, 2009). These might have been some of the reasons why the earliest civilization developed around estuaries. Around 3800 BCE, Ur (now Tall al-Muqayyar or Tell el-Muqayyar, Iraq) was built near the estuary where the Euphrates River meets the Persian Gulf (National Geographic Society, 2012). Cities next to estuaries are thus often densely populated, with nearly 70 percent of world's largest cities being closely surrounded by estuaries (Ashworth et al., 2015). The wetlands surrounding estuaries provide a natural protection from storm events, tsunamis and sea level rise.

However, these wetlands and flooding plains are often disturbed by humans with a desire for extra land space by converting the land resources to agricultural or aquacultural area (Kirwan and Megonigal, 2013, Goldberg et al., 2020). This has led to a process called 'land reclamation', the gain of land from the wetlands. Land reclamation and dredging can be seen in estuaries all over the world, influencing the wetland function of coastal protection (Kirwan and Megonigal, 2013). The protection offered by the wetlands is compromised when the wetlands are claimed for human use. Additionally, the population around estuaries leads to pollution, over fishing and subsidence (FAO, 2007, National Geographic Society, 2012, Brown and Nicholls, 2015). Current developments of climate change are further increasing the pressure on estuaries, with sea level rise, rising mean ocean temperatures, changing precipitation patterns, increasing frequency and intensity of coastal storms (Mehvar et al., 2019, IPCC, 2021). Furthermore, the interplay between sea level rise and coastal storm surges are predicted to lead to an increase in coastal flooding (IPCC, 2021). Therefore, it can be seen

that estuary systems are socio-economically and ecologically important. However, they are also determined by complex dynamics and under stress due to human interventions and climatic change, stressing the importance to investigate wetland changes under changing environment

Given the severe changes in climate and increasing pressure from humans, the importance of the vegetation on stabilizing estuaries against erosion and providing attenuation capacity has gradually obtained global recognition (Schuerch et al., 2018). Mangroves are one of the vegetation restricted to estuaries, in particular along the (sub)tropical shorelines. They offer important ecological and socio-economic functions, for example, due to their root system and stems, they stabilize the coastline and elevate the surface to withstand flooding from sea level rise (Mehvar et al., 2019, IPCC, 2021). Under the current conditions of sea level rise and increasing extreme weather events leading to coastal erosion and flooding, the services offered by mangrove forest gain importance (Duke et al., 2021). This has led to an interest in the use of mangroves for flood risk reduction as hybrid-engineering solutions (Gijsman et al., 2021) and as so called nature based solutions (NbS [1]) (Van Coppenolle et al., 2018, Amrit et al., 2021).

Events in the recent years however have shown, that the increasing stresses on the mangroves have effects on the mangrove resilience and growth. Mangroves are vulnerable to the changes in inundation, temperature and droughts (Duke et al., 2021). Thus, diebacks and a general decline in mangrove vegetation was observed in recent decades (FAO, 2007). As a recent example, unprecedented mangrove dieback with nearly 7400 ha of mangroves loss occurred in the Australian Gulf of Carpentaria, Queensland (Duke et al., 2017, Harris et al., 2017, Accad et al., 2019, Sippo, 2019, Duke et al., 2021, Abhik et al., 2021). However, the causes and consequences of such a large-scale mangrove dieback are barely investigated, particularly on the long-term impacts of morphological changes and vegetation recovery. This suggests a need to understand these ecosystems and their development to manage and conserve mangrove forests together with their valuable services. The processes governing establishment, growth and development of mangrove wetlands need to be further defined and quantified (Duke et al., 2021). Commonly used methods in mangrove research such as field studies and remote sensing are limited regarding the prediction of long-term development. However, the application of models is promising, as mangrove modelling has been applied in recent studies.

The aim of this research is to project the morphological and hydrodynamic changes caused by a large area of mangrove dieback as well as the subsequent mangrove recovery within an estuary. A numerical model is used to simulate mangrove colonization, dieback due to sea level drop and river discharge decrease and recovery within an estuary. Specifically, a process-based morphodynamic model is coupled to a vegetation model. The Leichhardt estuary in the Gulf of Carpentaria (Queensland, Australia) is used as a case study. The model domain and boundary conditions are based on this estuary. Thereby, this study aims to gain further insights into the conditions which led to the dieback as well as the recovery process of the mangroves in the decades to century following the dieback. Furthermore, the proposed model is validated in regards to the suitability for the use of simulating mangrove dieback and recovery by comparison to the case study.

[1] Nature-based Solutions (NbS) are defined by IUCN as "actions to protect, sustainably manage, and restore natural or modified ecosystems, that address societal challenges effectively and adaptively, simultaneously providing human well-being and biodiversity benefits".

This thesis is structured as follows. Firstly, a literature background about mangroves in general and their services, values and conservation is given in Chapter 2. In this chapter, the interactions of mangroves with morphology and hydrodynamics, as investigated in previous studies, are summarized. Furthermore, the morphodynamic model and the vegetation model, their application in previous studies and the coupling of the models is outlined. This serves as an introduction in the topics of this thesis and gives background information, which later serve as validation of the results. Secondly, in Chapter 3 the case study of the Leichhardt river is introduced regarding its location, climatic conditions and the mangrove characteristics. Particularly, the dieback event in the Gulf of Carpentaria of 2015/2016 is described, including a hypothesis on the causes of this event. Thirdly, the research approach is outlined including the research questions and hypothesis in Chapter 4. In Chapter 5, the methodology of this study is described in detail. Thereby, both the morphodynamic model, as well as the vegetation model are described on the basis of their governing equations. The parameters and initial conditions used in both models are summarized. Chapter 5 further includes a description of the modelling phases conducted during the study. Chapter 6 then outlines the results according to the four modelling phases. These results are subsequently discussed in Chapter 7. Here, the mangrove colonization under the influence of mud is discussed, the model dieback is compared to the dieback in the case study, the effects of the dieback on the estuary morphology and the mangrove recovery are discussed and the modelling approach is evaluated. Chapter 8 summarizes the conclusions from this research.

Chapter 2

Literature Review

This chapter serves as an introduction to the topic of mangroves as well as mangrove and hydro-morphodynamic modelling approaches. Firstly, background information about mangroves in general and their ecosystem services are compiled. Following, estuary morphology and the interactions of mangrove trees with their surrounding environmental factors is explained. Finally, previous studies of mangrove modelling and hydrodynamic modelling are summarized.

2.1 Mangrove Habitat and Their Functions

In this section, knowledge about mangrove distribution and the importance of mangrove ecosystems are first summarized (Section 2.1.1); next, the potential risk to mangroves from both climates and humans is addressed (Section 2.1.2); in the end of this section, mangrove conservation and restorations is reviewed with an emphasis on the natural recovery of mangrove characteristics (Section 2.1.3).

2.1.1 Mangroves Distribution and Economic and Ecological Functions

Mangroves are woody halophytes growing at the interface of land and sea along (sub)tropical shorelines (Asbridge et al., 2018). Estimates from the period of 1980 - 2005, suggest that mangrove forests cover a range of 12 to 20 million hectares worldwide (FAO, 2007). The majority of mangrove forests distributes in the Indo-Pacific regions, with a study by Giri et al. (2011) suggesting nearly 42 percent of global mangroves colonizing in Asia. Globally, mangroves can be found in about 124 countries with a varying total number of species due to differences in species definition (FAO, 2007). But the total number of 'true' mangroves was found to be a maximum of 80 taxa (including hybrids) (Shing et al., 2017). The highest species diversity, with 54 different species, can be found in the Indo-West-Pacific (Shing et al., 2017). Due to their specific distribution along the coastlines, mangroves are regarded as 'coast guards'.

In order to thrive in a highly transitional zone between land and sea, mangroves must adapt to their environment on a constant basis, which affects the mangrove forests in different ways. On the one hand, the physiological capability to adapt to varying environmental conditions such as fluctuations in tides, waves, varying salinity and oxygen conditions is required (Alongi, 2014). These adaptation include: 1) strong stems to resist water scouring, 2) small, streamlined leaves, thick or waxy leaves to reduce water loss, 3) salt excretion to persist in the saline water, 4) an above-ground root system to sustain oxygen uptake, 5) viviparous embryos to increase seedling survival rate, and 6) efficient nutrient-retention mechanisms to promote vegetation growth (Feller et al., 2010, Alongi, 2014, Naskar and Palit, 2015). Figure 2.1 , shows an example of the salt

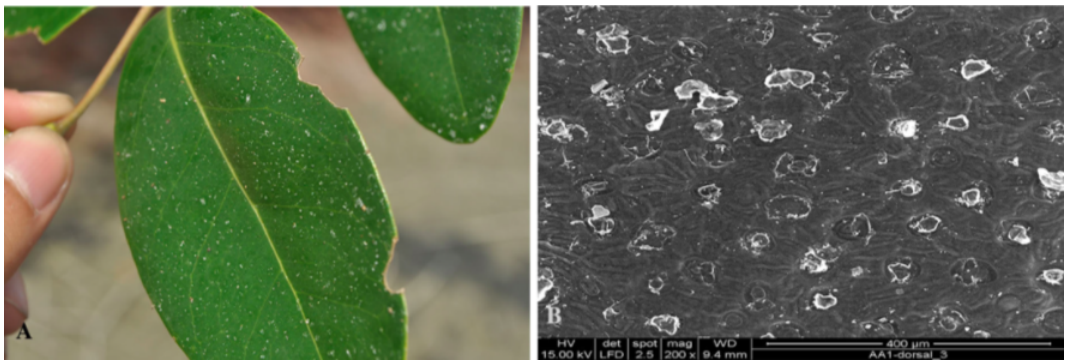

FIGURE 2.1: Salt excretion of A. marina. a Salt secretion through the leaves of A. marina. b Salt crystals under electron microscope (Naskar and Palit, 2015)

secretion of the mangrove species *A. marina*. The excess salt is excreted though pores or salt glands on the leaf surface (Naskar and Palit, 2015). Another possible adaptation is the uptake of oxygen through the pneumatophores or roots systems of the mangroves. Figure 2.2 shows root systems of different mangrove species.

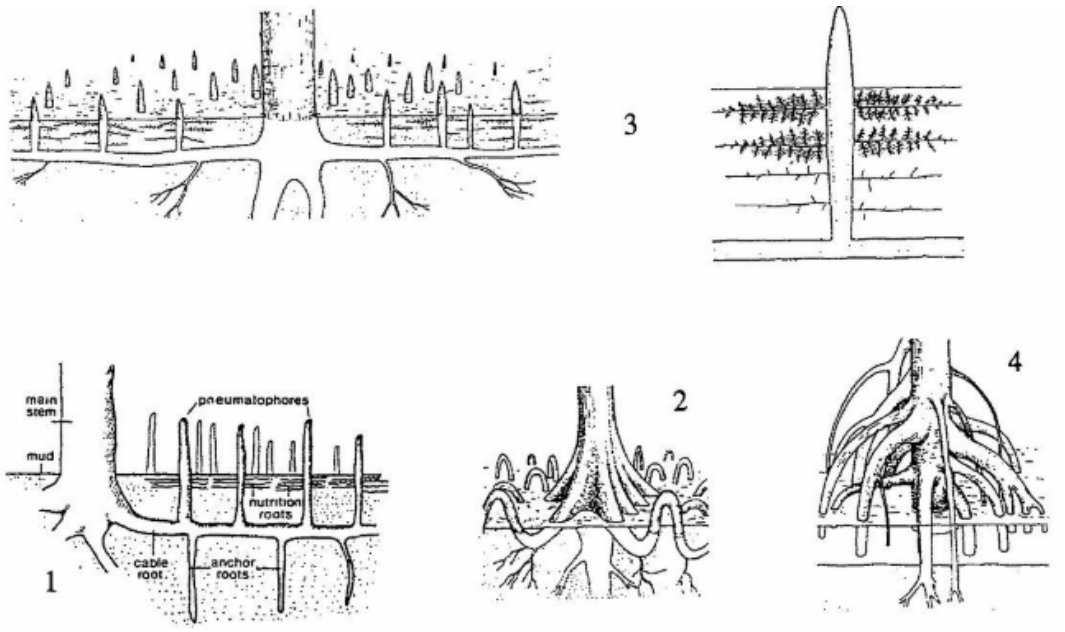

FIGURE 2.2: Root systems of (1) A. marina, (2) Bruguiera, (3) Sonneratia and (4) Rhizophora (from: Marchand (2008))

On the other hand, the varying environmental conditions have an influence on the productivity of the mangrove forest. Berger et al. (2008) identified different controlling factors for mangrove productivity, which are based on varying environmental conditions in the mangrove forests. These factors are divided into 'regulators', which are non-resource variables (including salinity, sulfide, pH and redox potential), and resource variables (including light, space and nutrients). A third influencing factor is the hydroperiod (Berger et al., 2008). These variables affect mangrove life traits. Mangroves that are exposed to prolonged periods of inundation for example grow slower and a densely populated forest enhances the competition and thereby decreases growth rates (Chapman, 1976, Ball, 1980, Berger and Hildenbrandt, 2000). Due

to the variations in mangrove species characteristics across the shorelines, a zonation in mangrove establishment can be observed, with mono-specific bands parallel to the shore, which are determined by the specific topography, soil composition, tidal ranges and salinity (FAO, 2007, Fagherazzi et al., 2017).

Furthermore, mangroves provide multiple ecosystem services. Thereby, they offer immense value not only for coastal population but for humanity in general. These ecosystem services include: the mitigation of water quality, shoreline protection, protection against coastal hazards, the creation of an ecologically important habitat, providing of natural resources (e.g. wood), as well as recreation, education and spiritual relevance (FAO, 2007, Horstman et al., 2013b, Duke et al., 2021). Furthermore, mangroves play an important role in small-scale local fisheries supporting food security and thereby achieving the first Sustainable Development Goal (SDG) 'No Poverty' as well as SDG 2 'Zero Hunger' (zu Ermgassen et al., 2021). Additionally, mangrove ecosystem gain increasing significance as blue carbon drivers [1]. Mangrove forests are able to capture and preserve a high amount of carbon and thereby play an important role in climate change mitigation (Alongi, 2014). Even though mangroves cover only about 0.5 percent of the global coastal area, they are responsible for approximately 10 to 15 percent of the global marine carbon burial (Alongi, 2014, Mullarney and Henderson, 2018). An extensive summary of the mangrove forest services of is given in Table 2.1. Based on the described ecosystem services, the total value of a mangrove ecosystems has been evaluated by Costanza et al. (2014) to be about USD 194,000 per hectare per year. Considering the total mangrove area estimated by Giri et al. (2011), the total value of mangrove ecosystems globally sums up to USD 2.7 trillion per year. This highlights the value of mangroves also from an economical viewpoint.

[1] blue carbon describes the burial of carbon within aquatic ecosystems (Alongi, 2014).

TABLE 2.1: Summary of Mangrove Services (adopted from: FAO (2007))

Category	Uses
Fuel	Fuelwood Charcoal
Construction	Timber, scaffolding Heavy construction Railway sleepers Mining props Boat-building Dock pilings Beams an poles Flooring, panelling Thatch or matting Fence posts, chipboards
Fishing	Fishing stakes Fishing boats Wood for smoking fish Tannin for nets/lines Fish-attracting shelters
Textile, leather	Synthetic fibres (rayon) Dye for cloth Tannin for leather preservation
Other natural products	Fish Crustaceans Honey Wax Birds Mammals Reptiles Other fauna
Food, drugs and beverages	Sugar Alcohol Cooking oil Vinegar Tea substitute Fermented drinks Dessert toppings Condiments (bark) Sweetmeats (propagules) Vegetables (fruit/leaves)
Agriculture	Fodder
Household items	Glue Hairdressing oil Tool handles Rice mortar Toys Match sticks Incense
Other forest products	Packing boxes Wood for smoking sheet rubber Medicines
Paper products	Paper - various

2.1.2 Threats to Mangrove Forests

However, in recent years, the stresses on mangrove forests have increased, mainly due to climate change induced processes of sea level rise, increasing coastal hazards and extreme weather events (IPCC, 2021). Considering mangrove landscapes are transition zones between different ecosystems (ecotones), which connect ocean ecosystem, periodically inundated by tidal currents, with terrestrial ecosystems, continually disturbed by human activity. Mangroves are affected by both natural processes and human activity. That makes mangroves a naturally stressed ecosystem and changing climatic conditions (e.g. increase in hurricanes and sea level rise) have a particular influence on the distribution of mangroves along environmental gradients (Twilley et al.,

1999). Additionally, with the increase in population of coastal areas and the destruction of mangrove forests for human use, further stresses and destruction is exerted on this high yielding ecosystems. For example, the construction of dams and reservoirs has led to changes in sediment transport, the extraction of oil in coastal areas leads to subsidence of deltas and aquaculture destructs mangrove forest area. All this causes further stress on mangrove forests (Mullarney and Henderson, 2018, Goswami, 2021). Thus, human activity has been identified as the main cause of mangrove forest loss, however, its impact has decreased since the year 2000, indicating the rising awareness for the values offered by mangrove forests (Goldberg et al., 2020). The combination of human activity and natural drivers of mangrove loss has led to mangroves being particularly threatened. Compared to pre-industrial times, half of the area covered by mangroves worldwide has already been lost (Mullarney and Henderson, 2018) and the mangrove coverage decreased at an average rate of 0.11 percent per year between 2010 and 2016 (Spalding and Leal, 2021). The loss of mangroves will in turn affect their ecological and economic functions, thus, assessing mangrove vulnerability is a global priority.

2.1.3 Mangrove Conservation and Recovery

Therefore, the conservation and restoration of this highly valuable ecosystem becomes increasingly important. However, mangrove ecosystems are highly complex systems, due to different physiological capabilities in species (e.g. tolerance to salinity (Joshi and Ghose, 2003)), environmental gradients as well as a highly variable environments, especially in face of climate change (IPCC, 2021). This makes it difficult to determine the optimal conditions for a healthy mangrove forest. Despite these uncertainties, studies have highlighted main recovery processes for the successful conservation and recovery of mangrove forests. Duke et al. (2021) defined the following recovery processes of importance - flowering and germination, production of mature propagules, dispersal to suitable sites, establishment despite tidal flushing, waves and predators, and finally, growth into mature individuals in preferably closed forest stands. Accordingly, management strategies have been pointed out, which include among others the development of models for restoration prediction. Additionally, Twilley et al. (1999) has shown that trajectories of mangrove restoration efforts depend on several factors. These are - the conditions of the initial disturbance, site modifications, the recruitment of new individuals, and environmental constraints of ecogeomorphic settings (e.g. wet versus dry climate, presence of river inflow and tidal amplitude) as well as local ecological factors such as nutrient resources and abiotic stressors. However, restoration and regrowth of mangroves is still subject to many uncertainties and is influenced by different factors whose interactions is not yet fully understood.

The recovery investigated in this thesis is based solely on the natural recovery of the mangrove characteristics such as mangrove area coverage and stem diameter. No restoration efforts are taken into account and other biotic or abiotic factors of ecosystem recovery are not considered.

2.2 Estuary Morphology and Mangrove Interaction

As pointed out in the above section, in order to protect and conserve mangrove forests, it is important to understand mechanisms underlying the relationships between mangrove dynamics and coastal environments. Below, previous studies on the interactions

between mangroves and their environment are reviewed. More specifically, the morphodynamic and hydrodynamic processes in estuaries are described, followed by an overview of what is known about the effects of mangrove vegetation on estuary systems and vise versa.

2.2.1 Morphology and Sediment in Estuarine Systems

Estuaries are characterized by a mix of fresh river water and saline sea water (Prandle, 2009). Describing the environmental and ecological factors influencing an estuarine system in detail, with their physical laws and equations would exceed the scope of this thesis. Therefore, this section merely serves as an overview of the morphological and hydrodynamic processes in an estuary as they represent the basis of the modelling approach adopted in this study. Figure 2.3 shows the hydro-morphodynamic interactions in estuaries with the flow influencing the sediment transport, this affects the morphology, which affects the flow. Therefore, this figure shows the feedback that underlies the hydro-morphodynamic system of estuaries.

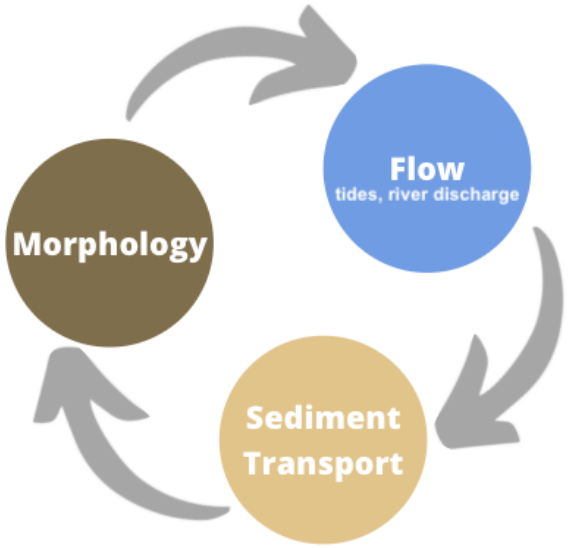

FIGURE 2.3: Concept of a Hydro-morphodynamic System

Estuaries are shaped and influenced by many factors. Hydrodynamic factors such as river discharge and fluvial load. The major sources of energy input are generally tides, river discharges, surges and waves (Prandle, 2009). Thereby, for example increased river discharge leads to erosion along the main channel and channel deepening (Luan et al., 2019). Along the estuary, the relative contribution of tides and waves as well as riverine contribution to the hydrodynamic energy gradually changes (Fig. 2.4) (Lokhorst et al., 2018). Furthermore, estuaries are influenced by morphological factors such as sediment sources and sinks, underlying geology, surficial sediments, as well as bank and marsh exchange. Additionally, they are influenced by anthropogenic influences such as dredging, land reclamation, coring and upstream damming (Prandle, 2009, Mullarney and Henderson, 2018). Lastly, estuaries are increasingly influences by sea level rise. Estuaries in general are deepening due to sea level rise, while large estuaries are exposed to the loss of intertidal area due to sediment limitation, small estuaries are subject to an increased risk for flooding (Leuven et al., 2019) due to sea level rise. Some of these factors are illustrated in Figure 2.5. All these factors lead to a highly variable ecosystems, with spatially and temporally varying conditions of flow, erosion, sedimentation and salinity. These conditions of high

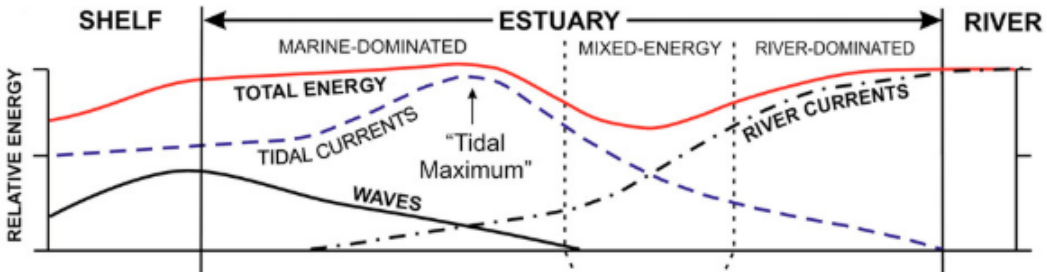

FIGURE 2.4: Longitudinal variation of the intensity of the three main physical processes, river currents, tidal currents and waves (Dalrymple and Choi, 2007).

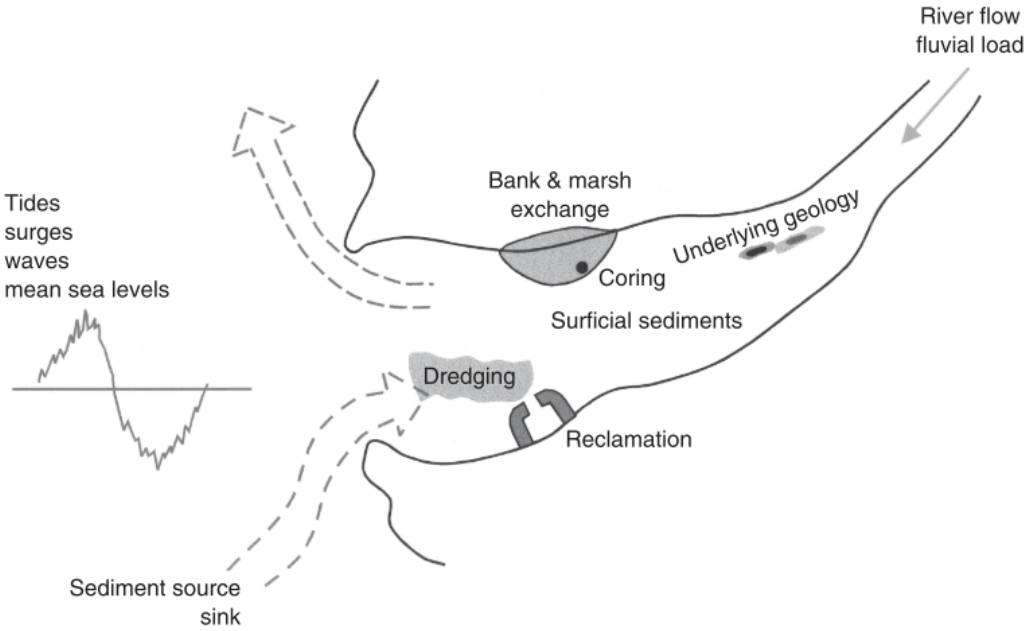

FIGURE 2.5: Schematic of major factors influencing estuarine bathymetry (Prandle, 2009).

variability and constant change, leads to the question of the resistance and influence of vegetation in estuaries.

2.2.2 Interactions of Mangroves with Hydrodynamics and Morphology

The full complexity of the dynamic processes governing estuaries becomes evident when considering the influence of vegetation on the morphology and hydrodynamics. Therefore, understanding the effects of vegetation on the geomorphological system as well as the hydrodynamic processes is an emerging field of research. In isolation, the effects of vegetation in general are fairly understood (Lokhorst et al., 2018). However, hydromorphodynamic and ecological processes interact across several spatial and temporal scales (Gijsman et al., 2021), and when it comes to consequences and effects at the scale of the entire system, they are rather poorly understood so far. For example, vegetation is known to increase bank stability, flow resistance and sedimentation. However, it is still mostly unknown, how these processes affect the whole

system of the estuary (Lokhorst et al., 2018). An overview of those processes is illustrated in Figure 2.6. Figure 2.6 shows how mangroves are interacting with hydrodynamic, morphological processes and how that affects the mangrove's functionality and persistence (Gijsman et al., 2021). These processes will be further described in the following paragraphs.

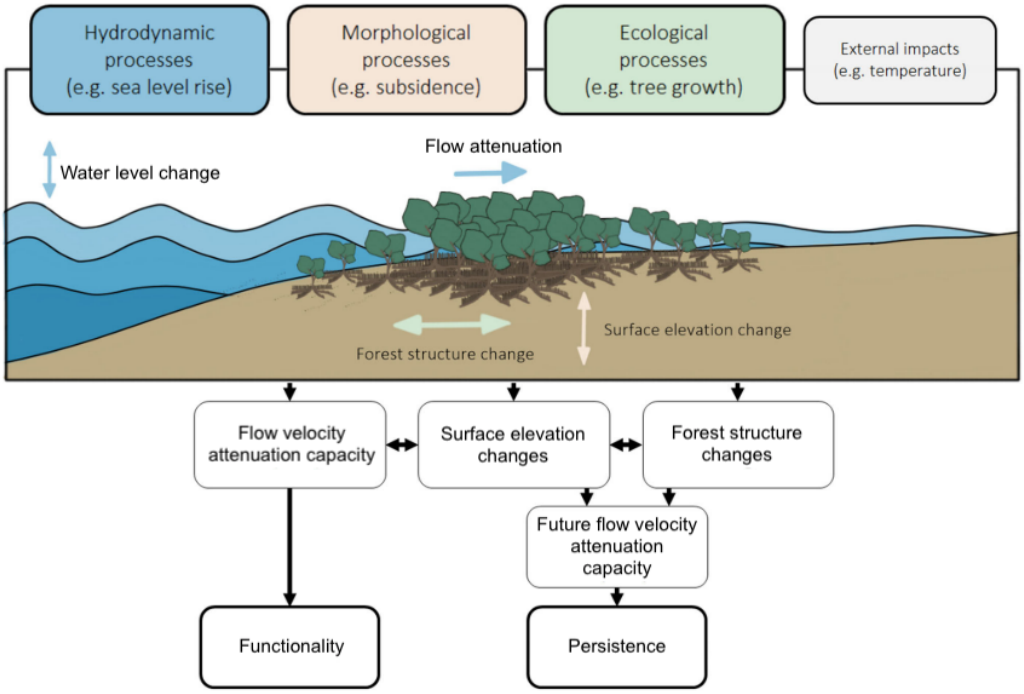

FIGURE 2.6: Interaction of hydrodynamic, morphological and ecological processes in mangroves (adopted from: Gijsman et al. (2021)).

Impacts on Hydrodynamic Processes

Mangroves interact with hydrodynamic processes to the extent that the magnitude as well as the direction of the flow is affected by their presence. In previous modelling studies, it was concluded that the magnitude of the flow in the vegetated areas is reduced due to the extra drag force. The drag force is caused by the stems as well as their pneumatophores acting as an obstacle forcing the flow to work against their friction. This leads to the dissipation of wave energy which results in wave height damping (Horstman et al., 2014, Amma and Bhaskaran, 2020). It was further observed that flow velocities decrease when mangrove vegetation becomes denser (Xie et al., 2020). Furthermore, the friction caused by the vegetation counteracts the alongshore velocity component leading flow velocities within the vegetated area to be mainly along the cross-shore water level gradients (Horstman et al., 2013c). On the other hand, in the unvegetated areas between the vegetated areas (e.g. within the channel), the flow is concentrated which leads to sediment erosion instead, and thereby to channel formation or channel deepening (Nardin and Edmonds, 2014). Further, it was found that flow velocities within the creeks have a noticeable peak during ebb tides with higher velocities than during the incoming flood tides (Willemsen et al., 2016). Based on the capacity of mangroves to attenuate surge levels and wind wave, it was concluded that mangroves have the potential to contribute to the reduction of coastal flood risk in coastal zones with a low elevation (Samiksha et al., 2019, Gijsman et al., 2021). In

Figure 2.6 these processes are summarized as flow attenuation capacity within the mangrove forest.

Impacts on Morphological Processes

Mangrove vegetation has several effects on its surrounding morphology. The above described attenuation of the hydrodynamics by mangrove vegetation initiates sediment deposition in the mangrove forest, as mangroves change the erosion threshold. Therefore, mangroves stabilize sediment, such as mud and lead to mud sedimentation. Firstly, when the flow encounters the mangroves, their presence leads to a reduction in sediment transport fluxes which causes net sediment deposition in the mangrove forest (Van Maanen et al., 2015). When studying the sediment deposition processes, Willemsen et al. (2016) found that there is a cross-shore decrease of deposition throughout the mangrove forest. Therefore, the largest deposition occurs on the mudflat. Furthermore, it was found that the cross-sections of the channels are influenced by the reduced erosion due to the vegetation. Mangroves increase bank stability and therefore steeper banks can develop in channels which are lined by mangrove trees. Due to the vertical growth of the vegetated areas, the volume of water stored in the vegetated platforms decreased, which lead to a reduction of the tidal prism and the current velocities within the platform (Van Maanen et al., 2015). In a long-term, the increased sediment depositions together with biogenic input especially due to organic matter production, leads to positive elevation change in the vegetated areas (Van Santen et al., 2007, Willemsen et al., 2016).

Studies further included the effects of a rising sea level due to climate change and the potential of mangrove forests to mitigate flooding (Mcivor et al., 2013). It was found that mangrove forests have the capacity to counteract sea-level rise. The vertical sediment accretion allows mangroves to avoid inundation and thereby keep the habitat suitable for their growth (Mcivor et al., 2013, Lovelock et al., 2015). Asbridge et al. (2016) for example observed seaward and landward migration of mangroves in the Gulf of Carpentaria prior to the dieback. However, there are limits to these processes. The decline in sediment supply due to for example upstream damming as well as the restriction of the mangrove habitat due to anthropogenic developments and structures, create limitations in the bed level increase and landward retreat of mangrove forests (Schuerch et al., 2018, Xie et al., 2020). Due to the outlined effects of mangroves on the morphodynamic system, they offer immense value. This results in an increasing interest to apply mangroves in flood risk engineering along with 'hard' engineering structures, forming "hybrid-engineering solutions" and as nature-based solutions (Gijsman et al., 2021, Kumar et al., 2021, van Zelst et al., 2021). However, these processes need to be further understood on an estuary scale, in order to utilise the full potential of this resilient ecosystem and profit from their values.

Impacts of Environmental Factors on Mangroves

The mangroves in turn are also influenced by the morpho- and hydrodynamics in different ways, such as for example their seedling recruitment. Mangrove propagules go through three phases which are influenced by different hydrodynamics and sediment dynamics (Balke et al., 2011). Initially, an inundation free period is needed for the propagules to develop sufficient roots to withstand displacement (Balke et al., 2011, Oh et al., 2017). Following, the roots growth must be fast enough to withstand hydrodynamic forces, and finally, sediment dynamics such as erosion and mixing can lead

to dislodgement of the seedling (Balke et al., 2011). Additionally, hydrodynamic factors such as the inundation period determines the mangrove growth rate and species-specific distribution (Chapman, 1976). Figure 2.7 shows that mangroves characteristically colonize the areas between mean tide level and high tide level.

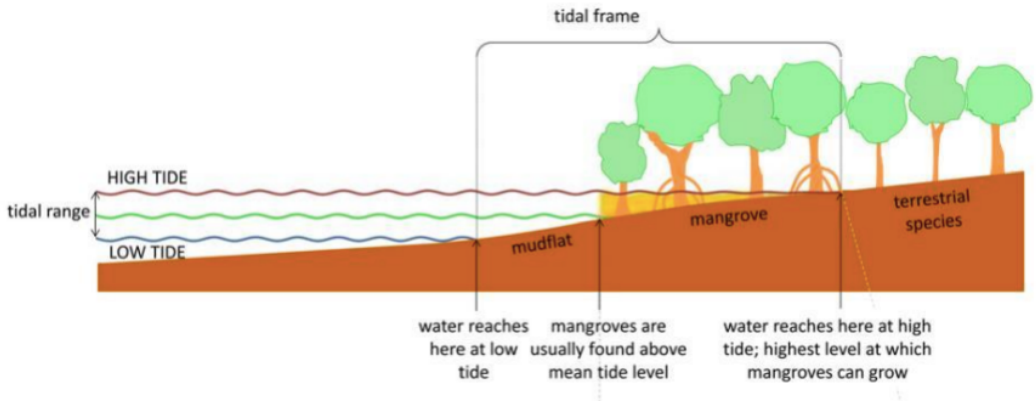

FIGURE 2.7: Mangrove colonization due to hydroperiod in cross-shore direction (from: Mcivor et al. (2013)).

In summary, it can be seen that external, hydrodynamic, and morphological factors have substantial impacts on mangrove forests. The mangrove vegetation on the other hand influences the hydro-and morphodynamics due to flow resistance and attenuation capacity. However, the question remains, on how this interaction influences the processes on an estuary scale and how the presence and absence of mangroves influence the long term processes in such a system. Further investigations are required to assess the effects of mangrove vegetation on a whole estuary, quantitatively and qualitatively. Furthermore, studies are needed to understand the potential of recovery of a mangrove forest after a perturbation event as well as the long term effects of such a event, in order to be able to quantify their resistance to future changes and their recovery potential.

2.3 Previous Modelling Approaches

In recent decades, modelling has proven to be a useful tool. It has been extensively used in the past decades to understand morphological and hydrodynamic processes as well as vegetation pattern (Broekema, 2013, Horstman et al., 2013a, Peters et al., 2014, Van Maanen et al., 2015, Kleinhans et al., 2018, Peters et al., 2018, Le Minor et al., 2019, Boechat Albernaz et al., 2020, Brückner et al., 2021, Brückner et al., 2020, Xie et al., 2020, van Veelen et al., 2021, Chen et al., 2021). Lesser et al. (2004) described morphodynamic models as "indispensable tools that hydraulic engineers working in coastal, river, and estuarine systems use to analyze erosion problems, assess morphological impacts of human interference (at several scales), and to aid the design of coastal defenses".

However, some considerations need to be made when simulating natural processes in a model. The model is not able to fully reflect the natural systems behaviour. There are uncertainties regarding initial conditions and applicable laws, which limits the verification of the model. Furthermore, models rarely predict well without calibration, and the question of the model boundaries needs to be considered. Additionally, the question of the scale arises. Since it is computationally impossible to include the processes on all scales in the system, the concept of separation of scales is important. For

example, it is virtually impossible to describe the processes of every single grain of sand in an entire estuary for every wave and tide over decades (Lesser, 2009). Therefore, modelling comes with uncertainties and limitations which need to be considered when analysing the results (Murray, 2003).

However, modelling helps to understand trends and behaviour of processes. This implies that models can help in comprehending results of complicated equations, and it can provide information about the sensitivity of different parameters, by manipulation of those parameters. Models can be further used to mediate between the theoretical laws of physics and the observations made in nature. And finally, models can offer long-term projections. To understand the early motivations to use modelling in ecology, Chen and Twilley (1998) pointed out the difficulty to capture both time and environmental gradients in experiments, which can be solved by using models to understand landscape patterns of forest dynamics. Furthermore, with regards to restoration of ecosystems it was pointed out that for rehabilitation processes, due to their time dependency (long-term), ecological modelling can determine the success and outcome of the restoration efforts (Twilley et al., 1999). Therefore, Twilley et al. (1999) recommend the development of interactive, spatially explicit models to simulate management scenarios and to evaluate their success. These previous studies are suggesting a modelling approach to simulate the (long-term) interactions between vegetation, hydrodynamic and morphological processes.. To put the modelling approach taken here in context, in the following subsections, a literature introduction into a state-of-the-art hydromorphodynamic model (Delft3D) and mangrove modelling is given.

2.3.1 Morphological and Hydrodynamic Modelling

The previously mentioned problem of scaling in the modelling of morphodynamic systems, leads to the fact that coastal morphological modelling must resort to some level of process aggregation (Lesser, 2009). 'Behaviour-oriented' models were developed as described by Stive and de Vriend (1995), in which a high level of process aggregation was incorporated. These models represent the general behaviour of large-scale morphological processes rather than modelling physical processes at a lower scale. 'Processes-based' modelling approaches on the other hand, rely on a lesser amount of process aggregation. In process-based models, it is attempted to represent all important physical processes influencing the sediment in a coastal environment. The process based models have been developed over the last century, from analytical models to one-dimensional-network, coastline, multiline and coastal profile models. These models simplify the occurring processes by integrating in two dimension and leaving one dimension free to respond, which leads to a certain amount of averaging (Lesser, 2009). Depth-averaging two-dimensional (2DH) models were developed in the 1980s and 1990s, which integrate solely the vertical dimensional, leaving two dimensions free to respond. This allows for the description of two-dimensional spatial patters of morphological change. de Vriend et al. (1993) reviewed some of those medium-term morphodynamic models and concluded that these models are applicable to certain problem classes. However, the complex nature of the natural system leads to processes that are fully-three dimensional and to a velocity profiles which deviate from the logarithmic one (e.g. channel curvature, current acceleration/deceleration, Coriolis force, wind- and wave-driven currents and density gradients) (Lesser, 2009). These conditions commonly occur near the river mouth, in estuaries and close to structures and obstacles.

In order to be able to predict and model such behaviour, a numerical model system was needed, which is "able to simulate arbitrary combinations of processes within broad classes of problems" (Lesser et al., 2004). This was realized in the DELFT3D package, which was developed by WLjDelft Hydraulics together with Delft University of Technology (Lesser et al., 2004). Due to the inclusion of integrated model, it allows for the simulation of different aspects within coastal systems. Thereby, hydrodynamic flow under the shallow water assumption, transport of water-borne constituents (e.g. heat or salinity), short wave generation and propagation, sediment transport, morphological changes, ecological processes and water quality parameters can be simulated within Delft3D (Lesser et al., 2004).

Delft3D was widely applied in previous studies as well as engineering constructions. Besides applications in rivers and tidal flats, it was also validated for different estuarine systems (Hu et al., 2009, Van Der Wegen et al., 2011a, van der Wegen and Roelvink, 2012, Lu et al., 2015). For example, to study the effect of tides on mouth bar morphology and hydrodynamics (Leonardi et al., 2013), to assess water quality and to study the controls on the evolution in a Yangtze Estuary Reservoir (Xu et al., 2017, Luan et al., 2017). It was further used to evaluate the effects of large-scale river diversions on fish and fisheries (de Mutsert et al., 2017), to evaluate the effects of mud supply on large-scale estuary morphology and development (Braat et al., 2017), and to improve the understanding of the hydrodynamics and morphodynamics of the tidal-influenced fluvial zone using a case study of the Columbia River Estuary (CRE), USA (Sandbach et al., 2018). Additionally, DELFT3D was used to investigate the effects of Shoal Margin Collapses and the impact of wind-waves and sea level rise on the morphodynamics of a sandy estuarine within the case of the Western Scheldt (van Dijk et al., 2019, Zheng et al., 2021, Elmilady et al., 2020), to determine the dominant Climate Change event for salinity intrusion in the GBM delta (Akter et al., 2019) and to investigate the influence of seasonal river discharge on tidal propagation in the Ganges-Brahmaputra-Meghna Delta, Bangladesh (Elahi et al., 2020). Most recently it has been utilized to study levee evolution under vegetation influence (Boechat Albernaz et al., 2020), to investigate pathways of micro plastic (Sousa et al., 2021) and marine debris (Juliandri, M. R., Radjawane, I. M., Tarya, 2020) within an estuary and to study salt marsh resilience to SLR (Pannozzo et al., 2021). This exemplary list shows that the DELFT3D package was extensively used for scientific research within estuaries and has produced results, which were validated on the basis of for example field observations. DELFT3D therefore provides a reliable tool for this study.

2.3.2 Mangrove Modelling

There are different approaches to investigate and monitor mangrove vegetation. A commonly used approach to monitor forest dynamics and document changes in vegetation cover is remote sensing imagery (e.g. Younes et al., 2020, Parida and Kumari, 2021). However, remote sensing cannot give information about ecological processes and processes that cause changes (Berger et al., 2008). Therefore, another approach which has provided insights in mangrove forest dynamics in the past and is gaining attention, is modelling (Doyle and Girod, 1997, Chen and Twilley, 1998, Doyle et al., 2003, Berger and Hildenbrandt, 2000, Berger et al., 2008). The use of models makes it possible to investigate the effects of environmental changes and disturbances on the recruitment, establishment, growth, productivity, and mortality of mangrove trees (Berger et al., 2008). Furthermore, models make it possible to understand rehabilitation processes and potential outcomes of such efforts (Peters et al., 2020).

In the past, different models were developed to capture the development of mangrove forests due to environmental effects. Early modelling approaches were made by Lugo et al. (1976) using a process-based model to simulate the effects of upland run-off and tidal flushing on the biomass production of a mangrove wetland. Further, a Leslie-Matrix was used by Burns and Ogden (1985) in order to simulate the development of a mangrove monoculture (*Avicennia marina*) under exponential population growth. And finally, a Lefkovich matrix, was used by Clarke (1995) to predict the recovery of a mangrove species (*Avicennia germinans*) after disturbances of different strengths (Berger et al., 2008). Furthermore, static trophic models were used to estimate the matter and energy flow in mangrove ecosystems (Berger et al., 2008). However, recently, individual based models (IBM) became most popular for mangrove modelling. IBM regard the trees autonomously with their varying characteristics, their interaction with neighbouring trees and their environment (Peters et al., 2020). Presently, different types of IBM for mangrove forests have been developed. A group of IBM take the effect of different abiotic factors on the tree growth into account, as species specific growth reducing factors. The growth-reducing factors include parameters such as salinity, nutrients, temperature, hydroperiod and competition of neighbooring trees (e.g. Chen and Twilley, 1998, Doyle et al., 2003, Berger et al., 2008, Grueters et al., 2014, Van Maanen et al., 2015 and Xie et al., 2020).

The descriptions of a single tree allometry and the tree growth, most commonly implemented in the mangrove models is based on the JABOWA model (Botkin et al., 1972). The empirical formula introduced by Botkin et al. (1972), describes the tree stem diameter at breast height (DBH) converging asymptotically to a species-specific maximum value. The further plant characteristics such as tree height or projected canopy area are then empirically related to the stem diameter. Furthermore, a dependency of the trees on water or nutrient availability as well as the increased stress due to salinity is implemented through a reducing factor (Peters et al., 2020). The following Table 2.2 summarizes IBM, developed in previous studies, concentrating on the used mechanism for tree establishment, the factors considered in tree growth, how the competition between neighbouring trees is considered, the process implemented to describe the mangrove mortality as well as the model application in a coupled model. Table 2.2 therefore serves as an overview of existing mangrove models.

TABLE 2.2: Mangrove Models Summary in Recent Decades

Model (Reference)	Use	Seedling Establishment	Tree Growth Factors	Competition Concept	Mortality	Coupling
FORMAN (Chen and Twilley, 1998	Simulate demographic processes of mangroves	Sapling number depending on light, flooding and seed consumption	Salinity, nutrient and light availability and temperature	-	-	-
KiWi (Berger and Hildenbrandt, 2000)	Study process of self-thinning by competition among individual trees	Random distribution, establishment dependent on competition strength	salinity and nutrient availability	FON	'memory function'	-
MANGRO (Doyle and Girod, 1997, Doyle et al., 2003)	Multi-species landscape dynamics of mangroves on a large spatial scale	$1 plant/m^2/year$ with equal probability for all species	Size (empirical growth curve) and light (shade tolerance)	-	Stochastic process of growth suppression, and hurricane impact	-
MANHAM (Sternberg et al., 2007)	Simulate sharp boundaries between mangrove stands and hammocks in costal economies of South Florida	-	Feedback between salinity and plants	Competition for space of mangroves and hammocks	Hard switch between mangroves and hammocks depending on fixed salinity threshold in soil porewater	In MANTRA model (Teh et al., 2013)
SEHM (Jiang et al., 2012)	Simulate spatial patterns of ecotone between mangroves and hammocks (intra- and interspecific competition)	Recruits produced monthly by mature trees, establishment depends on salinity and competition	Neighbourhood competition and salinity	FON	Mortality due to size-dependent factors or from reduced growth rate caused by competition or salinity	With a grid-based hydrodynamics submodel
mesoFON (Grueters et al., 2014)	Simulate Mangrove forest dynamics with including the crown plasticity of mangrove trees	Annual production by mature trees, number depends on reduction factor and offspring density per crown surface area	Salinity, nutrient availability and neighbourhood competition	2 FONs per tree (above- and below-ground)	Natural (dependent on dbh) and disturbance-related tree death (hurricane return period)	-
BETTINA ($_ibm$) (Peters et al., 2014; Peters et al., 2018)	Investigate the biomass allocation patterns of mangrove trees to environmental conditions	New biomass allocation in locations to improve uptake of limiting resource	Growth allocation is focused on improving the uptake of the limited resource (water uptake and light interception)	ZOI for above- and below-ground processes	Death threshold: If growth falls below a certain proportion of the tree volume, the individual dies	In MANGRA (Bathmann et al. (2020))
Van Maanen et al. (2015), Xie et al. (2020), Xie et al. (2022)	Simulate long-term morphological evolution of tidal basins due to interactions between hydrodynamics, sediment transport and evolving morphology	Initial establishment in bare cell with 5 percent probability, establishment only in grid cells inundated less than half of the time	Inundation (hydroperiod) and competition	Maximum density of 125 mature $trees/ha$ with ZOI	Mortality occurs after continuous periods of growth depression	With ELCOM or DELFT3D

Additionally to the models summarized in Table 2.2, further efforts have been made in modelling the vegetation impact on tidal dynamics along with wave and storm surge attenuation (Horstman et al., 2013b, van Veelen et al., 2021, Chen et al., 2021). Furthermore, a recent approach was made to model the wave dissipation of mangrove vegetation using a neural network modelling (Malvin et al., 2020).

The comprehensive overview given in Table 2.2 points out the gaps, which still exist in modelling the interaction of mangrove vegetation and their geomorphic environment. The past modelling approaches do not sufficiently consider the two way interaction between abiotic environmental conditions and the mangrove forest dynamics. The influencing factors such as salinity, nutrient and water availability are assumed to be constant over space and time in almost all of the past modelling approaches. The transport processes horizontally and vertically of water or nutrients are barely considered. Furthermore, it can be seen that the majority of the models listed in Table 2.2 predominantly focus on mangroves and the impact on mangroves of various factors such as light, salinity, nutrient abundance, temperature, water availability and competition (inter and intra-species), as well as the impact of hurricanes. While the studies listed below the table ((Horstman et al., 2013b, van Veelen et al., 2021, Chen et al., 2021), Malvin et al., 2020) focus on the effect of the mangroves on the flow and do not include the feedback on the mangrove establishment and growth.

2.3.3 Coupling of Morphology and Vegetation

To fill this gap, coupling of the mangrove vegetation model to flow and transport model was proposed and investigated (Peters et al., 2020, Xie et al., 2020). The coupled model used here from Xie et al. (2020), incorporates the interactions between mangroves and their environment instead of solely the influence of the environment on mangroves or vice versa. The coupling of the vegetation model with a flow or sediment transport model to account for feedback along with spatial as well as temporal variation of the relevant parameter, has shown promising results in previous studies (see Van Maanen et al., 2015, Brückner et al., 2020, Peters et al., 2020, Xie et al., 2020, Brückner et al., 2021, Xie et al., 2022).

Not many studies however have investigated these interactions on an estuary scale. A recent example is Brückner et al. (2020), where a model reflecting spatiotemporal growth of biostabilizers, saltmarsh and microphytobenthos is coupled with a 2-D hydro-morphodynamic model in Delft3D. Thereby, the interaction of mud, saltmarsh and microphytobenthos with morphology in an estuary was simulated. This previous study conducted in an estuarine system using the coupled vegetation model, shows that the method is suitable to model the eco-morphodynamic feedback on an estuary scale. In coupled modelling with mangroves as vegetation, two previous studies have been conducted. Van Maanen et al. (2015) modelled the evolution of tidal channel networks under the influence of A. marina mangroves in tidal sandy embayments. Furthermore, Xie et al. (2020) simulate the interactions between various mangrove species and hydro-morphodynamic processes in a coastal profile by extending the mangrove model (by Van Maanen et al., 2015, Xie et al., 2022) with comprehensive sediment transport processes (i.e. Delft3D).

This literature review shows a clear direction for further studies. Mangroves are an important ecosystem for coastal protection and carbon sequestration, whose interaction with hydro- and morphodynamics on an estuary scale need to be further understood. Additionally, considering restoration purposes and to preserve the valuable services

mangrove forests offer, it is important to find ways to understand the system in a way to increase their resilience. As previous studies have shown, filling these knowledge gaps can be archived using a modelling approach. The comprehensive summary of existing models has shown that a coupled model used by Xie et al. (2020) and Xie et al. (2022), is promising to investigate the processes in mangrove forests on an estuarine scale and the feedback with the morphological development.

Chapter 3

Research Region and Background

The purpose of this chapter is to provide an overview of the research region, the Leichhardt estuary in the Gulf of Carpentaria, Queenslands, Australia. In late 2015, a large-scale mangrove dieback event occurred in the Gulf of Carpentaria. This mangrove dieback event will be described and the information about the causes and consequences of this dieback event from recent studies will be recapped.

3.1 The Leichhardt River Estuary in the Gulf of Carpentaria

The Gulf of Carpentaria (hereafter also referred to as 'the Gulf'), situated in the Northern Territory and northern Queensland, Australia, is a U-shaped shallow gulf, which encompasses an area of 300,000 km^2 (Fig. 3.1). It is composed of three shores: the Arnhem Land coast, a southern shore and the Cape York Peninsula. The rather irregular Arnhem Land coast represents the eastern part of the gulf, while the southern shore has a low-gradient sediment-rich, rather low energy environment. Finally, the Cape York Peninsula is relatively straight and represents the west coast of the gulf (Short, 2020). With 280 creeks and rivers draining into the gulf, it represents a major catchment in Northeast Australia. Sediment is transported toward the coast through the river systems. In total, the rivers drain a relatively low-lying watershed with the size of about 0.5 million km^2 (Asbridge et al., 2016). In the estuaries tide-dominated deltas have formed (Short, 2020). Figure 3.1 shows a map of Australia with the Gulf in the North East, between Cape York and Cape Wessel. Overall, the Gulf is a diverse system with intertidal flats comprised of sand and mud, tidal creeks, salt marshes and beaches, island bars as well as mangrove forests (Short, 2020).

One of the biggest river flushing into the Gulf is the Leichhardt river with a catchment of about 33,000 km^2 (Short, 2020). An annually-average discharge of 2179 gigalitres is transported to the Gulf (Jaensch and George, 2019) and the Leichhardt estuary has an average tidal range of 2-3 m (Asbridge et al., 2016). The section of the Gulf adjacent to the Leichhardt estuary is dominated by extremely low near-shore gradients as well as especially low gradients across the supratidal salt flats. These salt flats can extend up to 50 km inland (Short, 2020). Regarding the catchment of the Leichhardt estuary, the main land-use in the catchment is rangelands for cattle. Several mines can be found upstream including the mining town of Mount Isa. Human population within the catchment is rare (Jaensch and George, 2019). In the upstream parts of the river, two major dams are impacting river discharge and sediment load (since 1958 and 1976). However, the ecological impact of the dams on the Leichhardt river are currently unknown (Jaensch and George, 2019). Nonetheless, the remoteness and the absence of human population result in the ecosystem of the Leichhardt estuary being

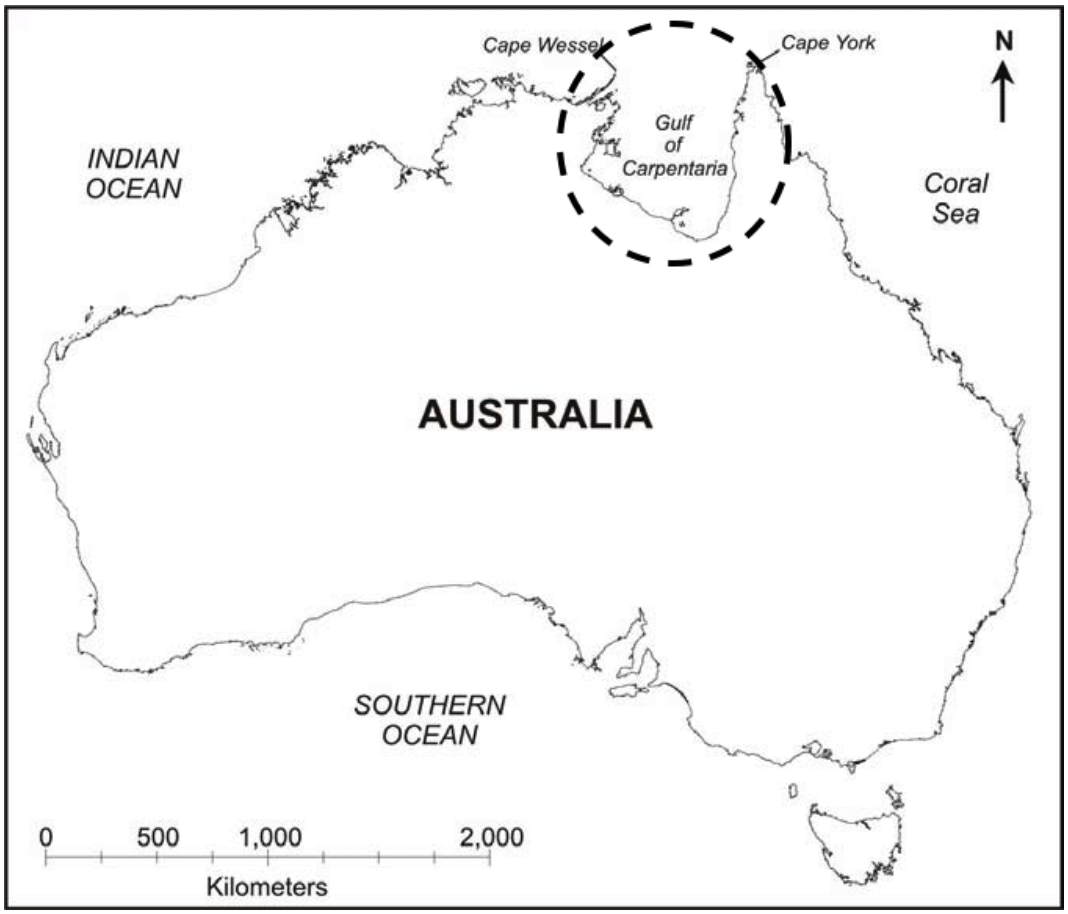

FIGURE 3.1: Map showing the location of the Gulf of Carpentaria, Queensland Australia (from Heap et al. (2006)).

hardly influenced by human interactions (Jaensch and George, 2019). Furthermore, designated conservation areas and marine national park zones are protecting the Gulf ecosystems (Asbridge et al., 2016). The undisturbed nature of the ecosystems as well as the numerous tidal wetlands around the river mouths provide an ideal substrate for mangrove growth (Asbridge et al., 2016).

3.2 Mangroves in the Gulf of Carpentaria

In 2005, 10 percent of the world mangrove area was found in Australia, with a species variety of more than 30 mangrove species (FAO, 2007). In total, Australia had an area of more than 1.4 million hectares of mangroves which equals to about 0.1 percent of its total land area (FAO, 2007). In the Gulf, mangrove forests can be found at most of the Gulf's shores and in all creeks and rivers. The eastern Gulf shore is home to about 20 mangrove species, while this number increases to more than 30 different species along the western shore (Short, 2020). The total area of mangroves in the Gulf sums up to 2440 km^2 which equals to about 21 percent of Australia's total area of mangroves (Short, 2020). Of this mangrove coverage, about 1600 km^2 can be found in the eastern Gulf (Asbridge et al., 2016). It was further found by Asbridge et al. (2016) that mangroves in the gulf were expanding both landward and seawards prior to the dieback event in 2015. The dominant species of mangroves in the Gulf of Carpentaria is *Avicennia marina* (A. marina, or: grey mangrove) (Duke et al., 2021). Furthermore,

the species *Rhizophora stylosa*, and *Sonneratia alba* are among the species thriving in the Gulf (Asbridge et al., 2016). In Figure 3.2, a photograph of the grey mangroves (A. marina) is shown.

FIGURE 3.2: Grey mangrove (*Avicennia marina*), Towra Point Nature Reserve.

Mangroves thrive in the Gulf especially along the coastlines of Leichhardt, Nicholson, Flinders River, and Mornington Inlet catchments (Asbridge et al., 2016). Around the western part of the Gulf, mangroves show zonation patterns, with *A. marina* populating the most seaward area, followed by the taller *Rhizophora* and *Bruguiera* further inland. In the most landward and saline zones, Ceriops are growing in some areas (Jaensch and George, 2019). Even further inland, above the highest tide line, communities of grasses, vines, shrubs and low trees are dominating the vegetation (Jaensch and George, 2019). The salt flats, enclosed by vegetation are itself quite bare. However, in some of the salt flats, algal mats, seawards of marine couch Sporobolus virginicus and short chenopod (samphire) plants can be found (Jaensch and George, 2019). As described in section 2.1, mangroves provide numerous, valuable ecosystem services. In the Gulf specifically, mangroves support the fish, crab and prawn resources which provide valuable resources for commercial fisheries and indigenous and recreational fisherman. In addition to the economic function, mangroves in the Gulf also provide coastal protection, act as carbon sink and protect the coast against the unpredictable weather conditions (Jaensch and George, 2019).

3.3 Climatic Conditions

The Gulf's climate is influenced by different factors. It is a hot and humid, tropic monsoonal climate, with dry and wet seasons (Short, 2020, Asbridge et al., 2016). Therefore, rainfall mainly occurs during the wet seasons of approximately four months (December to March), owing to the northwest monsoon being drawn by the ITCZ/Cloncurry heat low delivering heavy rains (Short, 2020). These rains produce runoff which often exceeds the capacity of the local river channels (Asbridge et al., 2016). Furthermore, during the wet season, tropical cyclones can occur, with an annual average of two to

three cyclonic events (Asbridge et al., 2016, Duke et al., 2021). The winters are rather warm and dry due to the sub-tropical high-pressure systems bringing drier south-east trade winds (Short, 2020). The annual rainfall is decreasing from the north to the south of the Gulf, with about 2000 mm of rainfall per year in the northern and 800 mm per year in the southern Gulf (Asbridge et al., 2016). The lowest rainfall occurs in Karumba at the southeast corner of the Gulf. The mean daily temperature in summer is approximately 30 °C, while in the winter an average temperature of about 25°C is reached (Short, 2020). Regarding climate change, the impacts on the Gulf are not sufficiently understood (Jaensch and George, 2019). However, it is known that the Gulf is impacted by a long term sea level rise of about 3.65 mm per year on average (Duke et al., 2021). Additionally, the Gulf is influenced by El Niño–Southern Oscillation (ENSO) events. The ENSO has an influence on sea surface and air temperature, rainfall, evaporation stress and reduces the sea level along the coast (Abhik et al., 2021,Hickey et al., 2021). A severe ENSO event occurred in 2015/2016 with an immense impact on the vegetation in the Gulf. The El Niño event is believed to be the strongest to have occurred within the past 145 years with an unprecedented warmth at the central equatorial Pacific (IPCC, 2021).

3.4 The Mangrove Dieback Event in the Gulf of Carpentaria

Figure 3.3 illustrated the consequences of the ENSO event 2015-2016 on the mangroves in the Gulf. The severe El Niño event of 2015/2016 led to a sea level drop, a lengthy

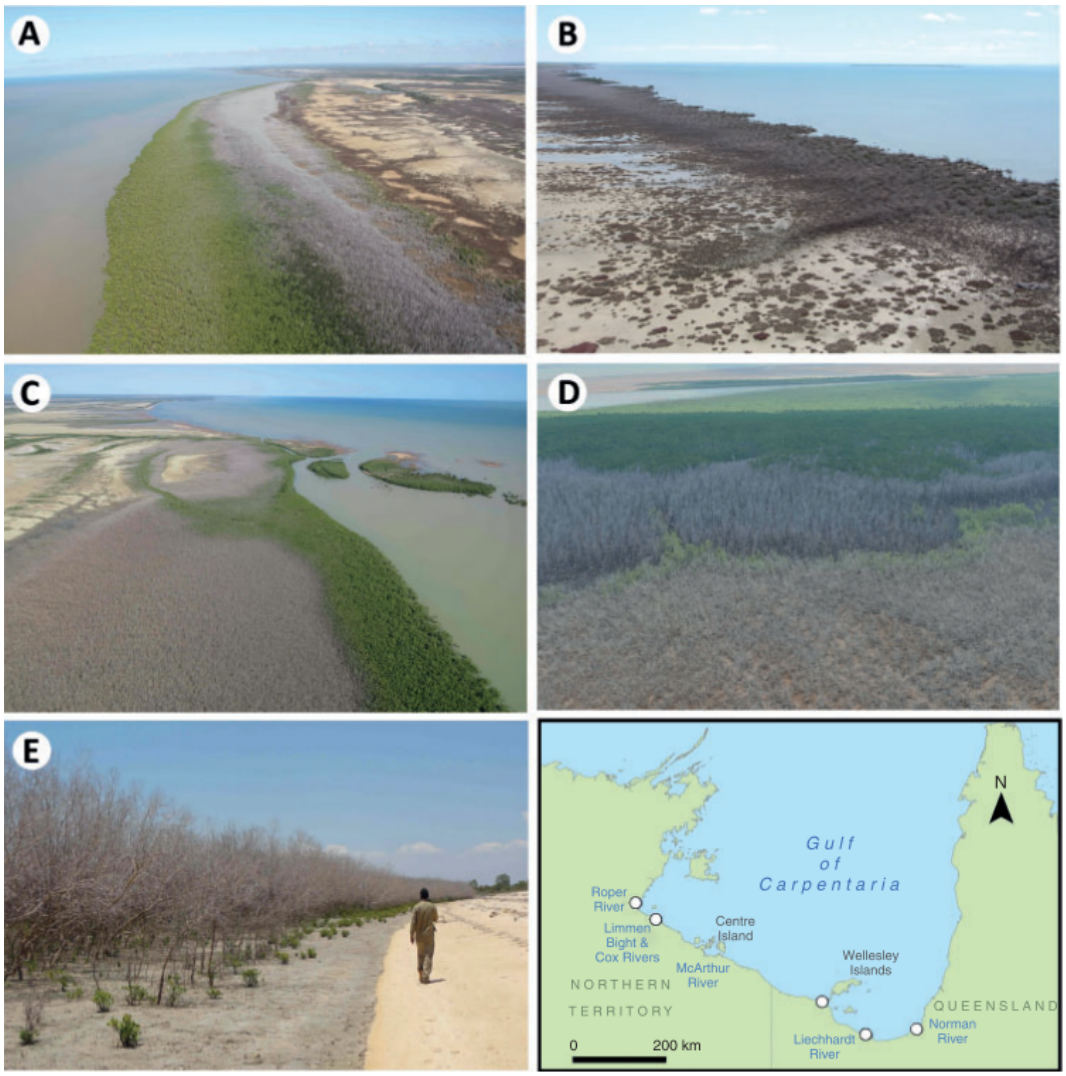

FIGURE 3.3: The mangrove dieback in the southern Gulf of Carpentaria in five different locations (A-E) as indicated in the map (bottom right). (A) Roper River shoreline, (B) Limmen Bight River shoreline (images taken by Tony Griffiths, 9.06.2016), (C) Gangalidda shoreline (image taken by Roger Jaensch, 13–14.04.2016), (D) Leichhardt River mouth (on 17.11.2016), and (E) Karumba, Queensland, Norman River shoreline (on 27.10.2016) (images from surveys reported in Duke et al. (2021)).

drought, low rainfall and a heatwave in the Gulf. All these factors resulted in a complex interplay, which created an extreme pulse event (Harris et al., 2017). The climatic anamolies in the Gulf due to the El Niño event compared to previous years are illustrated in Figure 3.4. Figure 3.4 shows an exceptionally (a) high temperature anomaly, (b) a low rainfall and (c) an unprecedented low sea level anomaly during the El Niño event in 2015-2016. Therefore, this event severely amplified the long-term stress in the mangrove forests (e.g. rising sea level due to climate change). The climatic stress

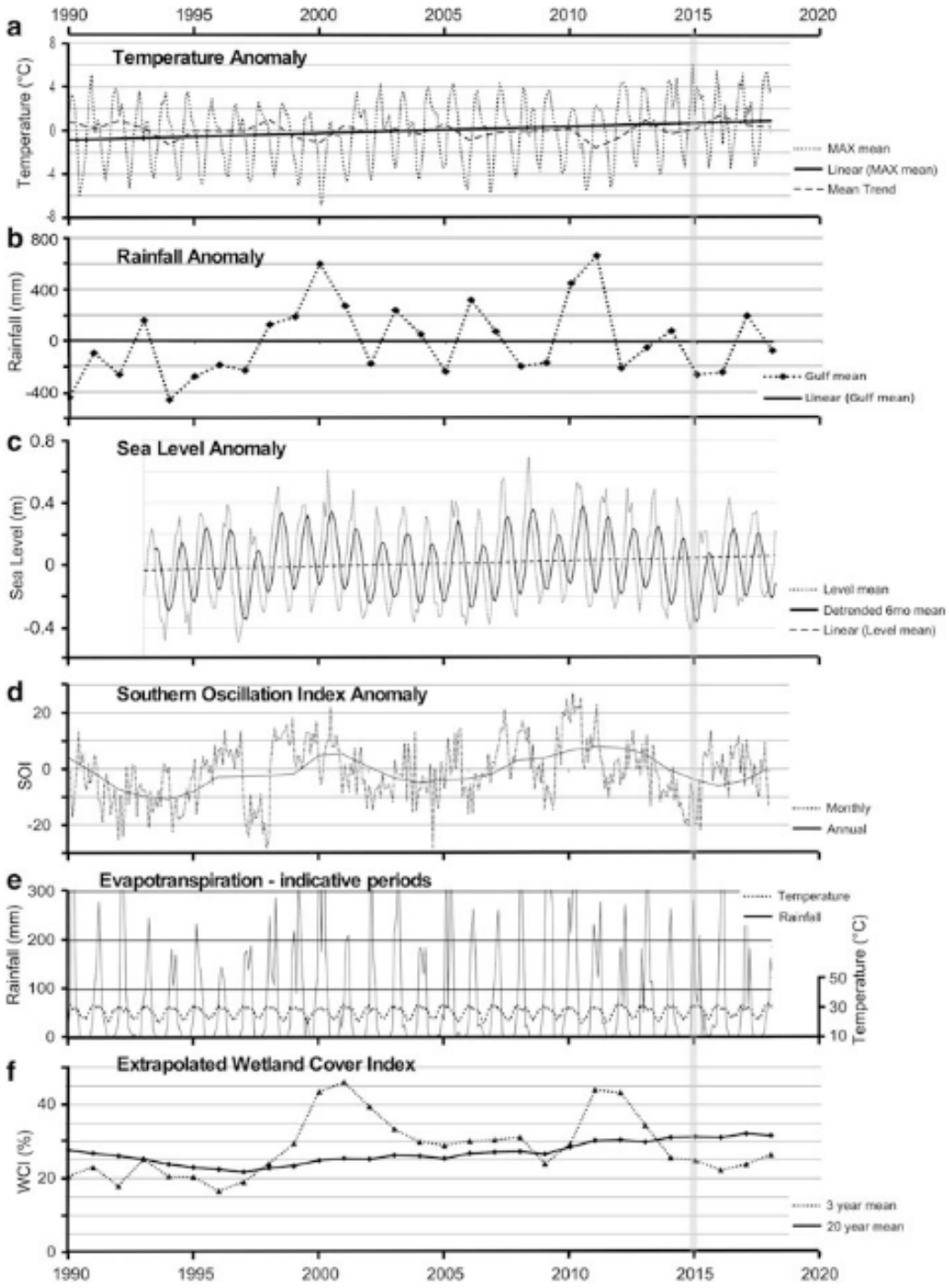

FIGURE 3.4: The condition of climate and environmental factors up to and after the 2015/2016 mangrove dieback event (from: Duke et al. (2021))

on the mangroves was increased in this short-term to such an extent, that the physiological and ecological tolerance and adaptability of the plants was exceeded. The mangroves were therefore forced into a degraded state which, according to Duke et al. (2021), might not be reversible.

Figure 3.5 shows the dieback of mangroves (in red) in the Leichhardt river catchment.

It can be seen that mostly the shoreline fringing zone of mangroves were affected by the dieback. Furthermore, a loss of mangroves bordering saltpans and saltmarshes in the upper margin occurred, while along the river channel, dieback occurred rarely. However, when looking at other sides within the Gulf, some dieback can also be observed along the river channels (Fig. 3.6).

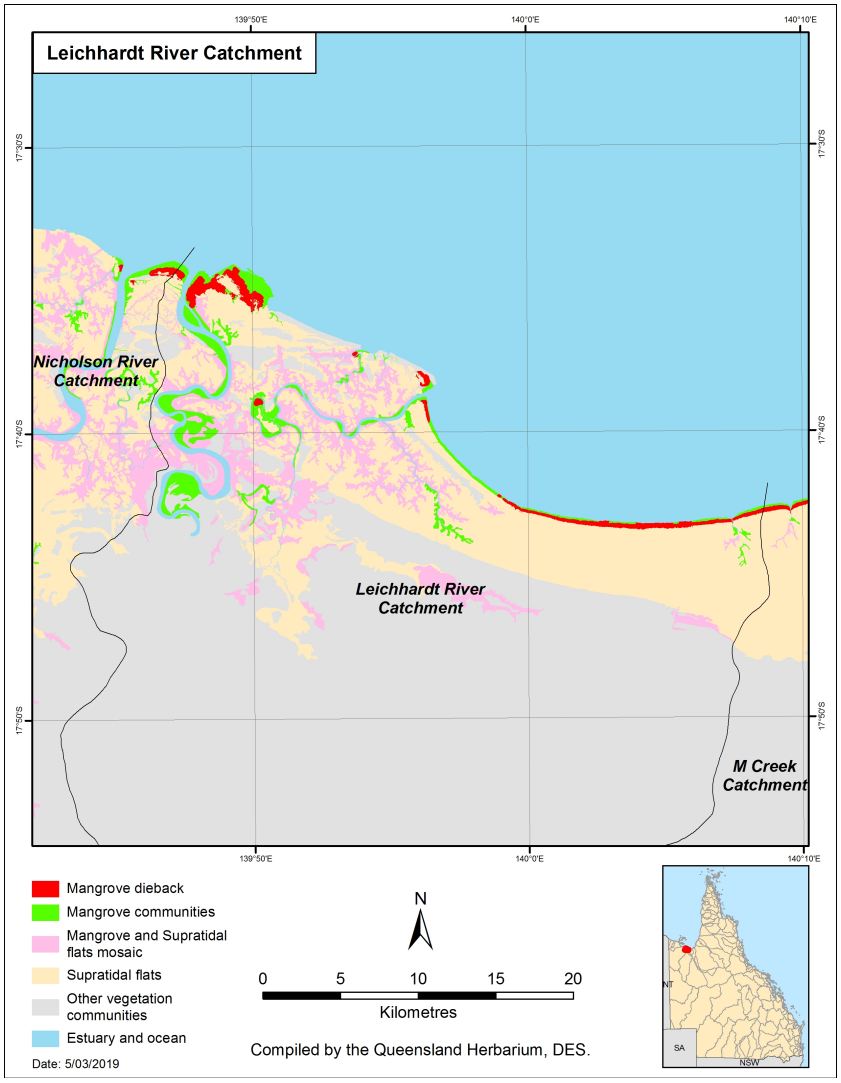

FIGURE 3.5: Leichhardt River Dieback Map (Accad et al., 2019).

This dieback had consequences for the ecosystems in the Gulf. These include for example, that the benefits of buffering and shoreline protection are lacking with the disappearance of mangroves, leading to more mobilized sediment and potential long-term influences on the adjacent reef systems (Duke et al., 2021). Furthermore, Sippo (2019) found consequences of the mangrove loss on the coastal carbon cycle. However, so far, there is little knowledge on the impacts of such a massive mangrove dieback on the estuary processes. It is therefore important to understand the causes of the dieback and how this situation affects estuary evolution in the future. Attempts to understand the processes leading to the dieback have been previously made (Duke et al., 2017,Harris et al., 2017, Accad et al., 2019, Sippo, 2019, Duke et al., 2021 and Abhik et al., 2021). These approaches mainly utilise satellite imagery, historic climate recordings and climate data of the 2015/2016 event to understand the causes of the dieback. However, according to Duke et al. (2021), one question still remains: "Was the drop in sea level

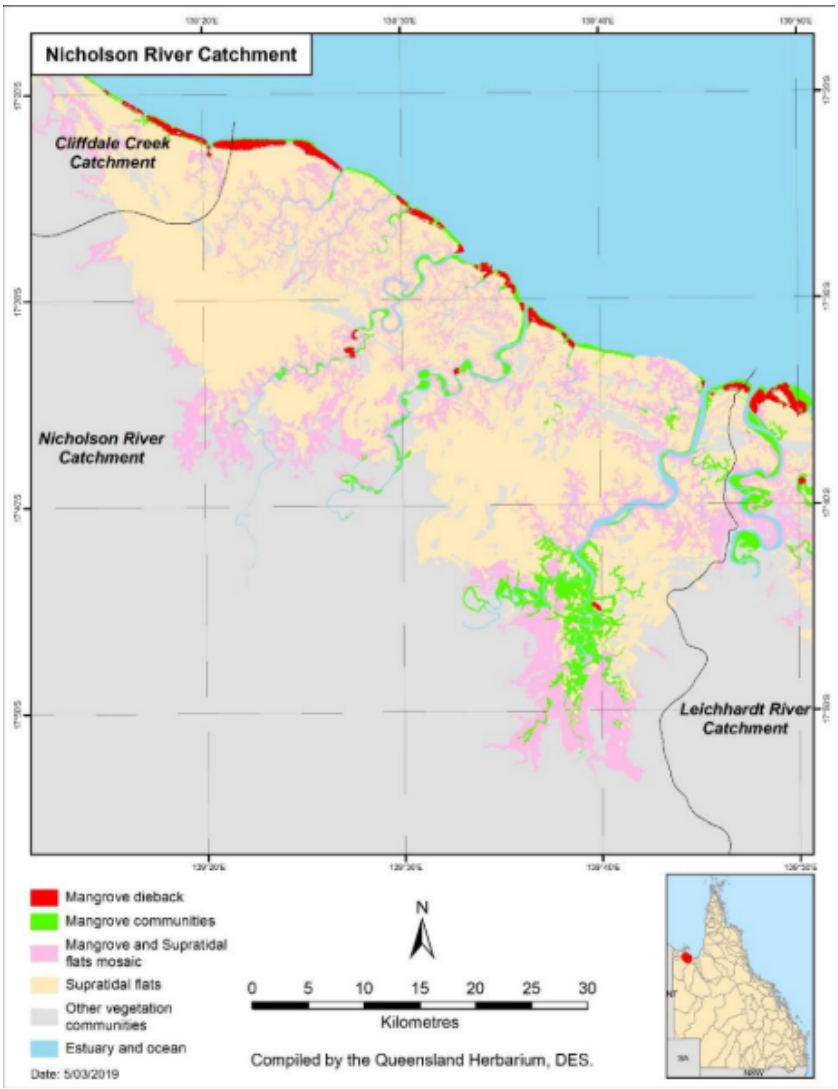

FIGURE 3.6: Nicholson River Catchment Dieback Map (Accad et al., 2019).

alone sufficient to have triggered the event? Or, had the impact of the temporary drop in sea level been enhanced by the extreme climatic conditions at the time?" (Duke et al., 2021). Furthermore, it is just as important to understand the mangrove recovery and predict changes and development of the mangrove characteristics as well as the whole estuary systems. Therefore, Duke et al. (2021) proposed, among other things, the development of forest growth and recovery models for the prediction of recovery and future events. They proposed the mapping of sediment elevation to simulate the mobilization of sediment as well as local erosion and deposition. Additionally, it was proposed to integrate climate factors such as temperature, rainfall, drought conditions, sea level and ENSO index, as well as evapotranspiration in order to understand their influence on forest development (Duke et al., 2021). In this study, the focus will lie on the influence of the sea level drop and drought conditions (i.e. decreased river discharge) on the mangrove forest development.

Chapter 4

Research Questions and Hypotheses

In this chapter, the research objectives and the research questions be outlined. Additionally, a hypothesis of the results will be presented.

4.1 Objectives and Research Questions

This thesis will investigate the processes of mangrove establishment, dieback and recovery within an estuary, to test the hypothesis of the causes as well as possible effects of the decreased mangrove coverage due to the dieback event. As highlighted during the literature review, mangrove modelling studies in the past have a limited inclusion of the two-way interaction between the mangrove trees and the morpho- and hydrodynamics on an estuary scale. In this study, a coupled modelling approach, to simulate the dieback based on sea level drop and river discharge decrease as well as the recovery of mangrove characteristics is used. As mangrove modelling on the scale of an estuary and the modelling of mangrove dieback due to changes in boundary conditions is not incorporated in previous studies, this will give new insights in the field of mangrove modelling and processes governing the eco-morphodynamic feedback. The coupled model developed by Xie et al. (2020) is used here to simulate the processes in the Leichhardt estuary. Thereby, the 2015 massive dieback event will be modelled and the results will be compared to the case study. Based on the literature review and the events occurring in the study area, the research questions are composed. Specifically, the focus lies on the biogeomorphic feedback and how the bio and morphological change is important relative to the physical forcing. Therefore, this study is guided by the following research questions.

- *Does mangrove area dieback occur in the model due to the change in boundary conditions of decreased sea level and river discharge?*
- *Which effects does the dieback have on the morphological and hydrodynamic factors (such as sedimentation, bed elevation, channel pattern and flow velocity) and which effects do the changed hydromorphology have on the mangrove resettlement?*
- *How suitable is the modelling approach to reflect the mangrove coverage during mangrove colonization, growth, dieback and recovery as compared to the case study?*

4.2 Hypothesis

Previous studies might already give an indication of the results which will be obtained in this study. It is hypothesised that mangrove loss is driven by sea level drop and river discharge decrease based on the observations made during a field study

(Duke et al., 2021). The effect of mangrove trees on morphology and hydrodynamics which are outlined in Section 2.2.2, are expected to be reversed with the dieback of the mangroves, as the flow resistance effect of the mangroves will be lost. Therefore, higher velocities in as well as lower sedimentation rates are hypothesised to occur in the dieback area compared to prior to the dieback.

Furthermore, within field studies, it was observed that the recovery of mangrove forest from disturbances in the Gulf is rather slow (Duke et al., 2021). This slow recovery could be possibly related to the hydrogeomorphic changes occurring due to dieback of mangrove area. As the presence of vegetation increase the relief and traps further sediment, removing the mangrove trees reduces relief. This feedback is expected to be seen from the model results, giving insights into the interactions of eco-morphodynamics during the recovery. Therefore, it is expected to see hydromorphodynamic changes in the dieback area affecting mangrove recovery. This possibly causes unfavorable conditions for the mangrove recovery, as they have to re-engineer a suitable habitat.

Chapter 5

Methodology

In this study, an existing hydro-morphodynamic model is coupled with a vegetation model. The vegetation model was designed to model mangrove colonization, growth and mortality (Xie et al., 2020, Xie et al., 2022). Using this method, the feedback between mangrove vegetation, morphological and hydrodynamic factors such as bed level, flow velocities, and inundation regime within an estuary are investigated. Therefore, the considered factors influencing mangrove growth, in this case inundation and competition, vary across location within the estuary and time. This allows for the simulation of the conditions occurring within the natural system. The model estuary is idealised, to avoid that local complexities in the natural system (e.g. inherited geology) hinder the comparison between model and case study. Furthermore, the inclusion of the hydrodynamics allows for the modelling of sea-level drop and a reduced river discharge to simulate the conditions which occurred during the dieback event. Thus, the coupled model is used to test the hypotheses of mangrove mortality and recovery after a disturbance. Undisturbed control runs allow for the quantification of the effects.

In the following sections, the hydro-morphodynamic model will be described by summarizing the main equations. Secondly, the dynamic vegetation model will be described. Following that, the coupling of the two models is summarized. Finally, the overall model set-up will be outlined.

5.1 Hydro-Morphodynamic Model

The Delft3D package was used to process the hydro-morphodynmaic simulations, specifically the Delft3D – Flow module. Delft3D is a hydrodynamic and morphodynamic numerical model (Lesser et al., 2004). Delft3D was used in this study to simulate the hydrodynamic and morphological processes in the estuary. In the following subsections the model is described on the basis of the main equations used, along with an explanation on the parameter and boundary condition choices.

5.1.1 Governing Equations

Delft3D is a process based model with open-source code and has been widely used and validated in previous studies (Chapter 2). The model can incorporate the main physical processes dominating coasts and estuaries, such as astronomic tides and wind waves, river discharge, salinity mixing, sediment transport (cohesive, non-cohesive sediment and interactions), as well as bed-level updating (online) based on mass conservation (Luan et al., 2017). The Reynolds-averaged Navier–Stokes equations is solved and the sediment load is calculated based on the generated flow field (Van Der Wegen

et al., 2011b). The hydrodynamics are calculated by solving the depth-averaged shallow water equations under assumption of hydrostatic pressure (Lesser et al., 2004). In the following, the main equations used in Delft3D will be summarized.

Mainly, the model relies on two hydrodynamic equations. Firstly, the conservation of mass (eq. 5.1), which describes a variation in water depth resulting form a discharge gradient.

$$\frac{d\eta}{dt} + \frac{dhu}{dx} + \frac{dhv}{dy} = 0 \tag{5.1}$$

where η is the water level [m], h is the water depth [m], u is the depth average flow velocity in x direction [m/s] and v is the depth average flow velocity in y direction [m/s]. Secondly, the model solves the momentum equations 5.2 and 5.3 (Braat et al., 2017, Xie et al., 2020).

$$\frac{du}{dt} + u\frac{du}{dx} + v\frac{du}{dy} + g\frac{d\eta}{dx} + \frac{gu\sqrt{u^2+v^2}}{C^2h} - v_w\left(\frac{d^2u}{dx^2} + \frac{d^2u}{dy^2}\right) + M_x = 0 \tag{5.2}$$

$$\frac{dv}{dt} + u\frac{dv}{dx} + v\frac{dv}{dy} + g\frac{d\eta}{dy} + \frac{gv\sqrt{u^2+v^2}}{C^2h} - v_w\left(\frac{d^2v}{dx^2} + \frac{d^2v}{dy^2}\right) + M_y = 0 \tag{5.3}$$

where C is the Chézy roughness [$\sqrt{m}$/s]; g is the gravitational acceleration (g = 9.81 m/s^2); v_w is the eddy viscosity [m^2/s] (Table 5.1) and $M_{x,y}$ is an extra momentum term linked to vegetation effects explained below. These three equations (5.1, 5.2, 5.3) combined describe the velocity variations in one grid cell over time under the influence of eddy diffusivity, friction and changing water depth. In the case of vegetation being present, an additional hydraulic resistance is included. This is incorporated through the Chézy friction coefficient and the additional resistance term: $M_x = -\frac{\lambda}{2}u^2$ and $M_y = -\frac{\lambda}{2}v^2$. The Chézy coefficient C and λ [1/m] are obtained from vegetation characteristics such as diameter, height and density of the vegetation objects (e.g. stems or roots) and the water depth (h) (Baptist et al., 2007):

$$\lambda = \begin{cases} C_D n \frac{h_v}{h}\frac{C_b^2}{C^2}, & \text{if } h \geq h_v \\ C_D n, & \text{if } h < h_v \end{cases} \tag{5.4}$$

$$C = \begin{cases} C_b + \frac{\sqrt{g}}{\kappa}\ln\left(\frac{h}{h_v}\right)\sqrt{1 + \frac{C_D n h_v C_b^2}{2g}}, & \text{if } h \geq h_v \\ C_b, & \text{if } h < h_v \end{cases} \tag{5.5}$$

where C_b, the Chézy coefficient for the bare bed without vegetation, is set to 65 [$\sqrt{m}$/s]; the Karman constant κ is constant with $\kappa = 0.41$ [-]; C_D is the drag coefficient; h_v is the vegetation height [m] and $n = Dm$, with m being the number of vegetation objects per m^2 and D being the respective stem diameter (Xie et al., 2020).

The sediment transport computed in Delft3D is induced by the flow, the sediment deflection due to the bed slope, bank erosion and the bed level update (Schuurman et al., 2018). The transport of the non-cohesive sediment and bed load is calculated in this

study using the equation by Van Rijn (1993). In the Van Rijn (1993) formula, it is distinguished between sediment transport below a reference height and above the reference height which are then handled as bedload transport and suspended load respectively (Deltares, 2021). This allows for the calculation of the non-cohesive sediment transport within the defined domain. In the calculation, bed slopes are considered as influence on the sediment transport. The influences of the bed slope on the magnitude and the direction of the bed-slope sediment transport are considered, resulting in an adjusted sediment transport vector ($\overrightarrow{S_r}$) (van der Wegen and Roelvink, 2012). The magnitude of the adjusted sediment transport is calculated according to the subsequent equations (eq. 5.6, 5.7, 5.8).

$$\overrightarrow{S'} = \alpha_S \overrightarrow{S} \tag{5.6}$$

with:

$$\alpha_S = 1 + \alpha_{bs} \left[\frac{tan(\phi)}{cos\left(tan^{-1}\left(\frac{dz_b}{ds}\right)\right)\left(tan(\phi) - \frac{dz_b}{ds}\right)} - 1 \right] \tag{5.7}$$

and

$$\left(\frac{dz_b}{ds}\right)_{max} = 0.9 tan^{-1}(\phi) \tag{5.8}$$

where $\overrightarrow{S}$ is the initial sediment transport vector [$m^3/m/s$]; $\overrightarrow{S'}$ is the magnitude adjusted sediment transport vector [$m^3/m/s$]; α_{bs} is the longitudinal bed gradient factor for bedload transport with a default value of 1 [-]; ϕ is the internal angle of friction [°] and $\frac{dz_b}{ds}$ is the bed slope in longitudinal direction [-] (van der Wegen and Roelvink, 2012). The direction of the bed-slope transport vector is adjusted calculating a further sediment transport vector which is perpendicular to the initial sediment transport vector (S_n) according to Ikeda (1982) (*Islope* = 2, compare Table 5.1) (eq. 5.9).

$$S_n = |\overrightarrow{S'}| \alpha_{bn} \frac{u_{cr}}{|\overrightarrow{u}|} \frac{dz_b}{dn} \tag{5.9}$$

where S_n is the transport vector perpendicular to the initial transport vector [$m^3/m/s$]; α_{bn} is the transverse bed gradient factor for the bedload transport, which is set to 1.5 [-]; u_{cr} is the critical, depth-average flow velocity [m/s], $\overrightarrow{u}$ is the depth average flow velocity vector [m/s] and $\frac{dz_b}{dn}$ is the bed slope with a direction normal to the initial sediment transport vector [-] ((van der Wegen and Roelvink, 2012)). This results in the adjusted (with respect to magnitude and direction) sediment transport vector ($\overrightarrow{S_r}$) (eq. 5.10) (van der Wegen and Roelvink, 2012).

$$\overrightarrow{S_r} = \overrightarrow{S'} + \overrightarrow{S_n} \tag{5.10}$$

The sediment transport of the mud fraction (cohesive sediment) is calculated using the Partheniades–Krone equations (Partheniades, 1965) with the erosion flux E_m (eq. 5.11) and the deposition flux D_m (eq. 5.12).

$$E_m = M_m \left(\frac{\tau_{cw}}{\tau_{cr,e}} - 1 \right) \tag{5.11}$$

for $\tau_{cw} > \tau_{cr,e}$.

$$D_m = \omega_s c_b \left(1 - \frac{\tau_{cw}}{\tau_{cr,d}}\right) \tag{5.12}$$

for $\tau_{cw} > \tau_{cr,d}$, with τ_{cw} being the maximum bed shear stress due to currents [Pa], $\tau_{cr,e}$ being the critical erosion shear stress and $\tau_{cr,d}$ being the critical deposition shear stress, M_m is an erosion parameter, ωs is the mud settling velocity [m/s] and c_b the depth average sediment concentration [kg/m^3] (Xie et al., 2020). Subsequently, the transport of suspended cohesive sediment is calculated on the basis of the advection-diffusion equation (eq. 5.13).

$$\frac{d(ch)}{dt} + \frac{d(uch)}{dx} + \frac{d(vch)}{dy} = Q_{mud,e} - Q_{mud,d}, \tag{5.13}$$

where c is the depth-averaged sediment concentration [kg/m^3].

Subsequently, the bed level update due to cohesive and non-cohesive sediment transport for every hydrodynamic time-step is based on the mass conservation (eq. 5.14).

$$(1-\varepsilon)\frac{dz_b}{dt} + \frac{1}{\rho_{s,S}}\left(\frac{dS_{sand,x}}{dx} + \frac{dS_{sand,y}}{dy}\right) = \frac{1}{\rho_{s,m}}\left(Q_{mud,d} - Q_{mud,e}\right) \tag{5.14}$$

where ε is the bed porosity with a default value of 0.4 [-], z_b is the bed level [m], $S_{x/y}$ is the sediment transport in x and y direction [m^3/m/s], and ρ_s is the density of the sediment (Table 5.1).

Furthermore, the bedlevel change which was calculated, is multiplied by a time varying or constant morphological scale factor (MorFac) for every hydrodynamic time step (Fig. 5.1). The MorFac is used to enhance the morphodynamic development and thereby also the morphodynamic computations (Van Der Wegen et al., 2011b, Duong et al., 2018). A constant MorFac of 180 is chosen in this study (Table 5.1), considering that Van Der Wegen and Roelvink (2008) concluded, that a morphological scale factor of up to 400 leads to acceptable results. Additionally, during a tidal cycle, the intertidal area is flooded and dries depending on the location due to water level change. Therefore, in order to avoid time-consuming hydrodynamic calculations, a threshold depth for flooding and drying is included in the computation. The threshold depth in this study is set as specified in Table 5.1. In dry cells, no sediment transport occurs since the velocity in those cells is zero. However, erosion can occur in the adjacent wet cell. Therefore, in order to create lateral bed lowering, the dry bank erosion was implemented. The dry bank erosion links the erosion of a dry cell to the erosion occurring in the adjacent wet cell using a user-defined factor (Table 5.1)(Braat et al., 2017). In order to illustrate the processes mentioned and considered in Delft3D as well as their interactions, Figure 5.1 shows a schematic model structure of Delft3D.

5.1.2 Boundary Conditions and Initial Bed

The initial domain and boundary conditions for Delft3D were created and set up to loosely resembles the Leichhardt estuary in Queensland, Australia (Fig. 5.2). Therefore, the most relevant boundary conditions from the Leichhardt estuary are considered. Those include the upstream river inflow, the tidal frequency and tidal amplitude, elevation characteristics (as estimated from Google Earth) and the overall dimensions of the estuary system (as estimated from Google Earth). Figure 5.2 shows the Leichhardt river estuary (the system on the right) on satellite imagery (Google, n.d.).

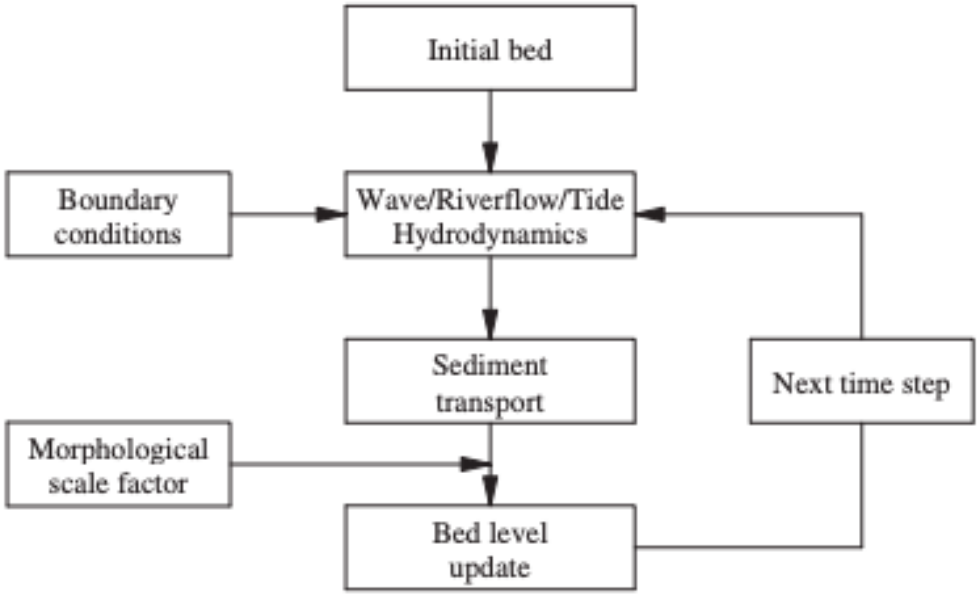

FIGURE 5.1: Delft3D Model Structure (from: Duong et al. (2018)).

FIGURE 5.2: Leichhardt River Top View.

The choice of this specific estuary was made based on several considerations. Firstly, the dieback event of 2015 and the recovery over the years are well monitored (Asbridge et al., 2016, Duke et al., 2017, Harris et al., 2017, Accad et al., 2019, Sippo, 2019, Duke et al., 2021). Furthermore, it was based on the severe impact that the dieback had on this estuary (Accad et al., 2019). Another factor considered is that the Leichhardt river is relatively natural with a low anthropogenic influence due to the remote location, which allows for the exclusion of anthropogenic factors when considering this estuary (Short, 2020). However, limitations arose during the creation of the domain due to the choice of estuary. The remote location and the low anthropogenic influence in this location meant, that little hydrological and morphological data is available for

this system. Therefore, some assumptions regarding the estuary bathymetry, the average river discharge, sediment supply by the river and tidal conditions had to be made. Subsequently, the different initial conditions, input parameter and boundary conditions chosen in this study will be outlined.

Grid The grid is rectilinear with a grid cell size of 50 x 50 m to 50 x 100 m (Fig. 5.3). The smaller grid size is used in the area of the river basin, while for the offshore part of the domain a coarser grid size of 50 x 100 m is implemented. This decision was made in order to reduce the computational time and simultaneously increase the resolution for the region of interest.

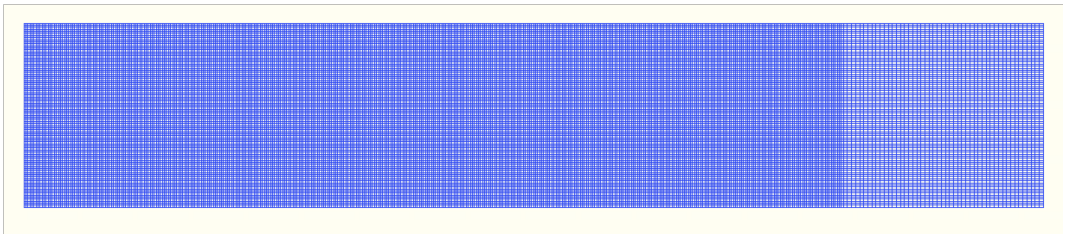

FIGURE 5.3: Delft3D Model Grid.

Initial Bathymetry It was decided to start with an idealised meandering estuary and let this domain develop over 400 years in an incipient phase (a detailed description of the model runs will be given in section 5.6), rather than starting of with a bathymetry which closely resembles the case study. This decision was made in order to determine and validate the input parameters. Due to the mentioned lack of data for the Leichhardt estuary, the initial formation was utilized as a validation of the chosen parameters. The aim was to elicit a similar morphological behaviour as seen in the Leichhardt estuary. But, as mentioned previously, this decision was also made to avoid that local complexities in the natural system and not in the model hinder the comparability.

The upstream width of the river is determined based on satellite imagery of the case study. The upstream boundary therefore has a width of 200 m (Fig. 5.2). According to previously determined characteristic meander dimensions, the upstream channel width correlates with the convergence length as following: $y = 81x^1$ (with $R^2 = 0.69$) (Leuven et al., 2018). Implementing this formula for the estuary results in an exponential increase of channel width for the last 16.2 km of the channel. The channel width at the seaward boundary is 1.5 km. Furthermore, Leuven et al. (2018) found a correlation between the local channel width and the meander length ($25x^{0.88}$) as well as the meandering amplitude ($2.5x^{1.1}$). These correlations are applied here to determine an initial idealized meandering of the estuary. The bed level has a linearly increasing elevation from -1m at the mouth to 1m at the upstream boundary and on dry land from 2m to 3m. The sea has a maximum depth of 50m. Figures 5.4 and 5.5 show the initial bathymetry and depth profile.

Boundary Conditions The domain has four boundaries, three at the seawards side and one upstream river boundary. For the eastward sea boundary, a harmonic water level is used with a tidal frequency of 30 degrees per hour (semi-diurnal) and a tidal amplitude of 1.5 m (Table 5.1). The northwards and southwards sea boundaries are defined as harmonic with the Neumann formulation. No wind-waves are included as the focus in this study lies on the impacts of tides and for reasons of computational cost. The river boundary is defined with a total discharge [m^3/s], which is set to a

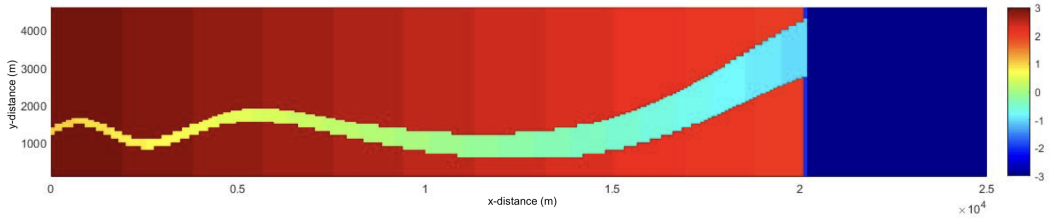

FIGURE 5.4: Initial bathymetry as input to the Delft3D model.

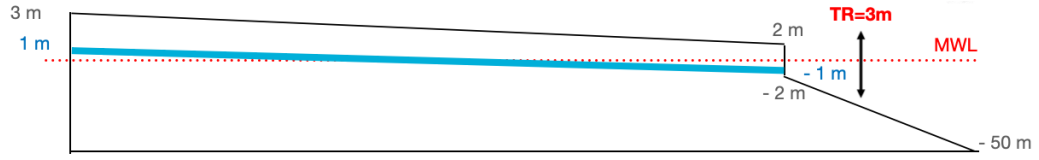

FIGURE 5.5: Depth profile of the initial domain.

constant value through time of 300 m^3/s (Table 5.1). Despite the strong seasonal variations of river discharge in the case study (i.e. wet and dry seasons), it was decided to include a constant river discharge based on the study carried out by Guo et al. (2015). Guo et al. (2015) concluded that the assumption of a constant river discharge is reasonable if the river discharge is small compared to the tidal discharge. It is assumed that this is the case for this study throughout most of the year. Regarding the sediment supply, the sand supply is determined by equilibrium conditions[1]. While the mud supply (SSC) is set to 10 mg/L (for the scenarios where mud is considered) at the river boundary. This decision was made based on the global satelite sediment concentration[2] within the estuary, due to lack of field data. The initial bed composition in the entire domain consists of sand. Mud is then supplied from the river boundary (in form of SSC) after the incipient phase. Thereby, the mass of mud transport depends on the hydrodynamic conditions. The parameters mentioned in section 5.1 as well as further parameters used in Delft3D are summarized in Table 5.1. These include the Delft3D input parameters describes in section 5.1.1, the initial bed settings as well as the boundary conditions.

[1]Meaning that the capacity of the flow to transport sand (eq. 4) at the boundary determines the sand supply rate. This therefore prevents erosion and deposition at the boundaries (Braat et al., 2017)

[2]GlobColour data (http://globcolour.info) used in this study has been developed, validated, and distributed by ACRI-ST, France

TABLE 5.1: Delft3D Input Parameter

Parameter	Value	Reference
Numerical Parameter		
Grid cell size	50x50 m, 50x100 m	Fig. 5.3
Time step	0.2 - 1 min	
Boundary conditions		
Tidal amplitude	1.5 m (mesotidal)	Asbridge et al. (2016)
Principle tidal period	12 h (semidiurnal)	model design
Tidal Frequency	30 deg/hour	model design
River discharge	300 m^3/s (strong seasonal variation	
Mud input at river (SCC)	10 mg/L	Global satellite sediment concentration (ACRI-ST)
Viscosity		
Horizontal eddy viscosity	1 m^2/s	Leonardi et al. (2013)
Horizontal eddy diffusivity	10 m^2/s	
Sand Properties		
Median sand diameter	250 μm	Brückner et al. (2021)
Dry bed density	1600 kg/m^3	Brückner et al. (2021)
Mud Properties		
Settling velocity	0.25 mm/s	Brückner et al. (2021)
Critical bed shear stress for deposition	1000 N/m^2	Braat et al. (2017)
Critical bed shear stress for erosion	0.25 N/m^2	Xie et al. (2020)
Dry bed density	500 kg/m^3	Brückner et al. (2021)
Morphology settings		
Active layer thickness	5 cm	Brückner et al. (2021)
Max. Storage layer thickness	5 cm	Brückner et al. (2021)
Morphological Scale Factor (MorFac)	180 [-]	
Factor for erosion of adjacent dry cells (ThetSD)	0.5 [-]	
Max depth for variable THETSD (HMaxTH)	0 m	
Islope	2 (Ikeda)	model design
Ashld	100	Baar et al. (2019)

5.1.3 Model Design

In this study, hydrodynamic and morphological parameters are determined so that the created domain shows similar characteristics compared to the Leichhardt estuary. Therefore, different test were performed to obtain properties sufficiently similar to the natural system. There are different parameters in Delft3D which can be changed for the model design. These include: choosing a roughness predictor, adding coarser grain sizes or a layer which is non-erodible in the channel to limit channel depth, including overtides at the seaward boundary, performing 3D instead of 2D calculations, increasing the river discharge and by modifying the transverse bed slope parameter

(van der Wegen and Roelvink, 2012, Baar et al., 2019). On the other hand, it was found that a change in mud characteristics (e.g. settling velocity or erosion parameter), modifying grain sizes, introducing different salt and fresh water densities and changes in the morphological scale factor will not greatly affect the general trends in the morphological development of the estuary (Van Der Wegen and Roelvink, 2008, van der Wegen and Roelvink, 2012, Baar et al., 2019). Based on these considerations the model design was conducted by modifying the initial bed elevations and channel outline, the bed slope parameter and by changing river discharge and tidal frequency. The formed estuary (after the initial phase of 400 years) was compared to the natural system. Specifically, the structure and patterns such as meandering and delta characteristics was compared. An important criteria for the choice of the bed slope parametrization was the bar formation [3], as it was needed for the later establishment of mangroves.

Firstly the initial bathymetry of the domain was varied in order to achieve meandering patterns which resemble the pattern seen in the case study. Using a straight channel the desired results were not achieved (Fig. A.1, A.3, A.2). Therefore, the channel was modified to an ideal meandering channel based on previous studies (compare section 5.1.2). Secondly, the transverse bed slope effect was varied. The transverse bed slope is commonly used for the calibration of morphological models. It is an important parameter which influences the bar dimensions and behaviour (Schuurman et al., 2018). Baar et al. (2019) found that for estuaries and rivers, a very high slope effect must be implemented to create a realistic morphology as the channel depth and braiding index are often over-predicted within Delft3D. The bed slope effect was one of the main parameter used for the model design. After several test runs with different Islope and Ashld parameters, it was decided on the bed slope formulation of Bagnold (1966) for longitudinal slope and Ikeda (1982, 1988) for transverse slope (Deltares, 2021) with an Ashld parameter of 100 (Table 5.1). This decision was made based on the recommendation by Baar et al. (2019) to use the Ikeda formulation for rivers with a relatively high Ashld parameter. With the specified parameters, the delta of the formed estuary showed a suitable reflection of the case study as a formation of channels and bars occurred which resemble the patterns observed in the case study. Especially, well formed meanders are established in the more downstream part of the estuary.

After adding the mangroves (compare section 5.5), some differences between the case study and the model behaviour were noted. Therefore, adoptions in river discharge and tidal frequency were made. The river discharge was increased to 300 m^3/s (initially 50 m^3/s), which was found to reflect the processes of the case study more accurately and the tidal frequency was increased to 30 deg/hour (semi-diurnal) instead of 15 deg/hour (diurnal). The later decision was made because it was seen in the model domain that the diurnal tidal flow reached the upstream boundary which can cause problems within the model since no outflow of sediment or water at the boundaries is allowed. Therefore, a semi-diurnal tidal cycle was implemented as the flow would not reach the upstream boundary then. Furthermore, the results have shown a higher resemblance of the estuary morphology to the natural system for the semi-diurnal tidal cycle simulation (Fig. 5.6).

Despite the design efforts, some limitations remain in this modelling approach. The hydrodynamic model is limited by the low data availability, such as local bathymetry and sediment compositions, which in this research the spin-up period is included to

[3] Bars are defined by Leuven et al. (2016) as: "discrete recognisable elements on what is essentially a continuous field of bed elevation that changes over time."

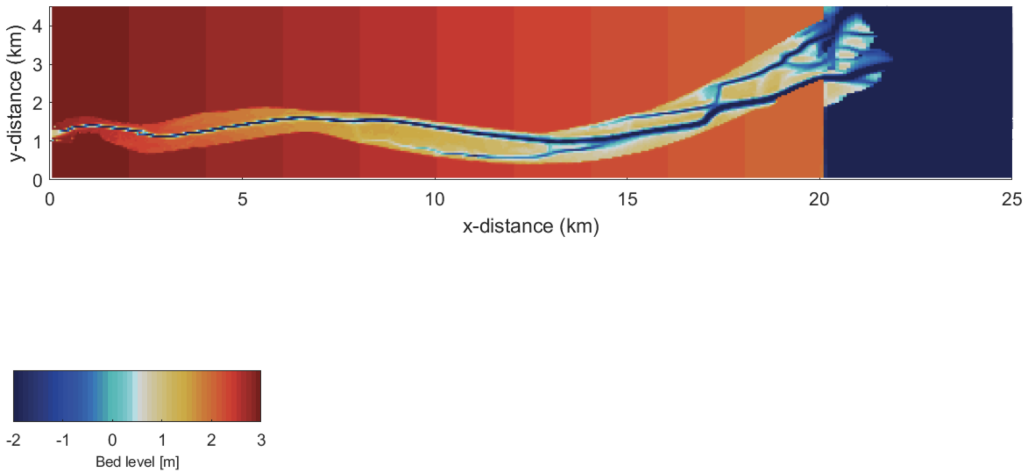

FIGURE 5.6: Bathymetry of the model estuary after 400 years of spin-up period.

attain an initial modelling environment. Some assumptions had to be made due to the lack of field data on hydrodynamics and morphology of the case study (e.g. SSC, river discharge, channel and dry bed depths and elevations). Furthermore, it should be noted, that in this study, the effects of wind, waves, storm events, salinity, 3D velocity patterns, temperature and Coriolis forces are neglected. As it is the aim to qualitatively capture the mangrove responses under the changes in external signals of sea level and river discharge.

5.2 Vegetation Model

The vegetation model includes the processes of mangrove (including their roots) colonization, growth, and mortality. These processes are based on competition and inundation stress (hydroperiod as determined by Delft3D), which is closely related to the bed elevation. The model is literature-based to study the response of the local mangrove species *A. marina*. In the following subsections, the governing equations of the vegetation model and the parameters characterizing the mangroves are described.

5.2.1 Governing Equations

Tree Growth The optimal growth of the mangrove trees is described by equation 5.15 (Chen and Twilley, 1998, Berger and Hildenbrandt, 2000, Van Maanen et al., 2015, Xie et al., 2020, Xie et al., 2022).

$$\frac{dD}{dt} = \frac{GD\left(1-\left(DH\right)/\left(D_{max}H_{max}\right)\right)}{\left(274+3b_2D-4b_3D^2\right)} \tag{5.15}$$

where D is the stem diameter [cm], D_{max} is the maximum stem diameter [cm] (Table 5.2) and H is the tree height [cm]. The physical settings of these vegetation parameters are based on local observations (Comley and McGuinness, 2005, Asbridge et al., 2016). G, b2 and b3 are species-specific growth parameters (Table 5.2). The growth parameters were determined, such that the maximum increase in stem diameter is $1cm/yr$ (Fig. 5.7b). The relation between the tree height and stem diameter is given in equation 5.16. It is assumed that when the stem diameter is 0 cm, the tree has a height of

137 cm (Fig. 5.7a).

$$H = 137 + b_2 D - b_3 D^2 \tag{5.16}$$

This assumption is made based on the fact that the diameter is usually measured at breast height (dbh) and breast height is set to be 137 cm above ground (Van Maanen et al., 2015).

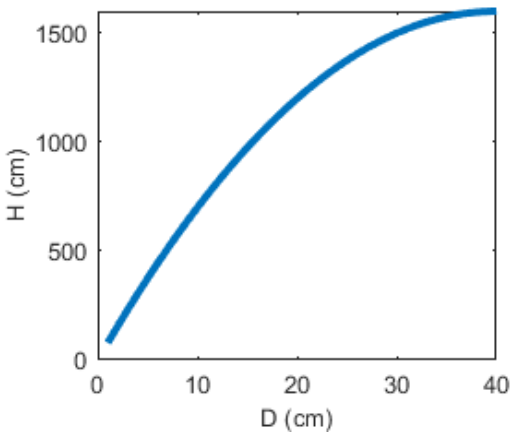

(A) Tree height over stem diameter.

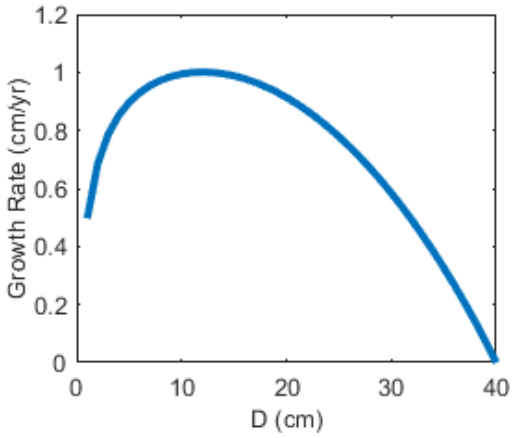

(B) Mangrove growth rate over stem diameter.

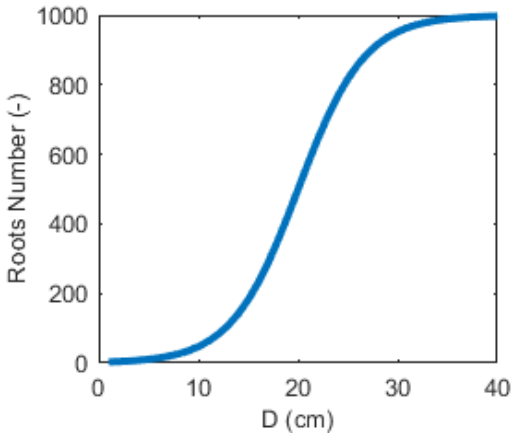

(C) Root number over stem diameter.

FIGURE 5.7: Growth Parameter for Mangrove Model over Stem Diameter.

Equation 5.15 reflects the growth of mangroves under optimal conditions. However, in reality the growth is limited by different stresses. In this model, the stresses of inundation (I) and competition (C) are considered (Fig. 5.8) (Xie et al., 2020, Xie et al., 2022), ranging from 0 to 1, from no growth to unlimited growth. Therefore, the resulting growth function includes the stress multipliers I and C (eq. 5.17) (Chen and Twilley, 1998, Berger and Hildenbrandt, 2000).

$$\frac{dD}{dt} = \frac{GD\left(1 - (DH) \,/\, (D_{max} H_{max})\right)}{(274 + 3b_2 D - 4b_3 D^2)} \times I \times C \tag{5.17}$$

with I and C being the inundation and competition stress respectively. The stress factors are described in equation 5.18 and equation 5.19.

$$I = a \times P + b \times P^2 + c, \tag{5.18}$$

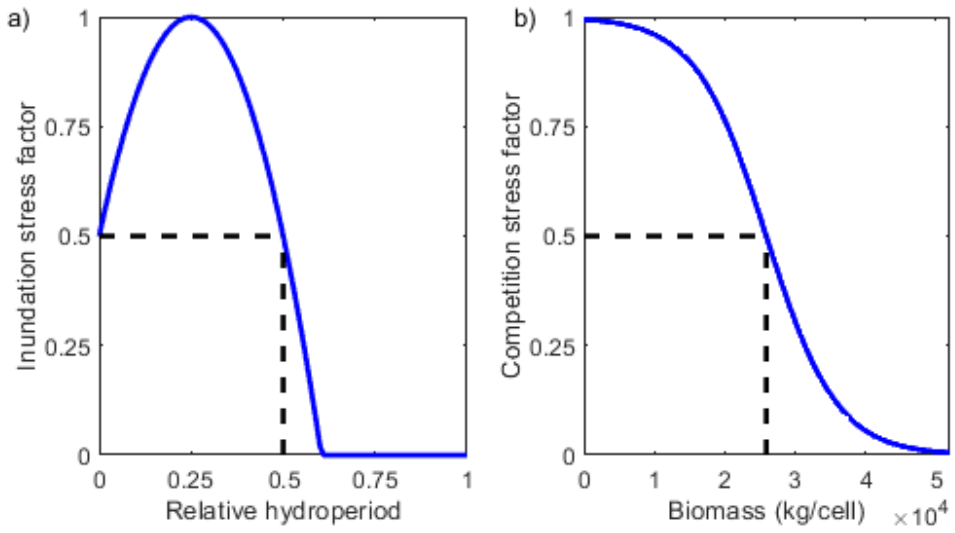

FIGURE 5.8: Mangrove Stress Factors with a) inundation stress over relative hydroperiod and b) competition stress over mangrove biomass (from Xie et al., 2020).

where P is the relative hydroperiod (supplied by Delft3D); a, b and c are the inundation stress factor constants (Table 5.2). The factors were chosen, that I=0.5 when the mangroves are inundated half the time (P=0.5) and when they are not inundated at all (P=0) (Fig. 5.8). The competition stress (C) is related to the total biomass B by a sigmoid function (eq. 5.19).

$$C = \frac{1}{1 + exp\left[d\left(B_{0.5} - B\right)\right]} \tag{5.19}$$

where d is a constant, set to -0.0002 (Table 5.2) and $B_{0.5}$ is the value for B when $C = 0.5$. In order to calculate the value for $B_{0.5}$, the total number of mangrove trees per grid cell as well as the weight of each single tree (W_{tree}), which is the sum of the above- ($W_{tree,a}$) and below-ground ($W_{tree,b}$) tree weight, is used (eq. 5.20).

$$W_{tree} = W_{tree,a} + W_{tree,b} \tag{5.20}$$

In order to calculate the above-ground and below-ground tree weight for *A. marina*, equations 5.21 and 5.22 are used (Van Maanen et al., 2015).

$$W_{tree,a} = 0.308 D^{2.11} \tag{5.21}$$

$$W_{tree,b} = 1.28 D^{1.17} \tag{5.22}$$

where D reflects the stem diameter [cm]. In order to estimate the number of trees that can be present in one grid cell, the 'zone of influence' (ZOI) concept (Berger and Hildenbrandt, 2000) was applied. The radius of this zone is described by equation 5.23.

$$R = 10\sqrt{0.5\frac{D}{100}} \tag{5.23}$$

where D is equal to $D_{max} = 40$ cm. Using the equations 5.20, 5.21 and 5.22, $B_{0.5}$ was calculated to be 25,894 kg per grid cell (2500 m^2).

Tree Mortality After a continuous period of growth depression, trees die (Van Maanen et al., 2015). Every year, the mangrove growth is evaluated. When the growth is less than 50 percent of the optimal growth rate for five consecutive years, the mangrove tree dies. In practice this means that when the product of I and C (eq. 5.14) is below 0.5 for five consecutive years, the mangrove tree dies and thereby the mangrove density in that grid cell decreases. When competition is the limiting stress factor, the resulting mangrove death leads to an increase in C and more favourable conditions for the growth of the remaining mangroves result. However, when mangrove die due to the prolonged or absence of inundation, mangroves within the area will be completely removed as the product of I and C will be below 0.5 for all trees. Furthermore, in case of inundation stress, the trees cannot reach the maximum density of trees possible for the grid cell. Such mortality process will be terminated when the product of I and C reach 0.5 again or there are no mangroves left within the cell.

Tree Colonization New mangrove trees can enter the domain either due to mortality of trees in a grid cell which reduces the density and therefore the competition stress in that grid cell reduces, or they can establish in a initially bare cell (Xie et al., 2020, Xie et al., 2022). Mangrove can colonize when a suitable hydroperiod (0 - 0.5) and simultaneously low bed shear stress (below 0.2 N/m^2) are prevalent. The number of mangrove seedlings establish in the grid cell depends on the number of existing mangrove trees. When mangroves trees are already present there, the inclusion of new mangrove seedlings cannot exceed the initial density and cannot lead to the product of I and C lower than 0.5. When there are no mangroves in the cell, an initial vegetation density will be assigned (3000 individuals per ha, Van Maanen et al. (2015)). When new mangroves enter the grid cell, they enter as young trees with a stem diameter of 1 cm (Van Maanen et al., 2015).

Roots Besides the mangrove stems, also the aerial roots of mangroves provide hydraulic resistance (Asbridge et al., 2016). Different mangrove species have different root system. However, due to the limitations in the model, the roots are added as cylindrical objects with a fixed diameter (1 cm) and height (15 cm) (Table 5.2). The number of roots of each tree is related to the tree diameter following equation 5.24 (Xie et al., 2020, Xie et al., 2022). The graph of the function is displayed in Figure 5.7c.

$$N_{roots} = m \frac{1}{1 + exp\left[f\left(\frac{D_{max,i}}{2} - D\right)\right]} \tag{5.24}$$

where m is the maximum number of roots per tree (1000 roots per tree) and f is a constant describing the rate of increase (Table 5.2). The parameters used within the equations as well as the characteristic parameters of the mangrove species *A. marina* are summarized in Table 5.2.

TABLE 5.2: Mangrove Input Parameter

Parameter	Value	Unit	Reference
Vegetation Parameters			
Initial stem diameter	1	cm	
Maximum root number	1000	-	
Root diameter	1	cm	Van Maanen et al. (2015), Xie et al. (2020)
Root height	15	cm	Van Maanen et al. (2015), Xie et al. (2020)
Roots function coefficient, f	0.3	-	
Drag coefficient of vegetation, CD	1	-	Xie et al. (2020)
Growth Parameter			
Maximum stem diameter	40	cm	Comley and McGuinness (2005)
Maximum tree height	1600	cm	Asbridge et al. (2016)
Growth constant, G	254	cm/yr	max. growth rate: 1 cm/yr
Growth constant, b_2	$2D_{max}b_3 = 80$	-	
Growth constant, b_3	1	-	
Inundation stress factor constant, a	-8	-	
Inundation stress factor constant, b	4	-	
Inundation stress factor constant, c	0.5	-	
Competition stress function $B_{0.5}$	2.589410^4	kg	Van Maanen et al. (2015), Xie et al. (2020), Xie et al. (2022)
Competition stress factor coefficient, d	-0.0002	-	Van Maanen et al. (2015), Xie et al. (2020), Xie et al. (2022)
Biomass above-ground index, inda	2.11	-	
Biomass above-ground constant, bioa	0.308	-	
Biomass below-ground index, indb	1.17	-	
Biomass below-ground constant, biob	1.28	-	

5.3 Coupling between Delft3D and Vegetation Model

The coupling of the hydro-morphodynamic model (Section 5.1) with the vegetation model (Section 5.2), allows for the modelling of the feedback between the tidal flow and river discharge, sediment motion, morphological change and mangrove vegetation (Xie et al., 2020, Xie et al., 2022).

Within the modelling approach chosen in this study, the mangroves influence the sediment transport in two ways. Firstly, there is a direct influence due to an increase in the erosion threshold. Secondly, there is an indirect effect due to a reduction in strength of the flow (tidal flow and river discharge). Mangrove trees add to the friction and roughness of the morphology and are thereby influencing the hydrodynamic processes. Specifically, mangroves increase the drag coefficient (C_D) due to their hydraulic resistance to the flow which influences the flow velocity and thereby also the sediment transport. At the same time, information on the inundation regime calculated in Delft3D are returned to the vegetation model. The inundation regime then influences the colonization, growth and mortality of mangrove trees through the inundation stress factor (Van Maanen et al., 2015, Xie et al., 2020, Xie et al., 2022). When the relative hydroperiod is suitable and the bed shear stress is not too large, mangroves are able to settle within the grid cell. In subsequent years, mangroves can grow based on the described growth function and under consideration of the growth reducing factors (I, C). These interactions within the model are summarized in a conceptual model in Figure 5.9.

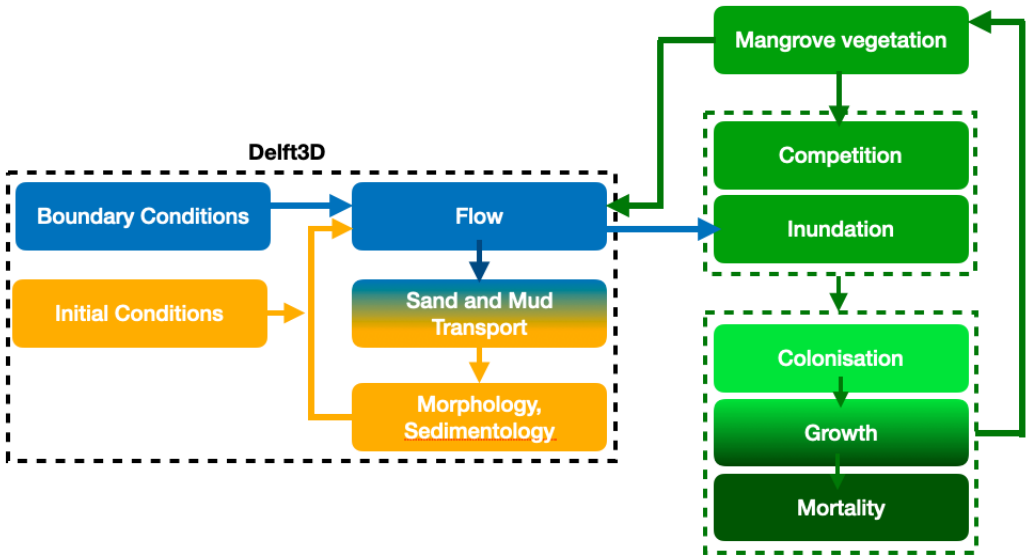

FIGURE 5.9: Coupling of vegetation and hydromorphodynamics in the model.

5.4 Model Scenarios

This section describes the planning of the individual model runs. The modelling consists of five phases, including the preliminary phase 0 for model design. The different phases are summarized in Figure 5.11.

Phase 0: Model Design During this model design phase, a suitable initial domain was created which reflects the main characteristics of the case study. The parameter choices made are described in detail in Section 5.1.3. In total 15 test runs were carried out with varying initial channel outline (straight, sinus and meandering), ISlope and Aschld as well as river discharge and tidal frequency (diurnal and semidiurnal).

Phase 1: Initialisation Phase 1 consists of the initial formation of the estuary (Fig. 5.11). The hydro-morphodynamic model was run over 400 years with the parametrization described in sections 5.1.1 and 5.1.2. Due to the assumption that sandy channels govern the development of the main morphological characteristics (van der Wegen and Roelvink, 2012), at this stage, only sand was included in the domain. This phase does not include mangrove vegetation nor mud inflow.

Phase 2: Vegetation Development In phase 2, vegetation was added to the model. Therefore, the coupling between the hydro-morphodynamic and the dynamic vegetation model was activated and mangroves were allowed to establish within the domain for a period of 200 years (Fig. 5.11). Here, different scenarios were considered, one scenario with solely non-cohesive sediment (sand) and mangrove vegetation and second scenario scenario with mud (cohesive sediment) inflow and mangrove vegetation (compare Table 5.1). These scenarios were selected in order to study the difference in vegetation establishment with and without the presence of cohesive sediment.

Phase 3: Disturbance In phase 3, the 'mud and mangroves scenario' from the previous phase was used as the starting domain to simulate the dieback event (compare Section 3.4). Two different methods were selected in order to describe the dieback (Fig. 5.11).

Firstly, the dieback was simulated by modifying the boundary conditions according to the condition which occurred during the 2015/2016 dieback event in the Gulf (Duke et al., 2021). Three different simulations were chosen for this method. The sea level was dropped by 20 cm, the river discharge was decreased to 10 m^3/s (Duke et al., 2021) and both sea level drop (SLD) and river discharge decrease (RDD) were considered to occur simultaneously. The SLD was implemented by adding a further tidal component in the bch file. Thereby, a smaller tidal frequency was used to create a near constant tidal amplitude. The combination of this additional tidal amplitude with the initial one leads to a drop in the tidal level. This is illustrated in Figure 5.10, with the black graph representing the initial tidal signal and the red graph representing the resulting tidal signal including the 20 cm sea level drop. The decrease in river discharge was included by reducing the discharge at the river boundary from 300 m^3/s (Table 5.1) to 10 m^3/s. Even though the dieback event in the natural system occurred within a period of a couple of months (Duke et al., 2021), the simulations were run for 10 years. This decision was based on the model set-up. As described in Section 5.2., a mortality state is assigned to every mangrove and only if the mangroves are in unfavourable conditions for five consecutive years, mortality occurs. Therefore, a period of 10 years was chosen to sufficiently model the dieback. However, in order to reflect the natural system dieback despite this limitation, the morphological change within the domain was turned off. This results in a domain after 10 years, having the same morphological features as before.

Secondly, a manual removal of mangroves was conducted after it was concluded that there are some differences between the model dieback simulations and the patterns

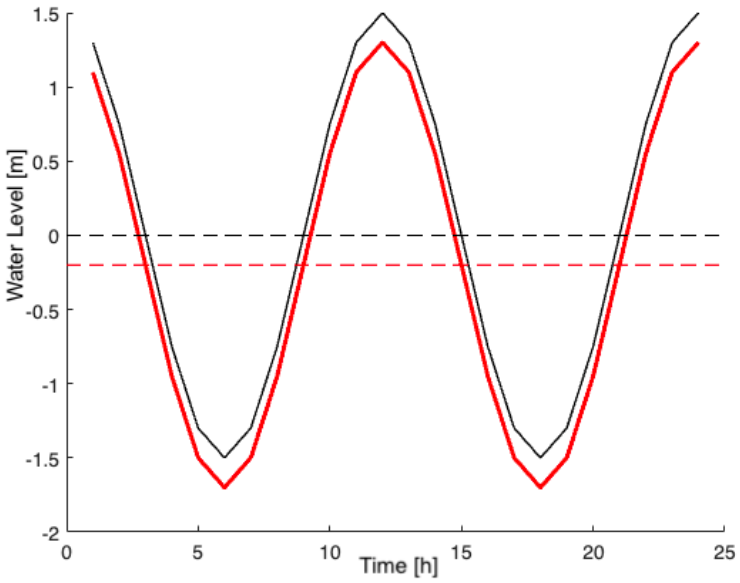

FIGURE 5.10: Implementation of the sea level drop with an additional tidal component.

observed in the natural system. Therefore, mangroves in specific areas were removed manually from the vegetation files. Three different scenarios were considered, the removal from all mangrove vegetation from 16 km, 18 km and 20 km seawards. Additionally, an undisturbed reference run was conducted for both methods, where where the initial boundary conditions were maintained and no vegetation was removed.

Phase 4: Recovery Three of the simulations: SLD and RDD (10 m^3/s), and manual removal 16 km seawards (Fig. 5.11) and the undisturbed reference scenario were then utilized as the starting point for phase 4. In phase 4, two different states were simulated: the recovery and the disturbed state (Fig. 5.11), over a period of 100 years. The recovery included the restoration of the initial boundary conditions (no SLD and river discharge of 300 m^3/s) while the morphological change as well as the vegetation change were allowed. For the simulation of the disturbed state, the boundary conditions were reset to the initial conditions and the morphological change was allowed. However, the mangrove vegetation development was not allowed, meaning that the mangroves were not able to colonize, grow or die within this simulation of 100 years. With the simulations in phase 4, it was intended to predict how the mangrove vegetation will recovery after the dieback (recovery) and which long-term influences the decrease in vegetation has on the morphology and hydrodynamics in the estuary (disturbed state).

Analysis of Results The results of the model scenarios were then analysed on the basis of bathymetry changes, changes in flow velocities, hydroperiod and mud deposition. The hydroperiod is a rate of time representing the frequency of inundation. Since mangroves mainly colonize between mean water level and mean high water level, a hydroperiod between 0 and 0.6 is assigned for the growth of mangrove trees. A hydroperiod higher than 0.6 leads to an inundation stress factor (I) of 0 (Fig. 5.8). The mud thickness is taken as the thickness of mud in either the upper layer or of the entire depth. In order to quantify the changes in bed level, the 5th and 95th percentile of bedlevel are compared over time. Thereby, the percentiles of the bedlevel within the

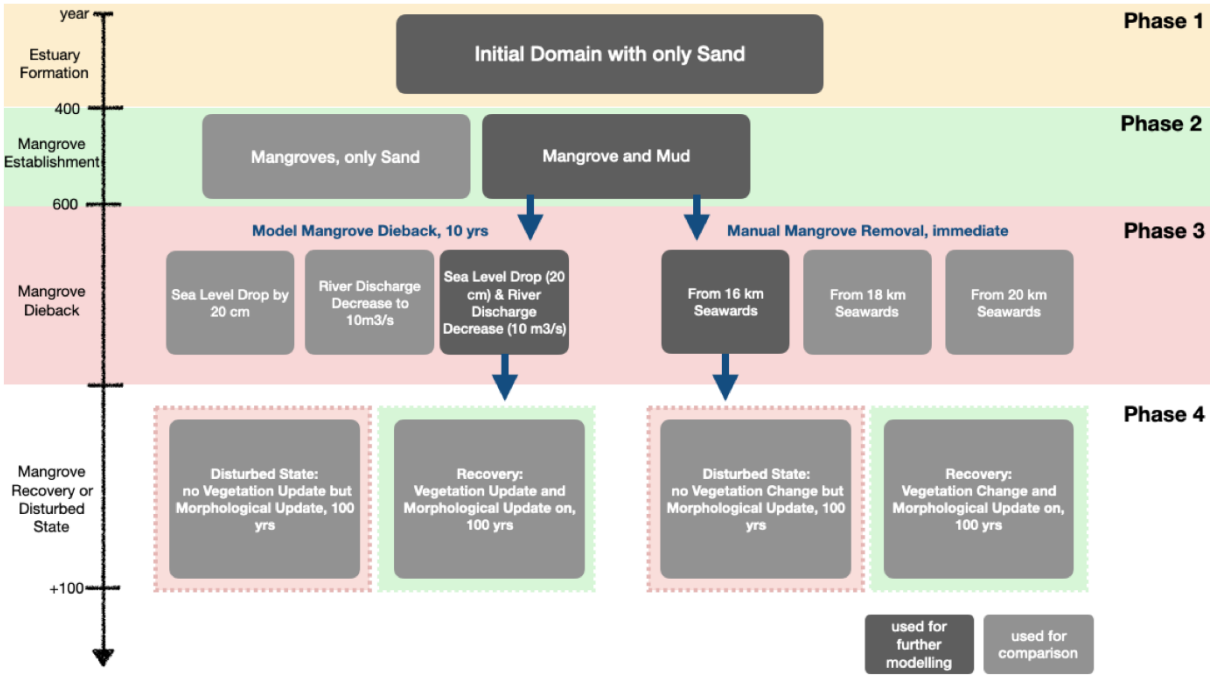

FIGURE 5.11: Overview of the conducted modelling phases (phase 1 - 4).

basin area is determined. For the same percentiles then the flood/ebb velocity ratio is determined. Therefore, the flood/ebb ratios over the whole basin are determined and then an average is taken from the ratios in those cells which represent the 5th or 95th bedlevel percentile (+/- 0.05 m). Furthermore, the vegetation was analysed based on the stem diameter and vegetation cover (basal area, eq. 5.25), geometry density (eq. 5.26), numeric density (eq. 5.27) and the hydraulic resistance of the vegetation, in the form of λ (eq. 5.3).

$$A_{Basal} = \sum_{i=1}^{n} A_{stem,i} \times N_i \tag{5.25}$$

where the area of a single stem is described as: $A_{stem,i} = (d_{stem,i}/2)^2 * \pi$

$$Density_i = (N_i \times d_{stem,i}) \, / \, A_{gridcell,i} \tag{5.26}$$

This geometric density is used in Delft3D for the Baptist equation and reflects the friction exerted by the mangrove stems based on their diameter.

$$Density_{tree,i} = N_i / A_{gridcell,i} \tag{5.27}$$

where $d_{stem,i}$ is the stem diameter in cell i [cm], and N_i is the number of mangroves in cell i [-]. This numeric density reflects the amount of trees being present in one grid cell, regardless their maturity.

Additionally, to quantify the recovery of the mangroves regarding their stem diameters, the recovery rate is determined. In literature, different approaches can be found regarding the best ways to quantify an ecosystem recovery. In this study, it was decided to follow the approach proposed by Jones et al. (2018). The recovery rate is thus

defined as:

$$Recovery = 100 \times (End - Start) \,/\, (Goal - Start) \,/ Time \tag{5.28}$$

with Start representing the average stem diameter at the start of the recovery, End representing the average stem diameter at the end of the recovery, goal being the average stem diameter of the undisturbed reference at the end of the recovery and Time representing the years of recovery (100 years). Further quantification provides the ratio of the actual growth rate to the optimal growth (eq. 5.29)

$$Growth\ Ratio = \frac{Actual\ Growth}{Optimal\ Growth} \tag{5.29}$$

The actual growth rate is here defined as the change of the average stem diameter over time. The optimal growth is calculated based on equation 5.15, using the average stem diameter. These parameters allowed for a conclusive analysis of the results from the different phases of the model simulations. The results will be presented in the subsequent chapter.

Chapter 6

Results

The results are presented according to the scheme illustrated in Figure 5.11. The colonization of mangroves in the 200 years of growth is firstly described, thereby the effect of mud on the growth of mangroves within the domain is analysed. Secondly, the results of the mangrove dieback using the two different methods is presented. Thirdly, the effects of the mangrove dieback on the morphology and the hydrodynamics of the estuary are outlined within the disturbed state. And finally, the result of the 100-year recovery of the different scenarios are presented. An overview of the different bathymetries and mangrove cover (if applicable) resulting from the model runs is presented in Figure 6.1. In the following sections, it will be zoomed in to each of those phases and detailed results regarding the hydrodynamic, morphological and vegetation change are presented.

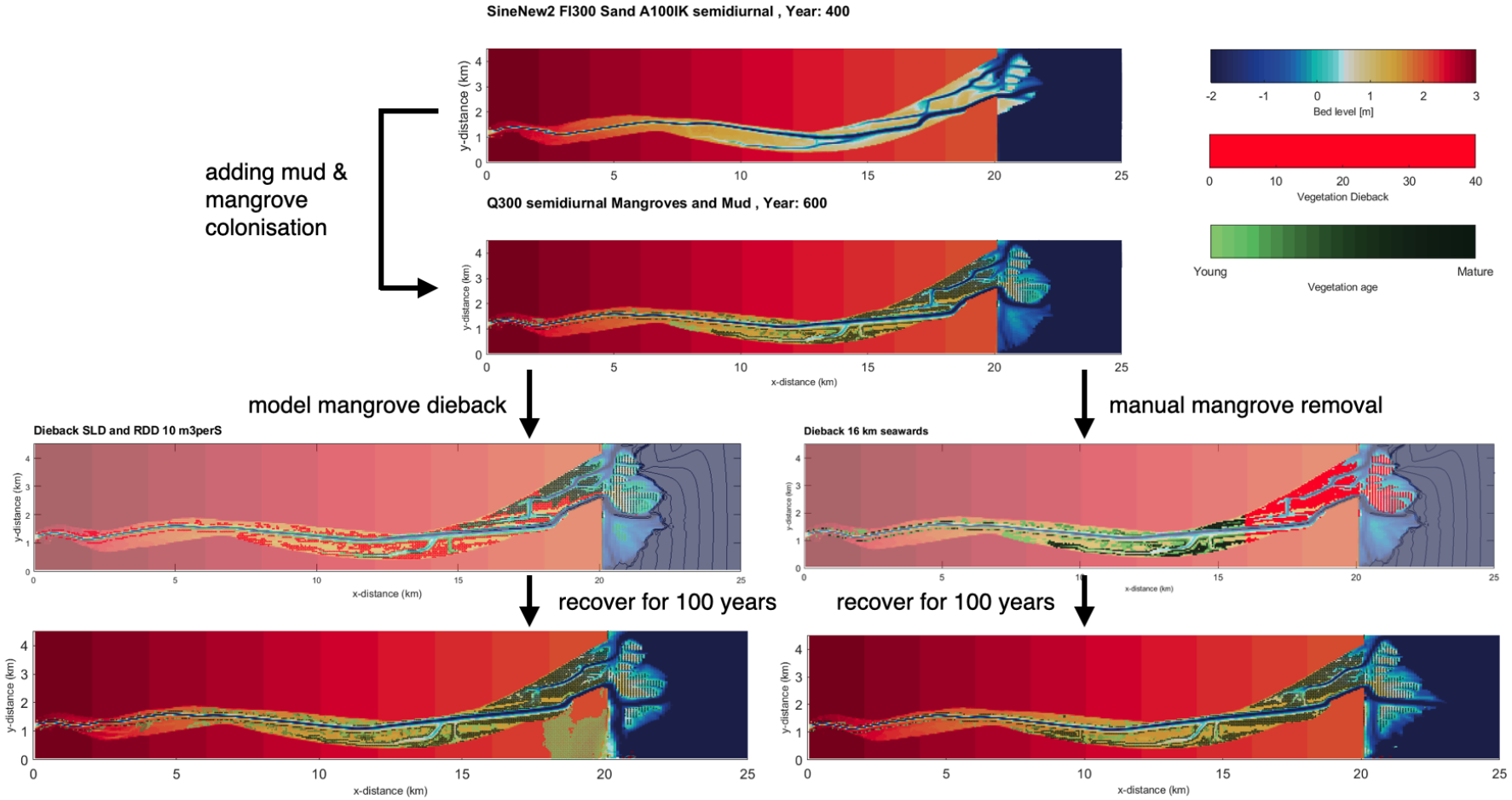

FIGURE 6.1: Overview of the bathymetry and vegetation distribution for the four different phases of model runs.[1]

[1]The bathymetry of the model dieback runs is illustrated using a higher transparency solely to make the dieback visible. However the depth according to the colorbar is still applicable.

6.1 Impacts of Mud Supply on Mangrove Distribution

After a 400-year spin-up period, simulations were first conducted for 200 years with fluvial mud supply and vegetation dynamics. For the 200 years of mangrove colonization, the effect of mud on the mangrove colonization was investigated by comparing the mangrove growth within the 'no-mud scenario' to the 'mud scenario'. An overview of the bathymetry and mangrove cover is given in Fig. 6.2.

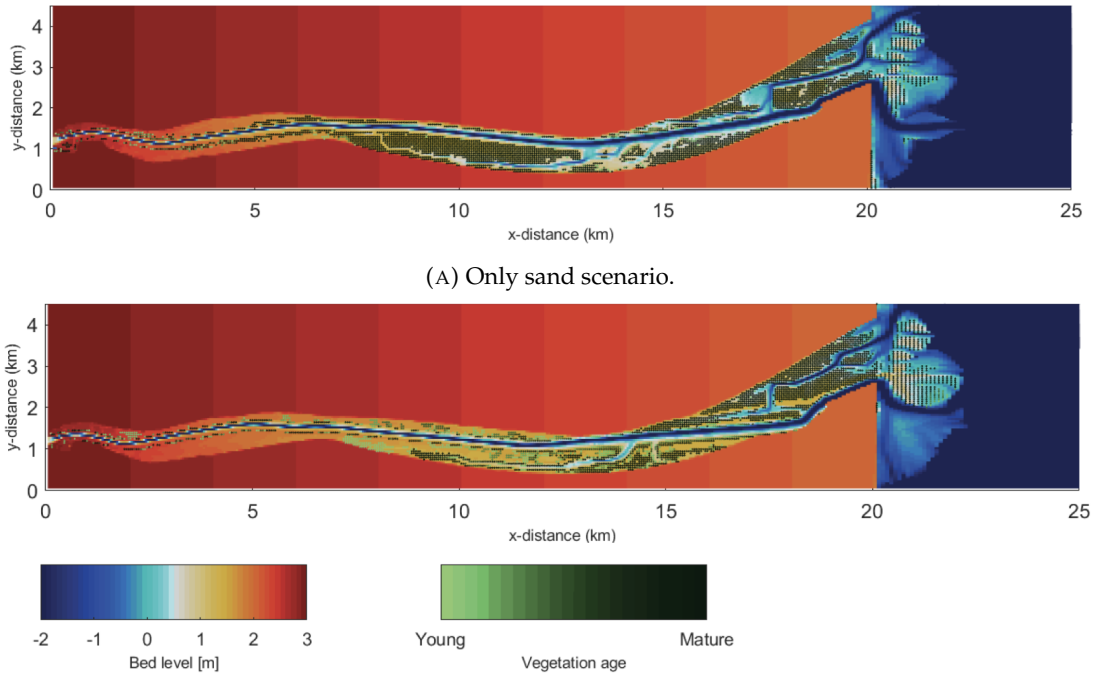

(A) Only sand scenario.

(B) Mud supply scenario.

FIGURE 6.2: Bathymetry and mangrove cover map after the 200 years of mangrove colonization for (A) the only sand scenario and (B) the scenario including fluvial mud supply.

In Fig. 6.2 and Fig. 6.3a, an overall lower mangrove coverage for the scenario including mud can be seen. Initially, both scenarios show a similar pattern of mangrove basal area. However, after 20 years of growth, the mangrove area as well as the geometric density increase further for the scenario without mud, while including fluvial mud supply leads to a smaller vegetation area and geometric density. The basal area however reaches the one of the no mud scenario for some time from year 540 until year 570. Then it decreases again. The geometric density of the mud scenario over the years is constantly below the one of the 'no-mud scenario'. The numeric density (Fig. 6.3c) however is higher for the scenario including mud from year 420 onward. For both scenarios the numeric density is decreasing from 410 years onward after an initial peak, indicating the maturation of tree over the years and therefore the thinning out due to competition stress within the cells. However, the numeric density for the mud supply scenario constantly lies above the one for the only sand scenario. This indicates that on average more trees colonize one grid cell in the 'mud-scenario', leading to the conclusion that more smaller trees are present in this scenario and maturation is limited compared to the scenario without mud. This leads to the conclusion that the presence of mud here leads to a decrease in suitable area for mangrove colonization and lower mangrove maturation.

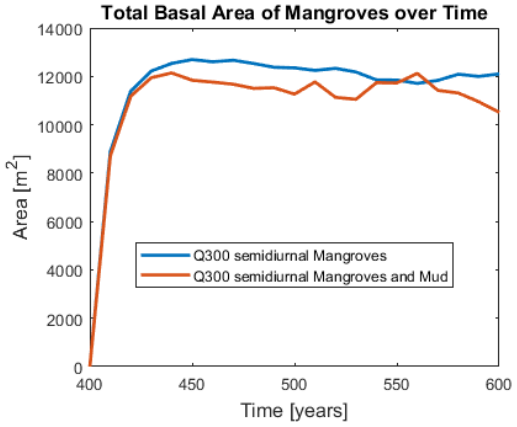

(A) Total area of mangrove coverage (excluding roots) over the 200 years of mangrove growth.

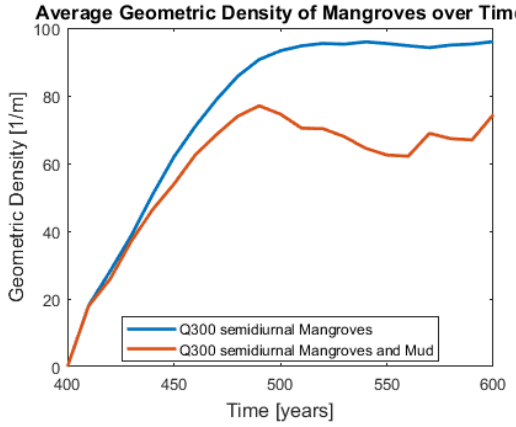

(B) Average geometric density of mangroves over the 200 years growth.

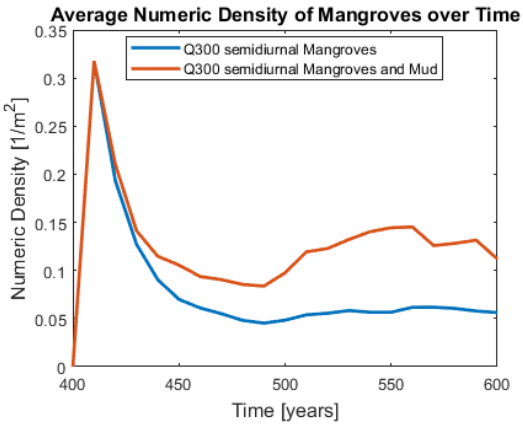

(C) Average numeric density of mangroves over the 200 years growth.

FIGURE 6.3: Comparison of (A) total mangrove basal area, (B) average geometric density and (C) average numeric density for the scenario with (orange) and without (blue) fluvial mud supply.

To investigate these differences, the hydroperiod is mapped in Fig. 6.4. Figure 6.4 shows the hydroperiod over the whole domain in year 600. Less mangrove coverage can be observed south of the main channel between approximately x = 8 km and x = 15 km (Fig. 6.2). When comparing this section within the hydroperiod plots (Fig. 6.4), it becomes evident that in those areas the hydroperiod is smaller for the scenario including mud compared to the scenario without mud. To quantify this observation, Fig. 6.5 shows the mud thickness, the bed level as well as the relative hydroperiod at a point within this section (x = 11 km and y = 0.8 km, marked in red circles in Fig. 6.4) for both scenarios. The mud thickness for the 'mud-scenario' increases constantly in that location indicating a sedimentation process of mud. The mud accretion then results in bed level increase at that location over the 200 years (Fig. 6.5b), while for the scenario without mud, the bed level is decreasing slightly (Fig. 6.5b). This mud accretion and bed level increase then leads to the effect that the hydroperiod in the location drops and reaches 0 for long periods for the mud supply scenario (Fig. 6.5c, orange). In summary, the presence of mud within the domain leads to a mud accumulation on bars which results in bed level increase to the extend that these locations are not inundated enough for mangrove colonization. Therefore, the scenario which includes mud shows an overall lower mangrove coverage and lower mangrove maturity but

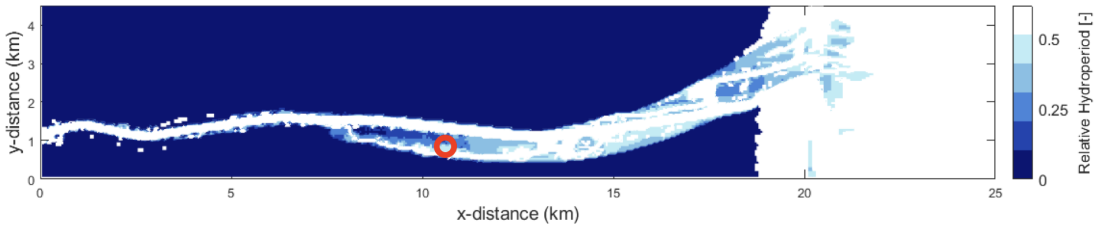

(A) Only sand scenario.

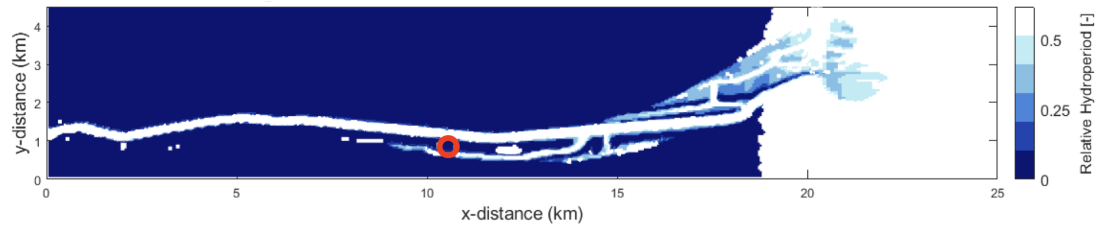

(B) Mud supply scenario.

FIGURE 6.4: Hydroperiod map after the 200 years of mangrove colonization for (A) the only sand scenario and (B) the scenario including mud supply, with the red circle indicating the area of interest mentioned in the text.

higher bed elevation on the bars.

6.2 Mangrove Dieback

In phase 3, the mangrove dieback was modelled using two different methods. The results for both methods are present in this section.

6.2.1 Dieback Induced by Model Boundary Conditions

The first approach is to model the dieback based on a change in boundary conditions of both river discharge decrease (RDD) and sea level drop (SLD), implemented as described in Section 5.5. The simultaneous decrease of river discharge (to 10 m^3/s) and drop of sea level (by 20 cm) has lead to a mangrove dieback over the 10-year simulation as presented in Figure 6.6. The dieback area is marked in red and the alive mangroves in shades of green, representing their maturity. It can be observed that a majority of the dieback occurs along the main river channel and along the channels between approximately 10 and 16 km x-distance. Some dieback can be seen within the upper delta platform. However, the most seaward parts of the mangroves are intact.

In order to understand the cause of the dieback, the hydroperiod before and after the dieback simulation is plotted (Fig. 6.7a, Fig. 6.7b). The white area represent the areas within the domain which have a hydroperiod of zero (not inundated). The darkest blue areas within the domain have a hydroperiod of 1 and are therefore inundated constantly. The main channel, the sea basin and some side channels are constantly inundated for both years. While the channel area, which is constantly inundated, is more narrow after the dieback (Fig. 6.7b). Within the delta, different hydroperiods can be observed. Fig. 6.7c shows the area which was initially suitable for mangrove growth (0<HP<0.6) but then due to the SLD and RDD the hydroperiod drops to zero. When comparing Fig. 6.6 to Fig. 6.7c, it can be observed that the hydroperiod dropped to zero in the zones where the dieback occurred. In order to quantify this observation,

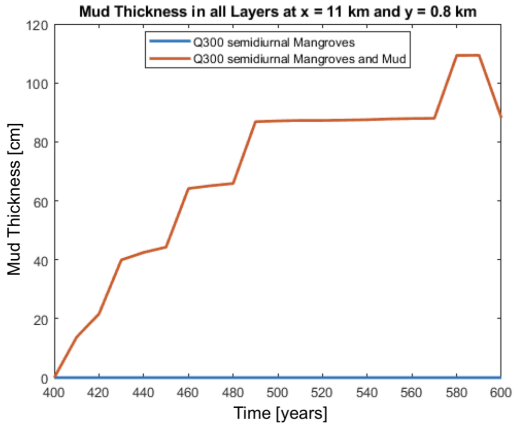

(A) Mud thickness in all layers.

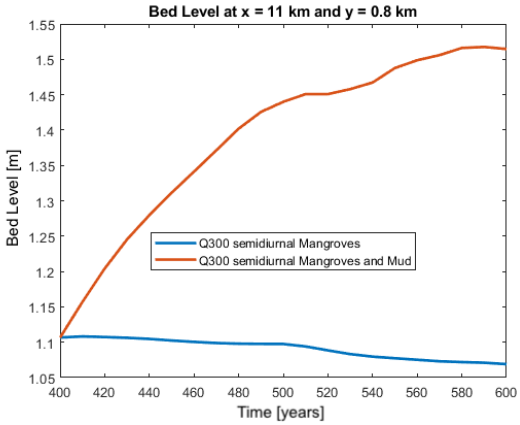

(B) Bed level.

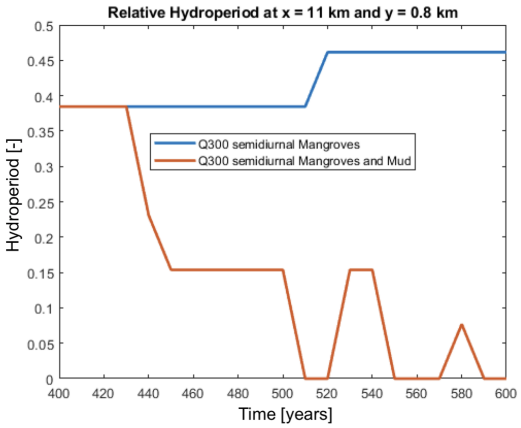

(C) Hydroperiod.

FIGURE 6.5: Comparison of (A) mud thickness, (B) bed level and (C) hydroperiod between mud and no mud scenario at the point x = 11 km and y = 0.8 km.

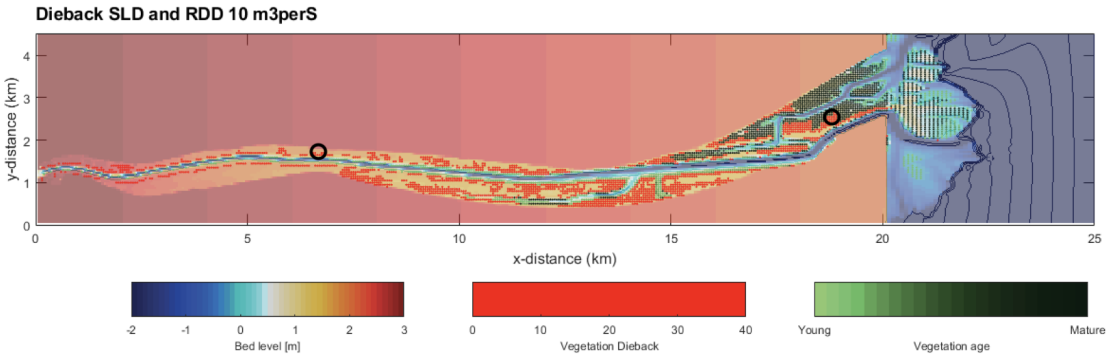

FIGURE 6.6: Bathymetry and mangrove coverage, including the dieback (in red), over the whole domain. The circles are upstream and downstream tidal flat locations discussed in the text.

Figure 6.8 shows the relative hydroperiod in two exemplary locations (as marked in Fig. 6.6, black circles), along the channel (Fig. 6.8a) and within the upper delta platform (Fig. 6.8b) over the 10 years of dieback. At both locations shown in Figure 6.8 the hydroperiod drops to zero within the first two years. In the following years, the hydroperiod is constant at zero, meaning that the mangroves in those zones are not

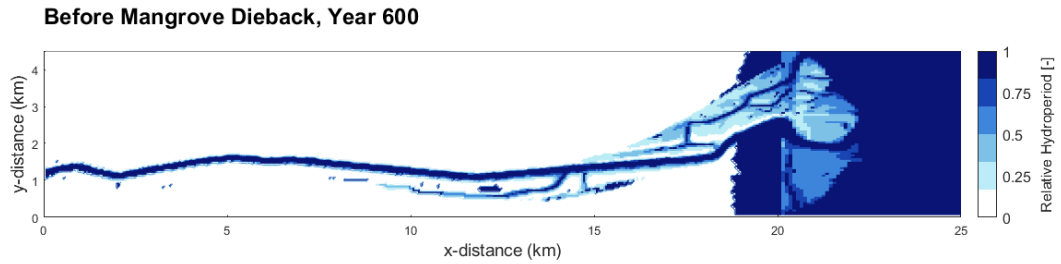

(A) Hydroperiod map before dieback.

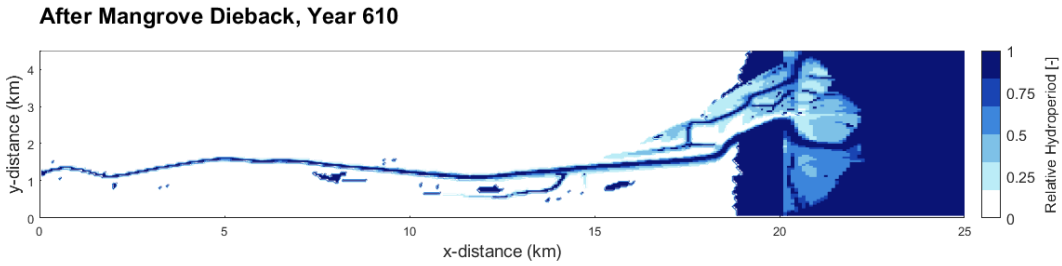

(B) Hydroperiod map after dieback.

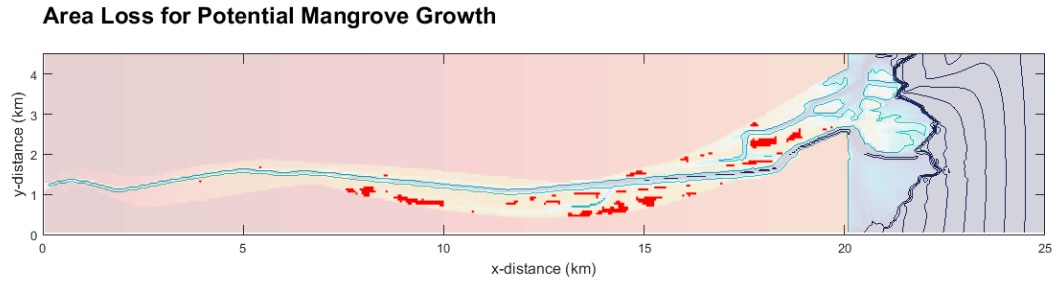

(C) Area of hydroperiod change from suitable for mangrove growth to unsuitable area (HP = 0).

FIGURE 6.7: Comparison of the hydroperiods over the whole domain (A) before the dieback (600 years), (B) after the dieback (610 years) and (C) the area where the hydroperiod drops from an initially suitable hydroperiod for mangrove growth to zero.

inundated and will die over time.

In order to quantify the mangrove dieback due to the sea level drop and river discharge decrease, three extra simulations (next to the SLD & RDD scenario) were incorporated: 1) only river discharge decrease (RDD) to 10 m^3/s, 2) only sea level drop (SLD) by 20 cm and 3) an undisturbed reference run which retains the initial boundary conditions without any sea level drop or river discharge decrease. Therefore, in total, four simulations were conducted, three of which are modelling mangrove dieback under different conditions, compared to the undisturbed reference scenario. Figure 6.9 shows a comparison of mangrove characteristics among these four simulations. The sum of the basal area of the mangrove vegetation (Fig. 6.9a), the average numeric density (Fig. 6.9b), the average geometric density (Fig. 6.9c) and the hydraulic resistance based on λ (Fig. 6.9d) over the 10 years of dieback simulation are shown. The total mangrove basal area (Fig. 6.9a) decreases over time for all three dieback scenarios, indicating the mangrove dieback in all scenarios. However, it is decreasing the most and the fastest for the scenario which combines SLD & RDD. Furthermore, the scenario including only SLD, has a higher dieback than the only RDD scenario. This leads to the

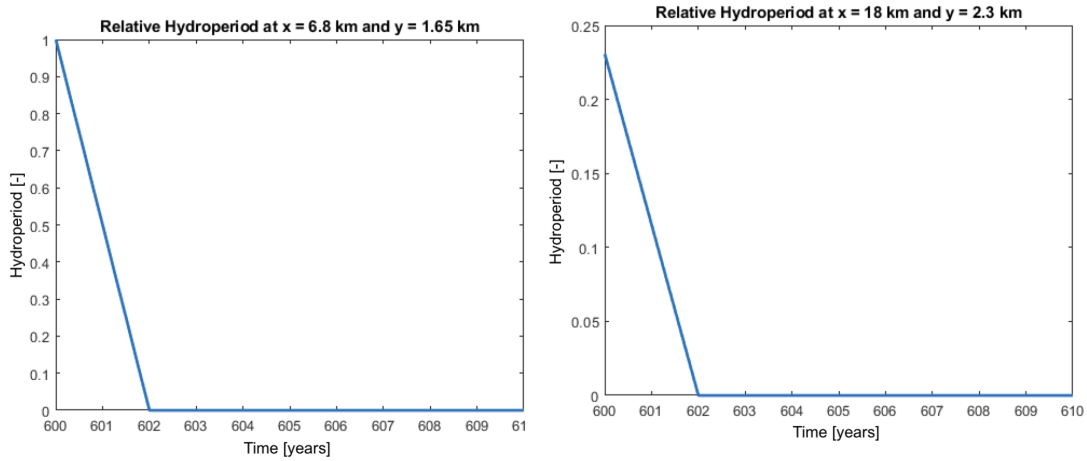

(A) Hydroperiod in dieback area next to channel.

(B) Hydroperiod in the dieback area at the upper delta platform.

FIGURE 6.8: Comparison of the hydroperiods over time at two different dieback locations: (A) along the channel upstream and (B) at the upper delta platform.

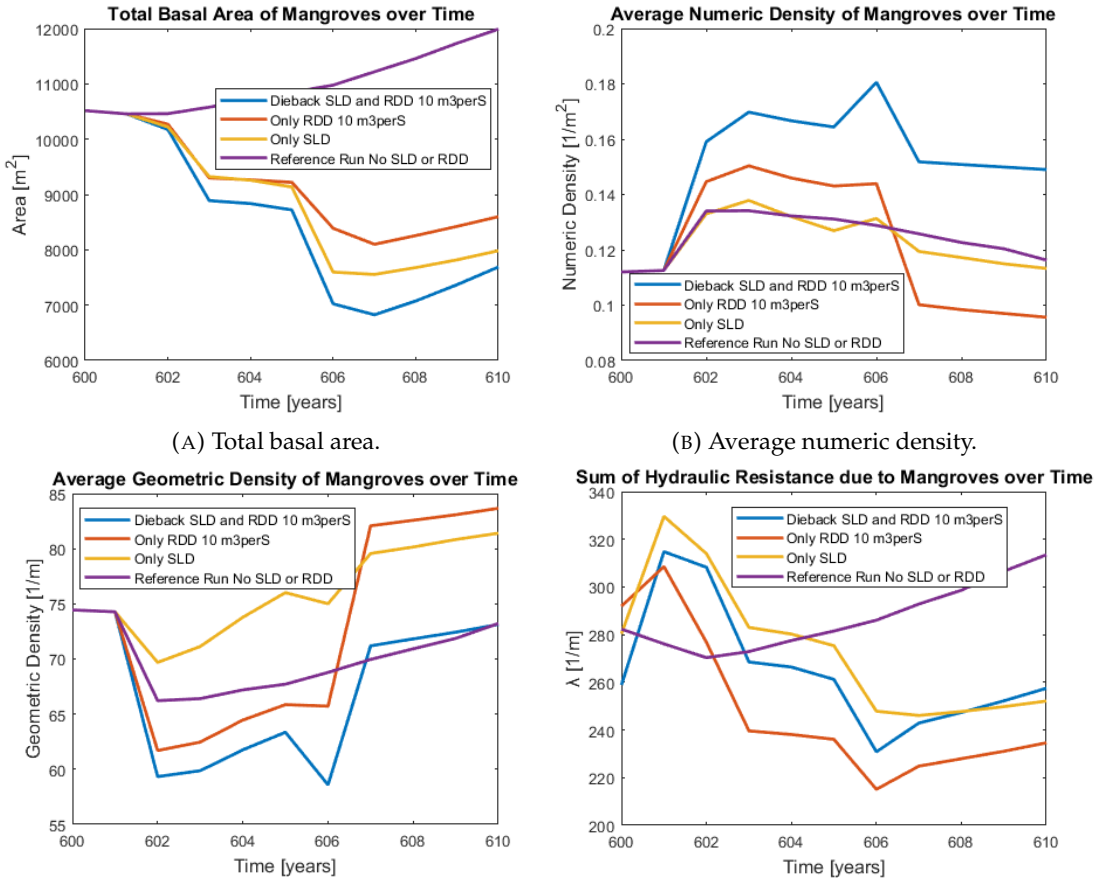

(A) Total basal area.

(B) Average numeric density.

(C) Average geometric density.

(D) Hydraulic resistance of mangrove trees.

FIGURE 6.9: Comparison of mangrove vegetation parameters: (A) total basal area, (B) average numeric density, (C) average geometric density and (D) hydraulic resistance, over the 10 year dieback event for the different dieback scenarios and the undisturbed reference.

conclusion that most mangroves die when the effect of both SLD and RDD are combined, while more mangroves area dieback occurs from the effects of the SLD than from RDD. The average numeric density over time increases initially for all 4 simulations. It increases the most for the scenario which combines SLD & RDD (Fig. 6.9b, blue graph) and it increases the least for the reference run (violet graph) and the only SLD scenario (yellow graph). For the only RDD scenario it even decreases slightly in the overall trend. Thus, the combined effects of SLD and RDD lead to an increase in the average numeric density compared to the other scenarios. This leads to the conclusion that predominantly mangroves within less densely populated grid cells die, as the average numeric density only considers vegetated cells. The dieback of more mangroves in more sparsely populated grid cells therefore leads to an overall increase of the average numeric density. Fig. 6.9c shows the same pattern with the geometric density decreasing the most for the SLD & RDD scenario (blue graph) compared to the other dieback scenarios. Therefore, it can be concluded that even though the average amount of trees per cell increase, the average geometric density is decreasing for the scenario showing the highest dieback (SLD & RDD). Both observations combined therefore indicate the dieback of more sparsely populated, more mature mangroves within the scenario combining SLD and RDD. This is also reflected within the sum of the hydraulic resistance exerted by all trees within the domain. The hydraulic resistance (Fig. 6.9d) reflects the combined, complex effects of total basal area as well as their density and thereby also maturity due to the competition stress and the root number. For all three dieback scenarios, the hydraulic resistance overall decreases over the 10 years dieback, reflecting the pattern of mangrove death, as the sum of all present trees is considered here. However, the pattern of the sudden decreases (e.g. year 606) reflects the patterns seen within the geometric density. Indicating that the decrease in hydraulic density does not solely originate from the overall decrease in mangrove coverage but also from the decrease in geometric density with the death of more mature trees including their higher number of roots. For the reference scenario however, the hydraulic resistance increases over the 10 years due to the increase in mangrove coverage (Fig. 6.9a). In summary, the combined effects SLD & RDD are most severe for the mangrove coverage as well as their hydraulic resistance with the highest area dieback, the dieback of more mature trees and the lowest hydraulic resistance after the dieback in this scenario.

Additionally, Figure 6.10 shows that even though the morphological change was not allowed during the dieback simulation (Fig. 6.10, top row), the mud distribution and relative flood ebb velocity ratio changed over the 10 years of dieback (Fig. 6.10, bottom row). This can be explained by the changes in hydrodynamic forces due to the drop in sea level and decrease in river discharge leading to a decreased ebb flow (Fig. 6.10, second row). This leads to decreased sediment transport downstream and mud accumulation in the upstream channel (Fig. 6.10, bottom row).

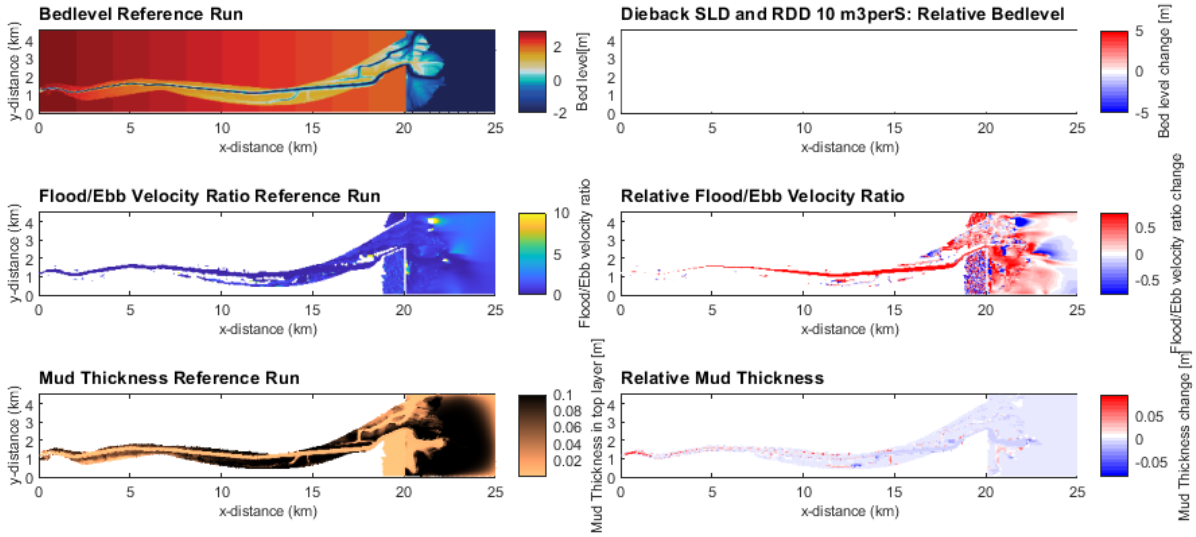

FIGURE 6.10: Bed level, Mud thickness in top layer and flood/ebb velocity ratio over the whole domain of the reference run and relative bedlevel, mud thickness and flood/ebb velocity ratio of the SLD & RDD dieback scenario compared to the reference run.

6.2.2 Dieback by Manual Removal

The second method to include the dieback within simulations was the manual removal of mangrove trees in a certain area. Based on the case study, it was here decided to simulate an extreme case and remove all the mangroves from 16 km seawards. Figure 6.11 shows the area where the mangroves were removed (red) and the mangroves which remain in the estuary including their age (shades of green).

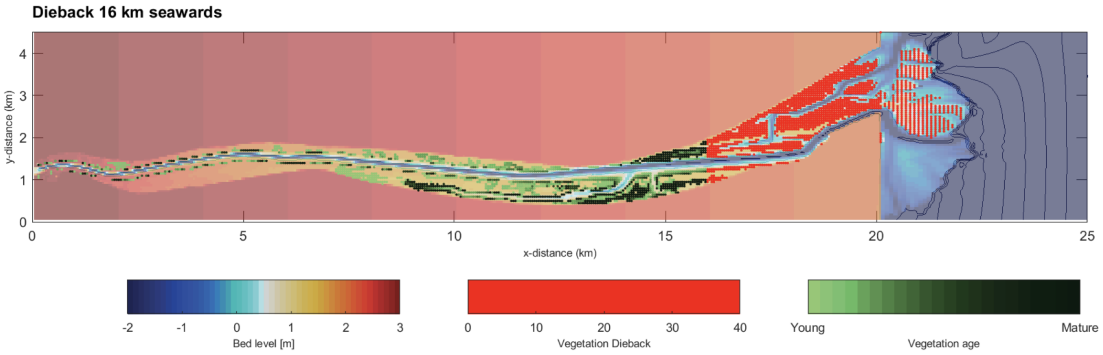

FIGURE 6.11: Map of bathymetry and mangrove coverage (green) including the dieback area (red).

Figure 6.12 further shows the vegetation characteristics of the mangrove removal. It can be seen that more than half of the total mangrove basal area was removed (blue bars). Furthermore, the average geometric density decreases with the removal from above 70 to approximately 50 stems per m. This leads to the conclusion that using this method, a high amount of more mature trees (higher stem diameter) were removed, as was also seen in the SLD & RDD (Fig. 6.9d) scenario.

The SLD & RDD dieback scenario and the 16 km seaward manual removal scenario were then used as the initial states for the further simulations of the disturbed state and the recovery (Fig. 5.11).

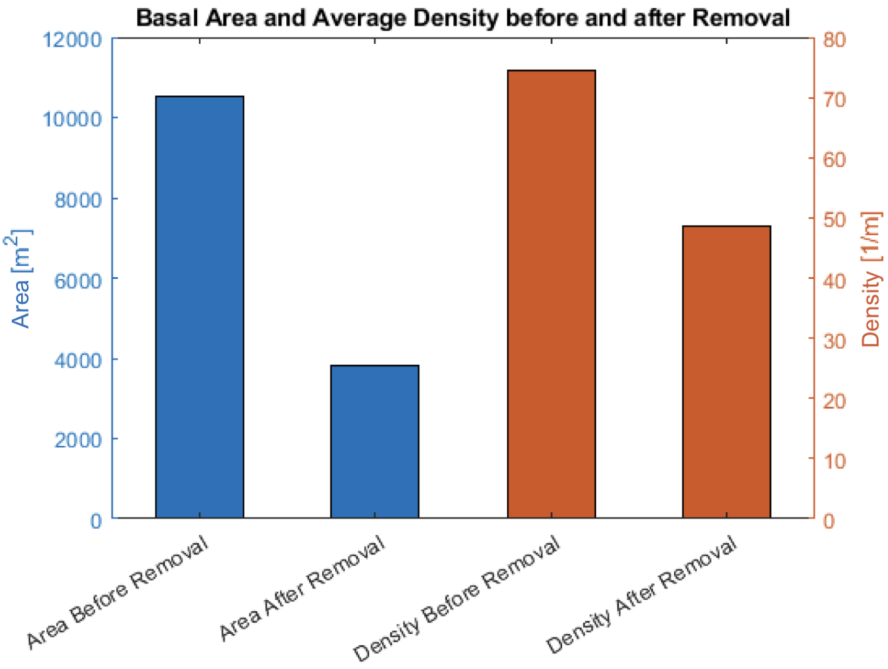

FIGURE 6.12: Basal area (blue) and geometric density (orange) of mangroves before (left) and after (right) the manual removal.

6.3 Influences of Dieback on Morphology - Disturbed State

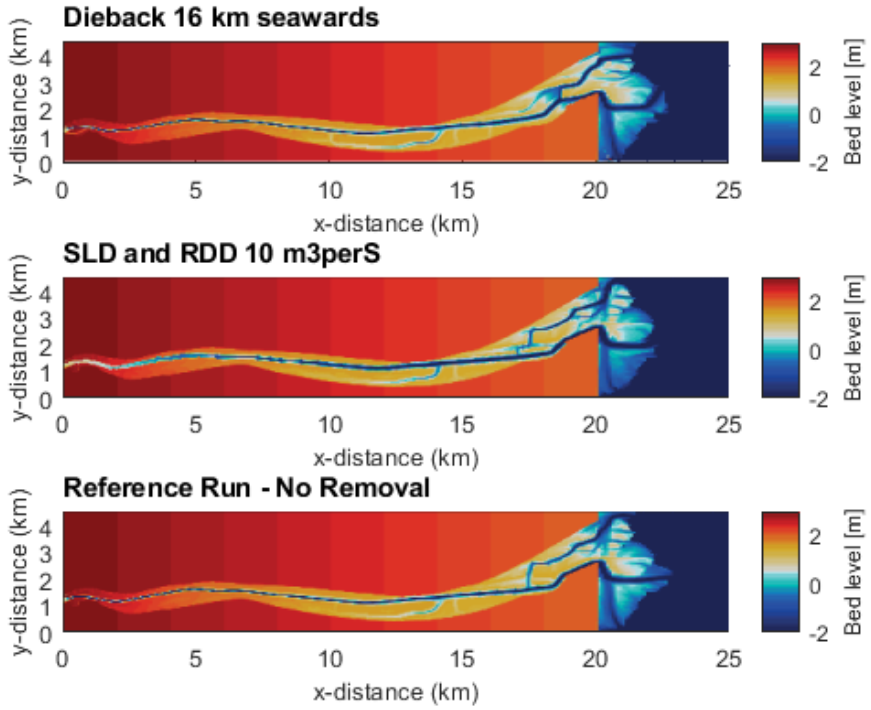

FIGURE 6.13: Bed level of the two dieback scenarios (top and middle) and the reference run (bottom).

During the disturbed state (phase 4), no mangroves were allowed to recolonize. Therefore, the effect of the dieback on the morphology and hydrodynamics over 100 years can be investigated. In order to do so, the undisturbed reference scenario (no dieback)

is compared to the two different dieback scenarios (dieback 16 km seawards and SDL & RDD). Regarding the bathymetry (Fig. 6.13), different observations can be made. Firstly, differences in the upstream river boundary can be observed for the SLD & RDD scenario. For this scenario, the upstream channel is wider and shallower than for the other two simulations (Fig. 6.13). This can be attributed to sediment deposition in that area, which is visible when comparing the mud thickness map (Fig. 6.16), showing an increased mud thickness within the upstream channel. When comparing to Fig. 6.10 it can be seen that this can be attributed to the sediment deposition in this area during the 10 year dieback simulation. Within the delta (near 17 - 20 km), it can be observed that the main channels have different shapes and locations, which can be attributed to the mangroves or missing mangroves in that area. Especially for the 16 km seawards dieback scenario differences can be observed, with a channel mitigation seawards (at x = 18 km) due to the absence of mangroves in that area. Thus, it can be seen that the difference in mangrove cover have an impact on shaping the morphology.

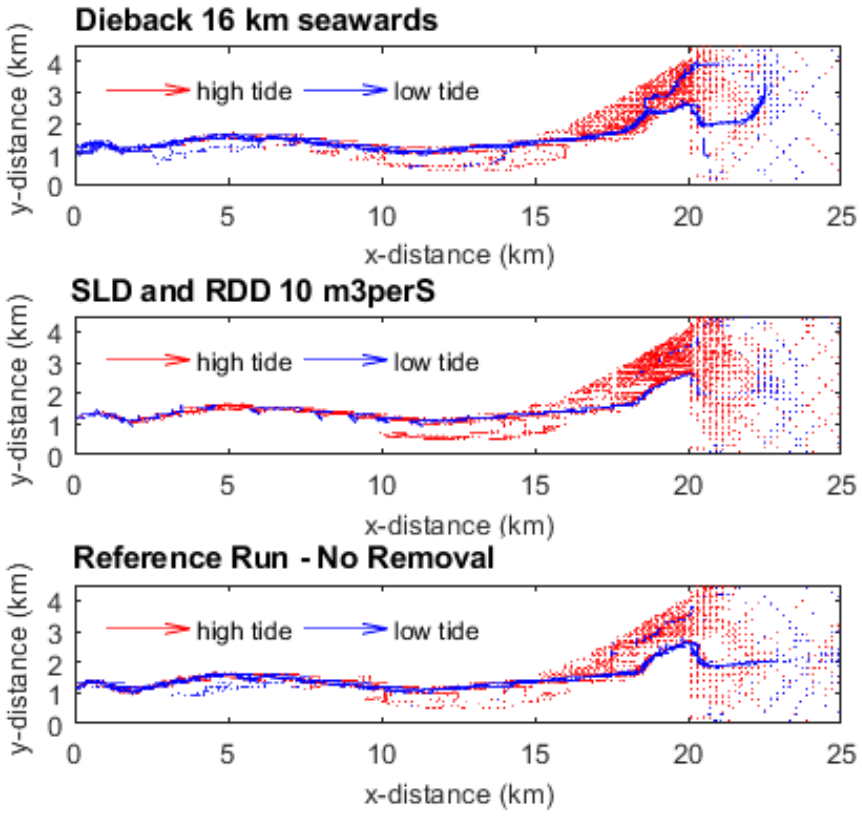

FIGURE 6.14: Ebb and flood velocities (top and middle) of the two dieback scenarios and the reference run (bottom).

Figure (Fig. 6.14) further shows differces in the ebb and flood flow velocities. It can be seen that for the SLD & RDD scenario, the ebb flow (blue arrows) is reduced compared to the other scenarios. This can be attributed to the above mentioned sediment infilling of the upper channel area due to reduced river discharge. Therefore, the flow velocities in teh channel upstream are lower and the ebb tidal currents mainly flush the bottom channels (Fig. 6.14).

Additionally, it can be observed that the flow velocities in the delta area for both dieback scenario are higher compared to the undisturbed reference scenario (Fig. 6.14). This indicates that the absence or reduction in mangrove cover in this area has lead to a higher flow velocity on the platform in the delta. To quantify this observation,

Figure 6.15 shows the average flow velocities of a tidal cycle for the 100 years of recovery in one point within the delta (x = 19 km, y = 2.5 km). It can be seen that for both dieback scenarios, the average velocity is higher than the velocity seen in the undisturbed reference over the years in that point. The 16 km seawards scenario shows a higher increase especially in the last 10 years of the simulation compared to the SLD & RDD scenario.

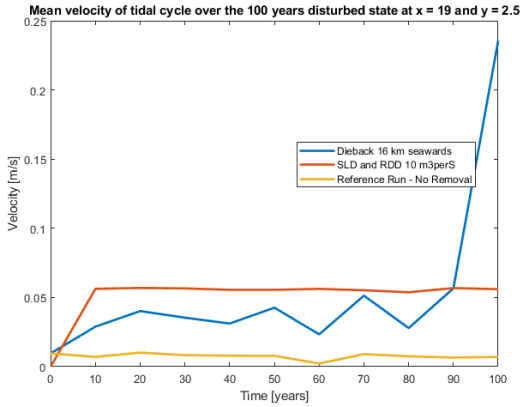

(A) Average velocity over a tidal cycle at location x = 19 km and y = 2.5 km over the 100 years of simulation.

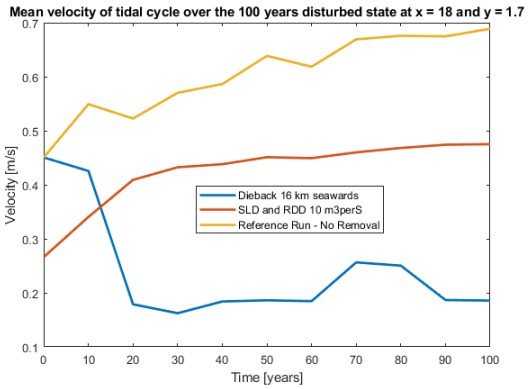

(B) Average velocity over a tidal cycle at location x = 18 km and y = 1.7 km over the 100 years of simulation.

FIGURE 6.15: Average velocities over tidal cycle (A) in the channel and (B) on the platform.

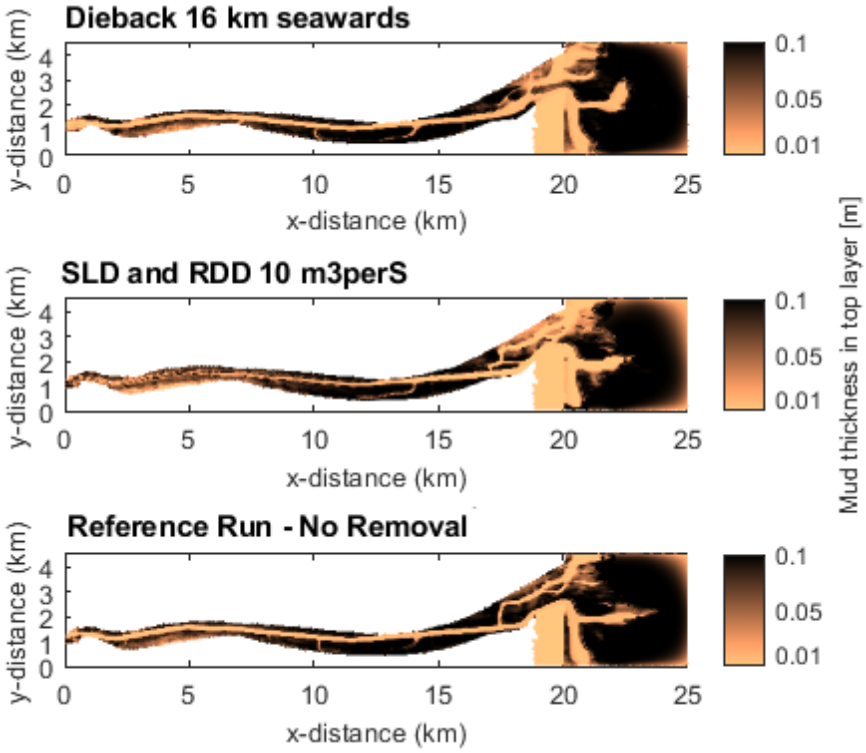

FIGURE 6.16: Mud thickness (in top layer) of the two dieback scenarios (top and middle) and the reference run (bottom).

Finally, the mud thickness shows different pattern within the delta for the three scenarios (Fig. 6.16). The reference run shows the highest mud thickness within the delta. This can be attributed to the fact, that for both dieback scenarios the flow velocity within the delta increase compared to the reference scenario (Fig. 6.16) leading to lower sedimentation in this area. Furthermore, the absence of mangrove vegetation leads to a decrease in erosion threshold compared to the vegetated area. This therefore causes the lower mud deposition in the dieback area.

6.4 Mangrove Recovery

In the final simulations, the recovery process over 100 years was assessed. In this simulation mangroves development and morphological change occurs (Fig. 5.11). During the mangrove recovery, changes in morphology and hydrodynamics are observed between the dieback scenarios and the undisturbed reference scenario. In order to illustrate these differences, Figure 6.17 shows the relative bed level, the relative flood/ebb velocity ratio and the relative mud thickness compared to the reference run for both scenarios.

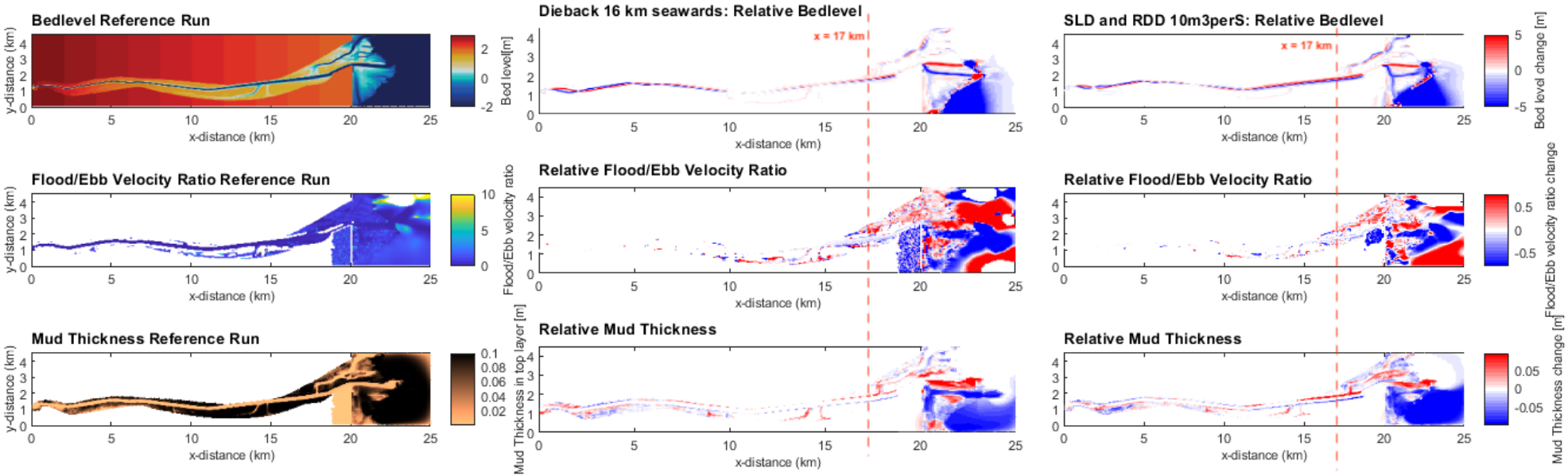

FIGURE 6.17: Comparison of the bed level, flood/ebb velocity ratio and mud thickness to the reference run after 100 years of recovery.

Regarding the bed level, in the channel area major bed level changes (+/- 5m) can be observed between the reference run and the two dieback scenarios. Figure 6.18 shows that this is caused by a shift in the main channel course.

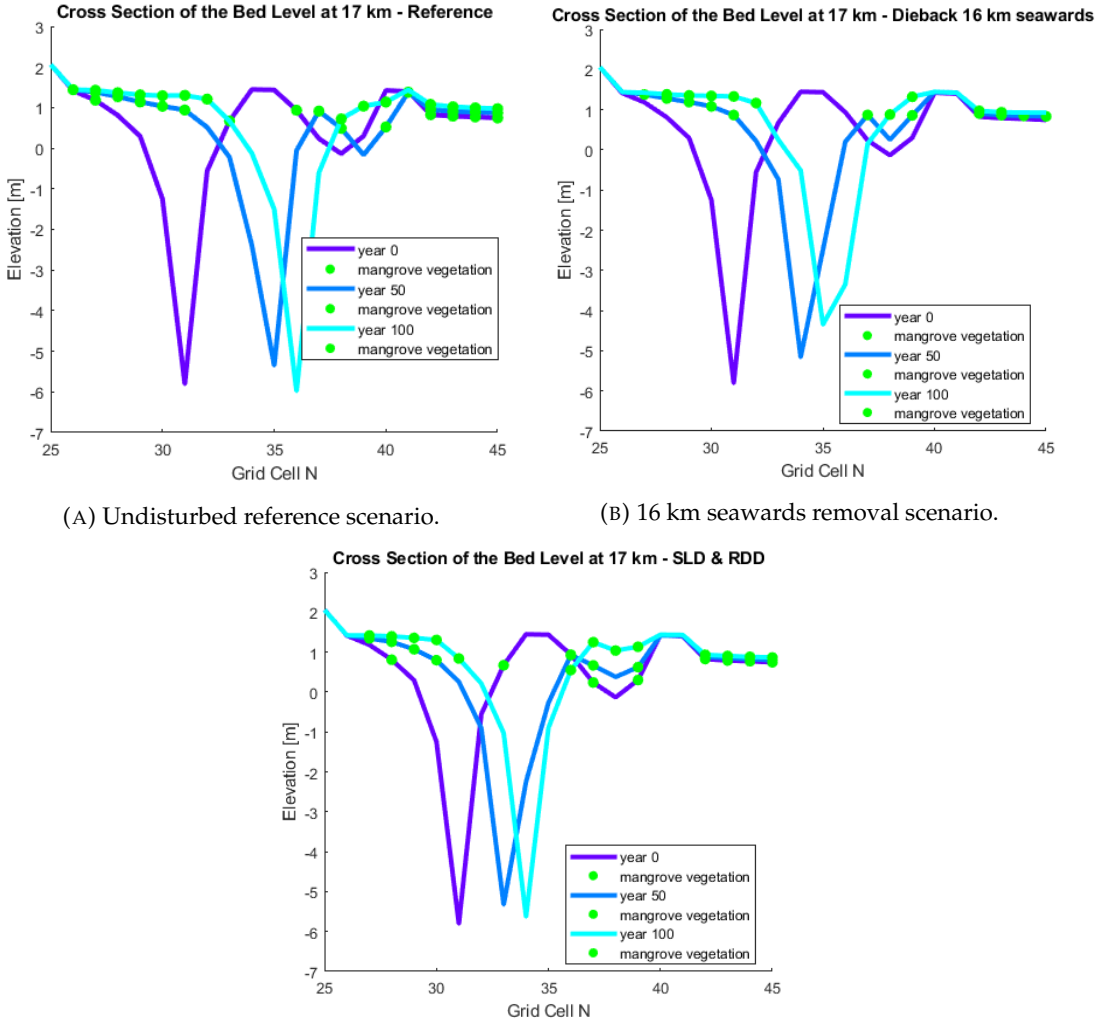

(A) Undisturbed reference scenario.

(B) 16 km seawards removal scenario.

(C) SLD & RDD scenario.

FIGURE 6.18: Cross section of channel bed elevation with locations of vegetation indicated over the 100 years recovery for (A) reference run, (B) 16 km seawards for manual removal and (C) SLD & RDD.

When comparing the reference run (left top) to the two dieback scenarios (right top and bottom) (Fig. 6.18), it can be seen that the channel of the reference run moves further north than the channel in the dieback scenarios after 50 and 100 years, causing the high differences in bed level within the channel area observed in Figure 6.17. The relative mud thickness within the channel area shows this pattern as well, as south of the main channel, there is a lower mud thickness than in the reference run for both scenarios. North of the channel there is a higher mud thickness than in the reference run. This further reflects the channel shift (Fig. 6.17, bottom).

Thus, in both scenario of dieback, the main channel northward shifting is less evident than in the reference run. This can be explained when looking at the velocity fields displayed in Figure 6.19. Here the velocities in x-direction (top) and y-direction (bottom) in the deepest part of the channel at x=17 km can be seen. It can be observed that

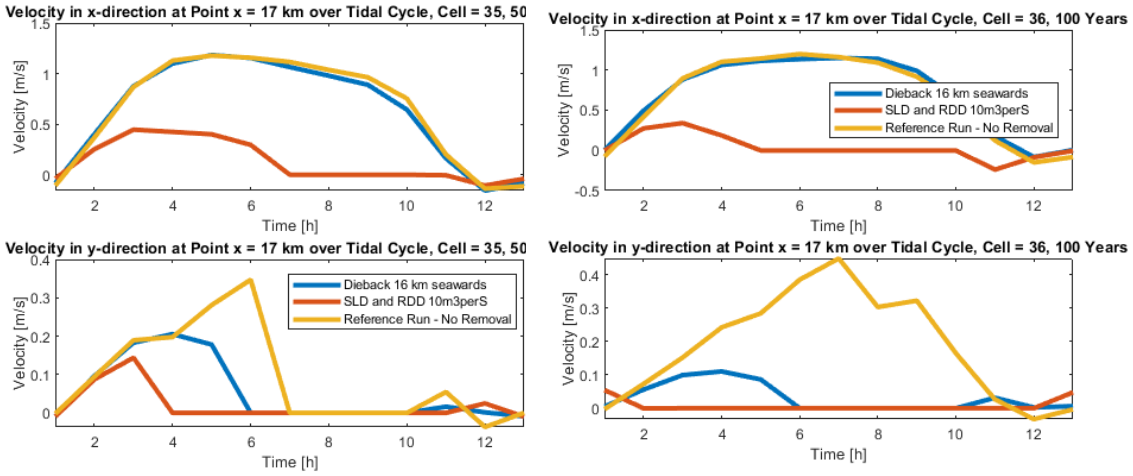

(A) x- and y-direction velocity over tidal cycle after 50 years of recovery.

(B) x- and y-direction velocity over tidal cycle after 100 years of recovery.

FIGURE 6.19: Flow velocities in x- and y-direction at x = 17 km in the deepest channel part of the reference run over a tidal cycle (A) after 50 years of recovery and (B) after 100 years of recovery.

the velocities in x-direction (top figures) after 50 (left) and 100 years (right) are similar for the reference run and the manual removal scenario. While it is lower for the SLD & RDD scenario. The velocity in y-direction (bottom figures) however is higher (positive) for the reference run than for the two dieback scenarios after 50 and 100 years. The higher y-direction velocity within the channel in that location (x = 17km) therefore leads to this higher channel mitigation northwards (positive y-direction). Figure 6.21c and 6.18 (left) show a relatively higher mangrove cover in the reference run south of the channel at x = 17 km. As the reference scenario has a higher presence of mangroves in this area, it can be concluded that the presence of vegetation modulates the velocity field.

Furthermore, the relative flood/ebb velocity ratio for the dieback scenarios is higher in parts of the delta than in the reference run (Fig. 6.17, middle row). For the 16 km seawards dieback scenario, this holds true for a bigger area than for the SLD & RDD scenario, indicated by the larger area in red within the delta area. When comparing this observation to the flood/ebb velocity ratio in the 95th percentile of the bed level (Fig. 6.20d), it can be seen that the dieback 16 km seawards scenario shows an increasing ratio after 30 years of recovery indicating a higher flood dominance on the tidal floodplain. Furthermore, Fig. 6.20b indicates that the 95th percentile of bed level for the SLD & RDD scenario is slightly increasing (about 1cm) during the 100 years of recovery. Overall, Fig. 6.20 shows differences in bed elevation and flood/ebb velocity ratio on the tidal flat and in the channel between the three scenarios. It was seen that when regarding specific locations in the estuary, trends can be observed. However, when regarding the parameters for the whole estuary, more complex interactions emerge as no clear trends can be seen between the amount of mangrove coverage and the bed level and velocity ratio in these scenarios (Fig. 6.20).

This feedback between in morpho- and hydrodynamics and mangrove vegetation is also visible within the mangrove vegetation pattern. Figure 6.21 shows the resulting bathymetry as well as the mangrove coverage after the 100 years of recovery over the entire domain for the two dieback scenarios (16 km seawards manual removal

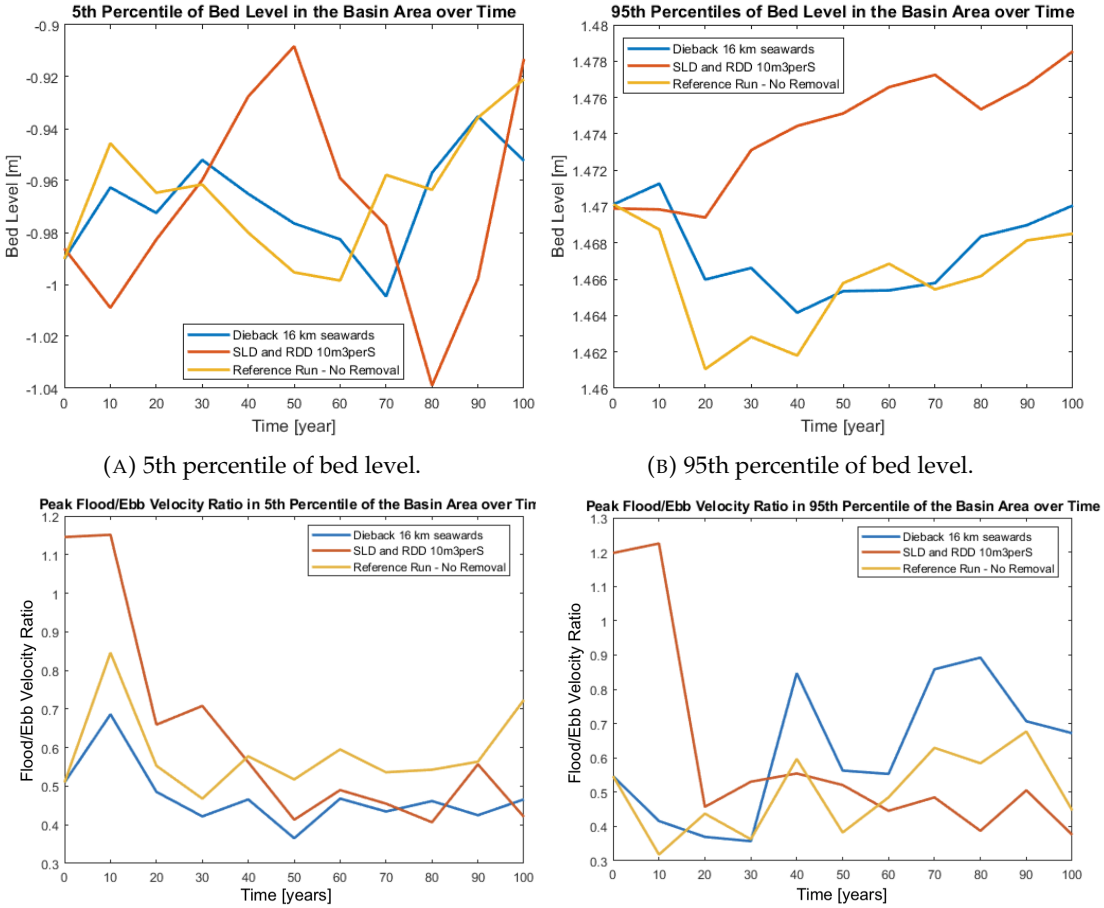

(A) 5th percentile of bed level.

(B) 95th percentile of bed level.

(C) Flood/ebb velocity ratio in 5th percentile of bed level.

(D) Flood/ebb velocity ratio in 95th percentile of bed level

FIGURE 6.20: Time series of the 100 years of recovery of the (A) channel depth represented by the 5th percentile of bed level, (B) tidal flat elevation represented by the 95th percentile of bed level, (C) flood/ebb velocity ratio within the channel area (5th percentile of bed level) and (D) flood/ebb velocity ratio on the tidal flat (95th percentile of bed level).

(Fig. 6.21a), SLD & RDD model dieback scenario (Fig. 6.21b) and the undisturbed reference scenario (Fig. 6.21c). It can be seen that the mangrove vegetation areas increase again for the two dieback scenarios. Even though all three maps show slightly different patterns, the overall coverage seems similar in the estuary area. These differences in coverage seen in Figure 6.21 can be explained by the different hydroperiods for those locations (Fig. 6.22). Accordingly, some differences are noticeable between 10 and 15 km, as the 16 km seawards scenario shows more areas with a hydroperiod above 0.6 (Fig. 6.22a, red circle), which makes them uninhabitable for mangrove vegetation. While for the SLD and RDD scenario, the area in the back of the delta (Fig. 6.22b, red circle) shows higher amounts of zero inundation compared to the reference run after the 100 years of recovery. Therefore, differences in the inundation regime within the three scenarios lead to differences in mangrove vegetation coverage.

The vegetation characteristics during the 100 years recovery of the two dieback scenarios and the reference run are displayed in Figure 6.23. The total basal area of the

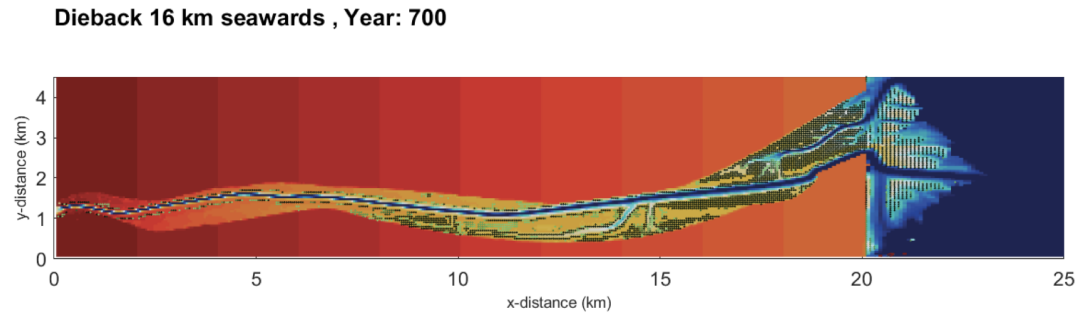

(A) 16 km seawards manual removal.

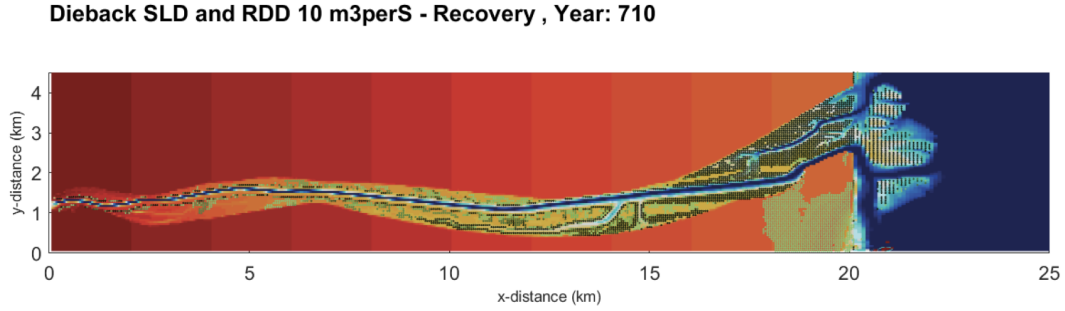

(B) SLD and RDD model dieback.

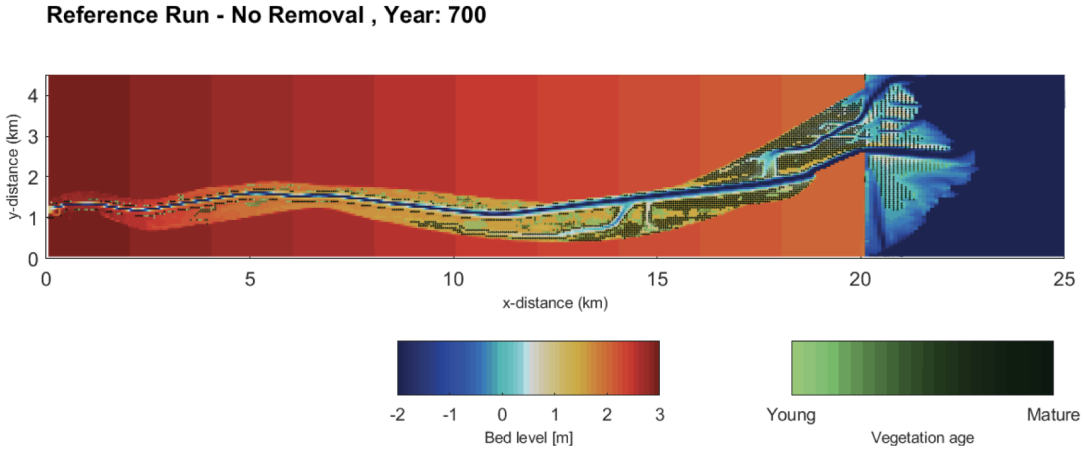

(C) Reference scenario.

FIGURE 6.21: Bathymetry and mangrove cover map after 100 years of recovery for three scenarios: (A) 16 km seawards manual removal, (B) SLD & RDD model dieback and (C) undisturbed reference scenario.

mangroves (Fig. 6.23a), the average numeric density (Fig. 6.23b), the average geometric density (Fig. 6.23c) and the sum of the hydraulic resistance due to the mangrove trees within the whole domain (Fig. 6.23d) are displayed. During the recovery of the manual removal scenario, the amount of total basal area seen in the undisturbed reference run, is reached in less than 20 years. Within the SLD & RDD scenario, it takes about 70 years to reach the sum of basal area seen in the undisturbed reference. The average numeric density (Fig. 6.23b) is initially close to the reference run for both dieback scenarios. For the SLD & RDD scenario the numeric density is relatively constant and close to the reference run over the 100 years. For the dieback 16 km seawards scenario, the tree density increases to reach its peak in the first 10 years of the recovery, it then decreases again to the level of the other two scenarios. This initial increase can be explained by the sudden recolonization of new, small trees in the area

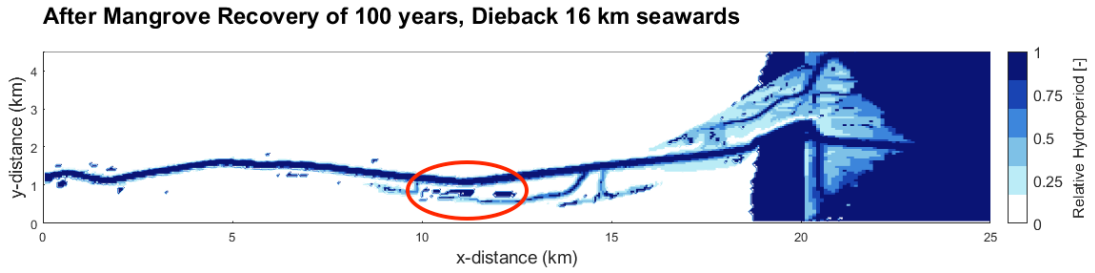

(A) Hydroperiod of 16 km seawards manual removal scenario.

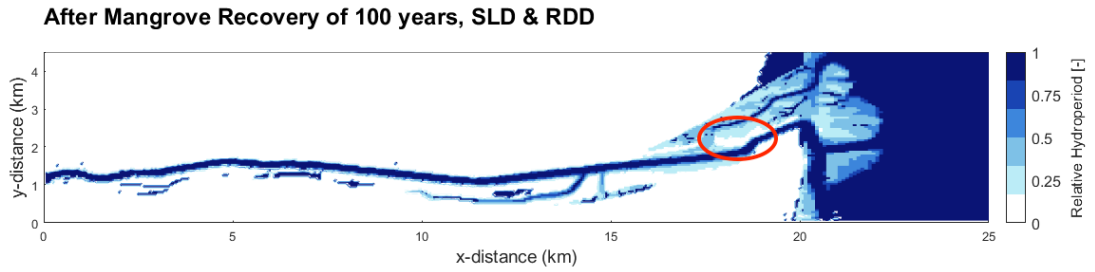

(B) Hydroperiod of SLD and RDD dieback scenario.

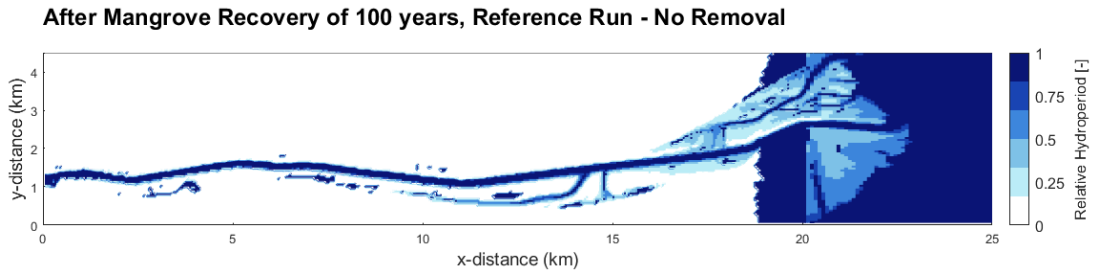

(C) Hydroperiod of undisturbed reference scenario.

FIGURE 6.22: Hydroperiod maps after 100 years recovery of the three scenarios: (A) 16 km seawards manual removal, (B) SLD and RDD model dieback and (C) the undisturbed reference run.

of the manual removal. During the recovery process, numerous trees enter at the new habitats as small trees, leading to this peak in numeric density. As the trees become more mature, less trees fit on one grid cell due to the competition stress, causing the tree density to decrease again with maturation of the trees. Looking at the hydraulic density (Fig. 6.23c), this pattern can be observed as well. An initial drop in average geometric density can be observed within the first 10 years of the dieback 16 km seawards scenario. The density then increases with the maturing of the trees, to the level of the reference run and of the other dieback scenario. Similar patterns can be observed within the hydraulic resistance over the 100 years recovery of the dieback 16 km seawards scenario (Fig. 6.23d, blue). Initially low hydraulic resistance is observed, which then increases with increasing sum of mangrove basal area (Fig. 6.23a). For the SLD & RDD scenario, the hydraulic resistance initially shows a higher value than for the 16 km seawards scenario. However, it drops to a lower value due to the slow increase and slight drop in total basal area (Fig. 6.23a) as well as the geometric density (Fig. 6.23c) after 20 years of recovery. In the following decades, it increases to the level of the reference run which it reaches after about 50 years of recovery. To quantify the effect the stems (excluding the roots) have on the hydraulic resistance, Figure 6.24 shows the hydraulic resistance over the 100 years of recovery, including solely the effect of the stems. When comparing Figure 6.24 with Figure 6.23d, it can be seen,

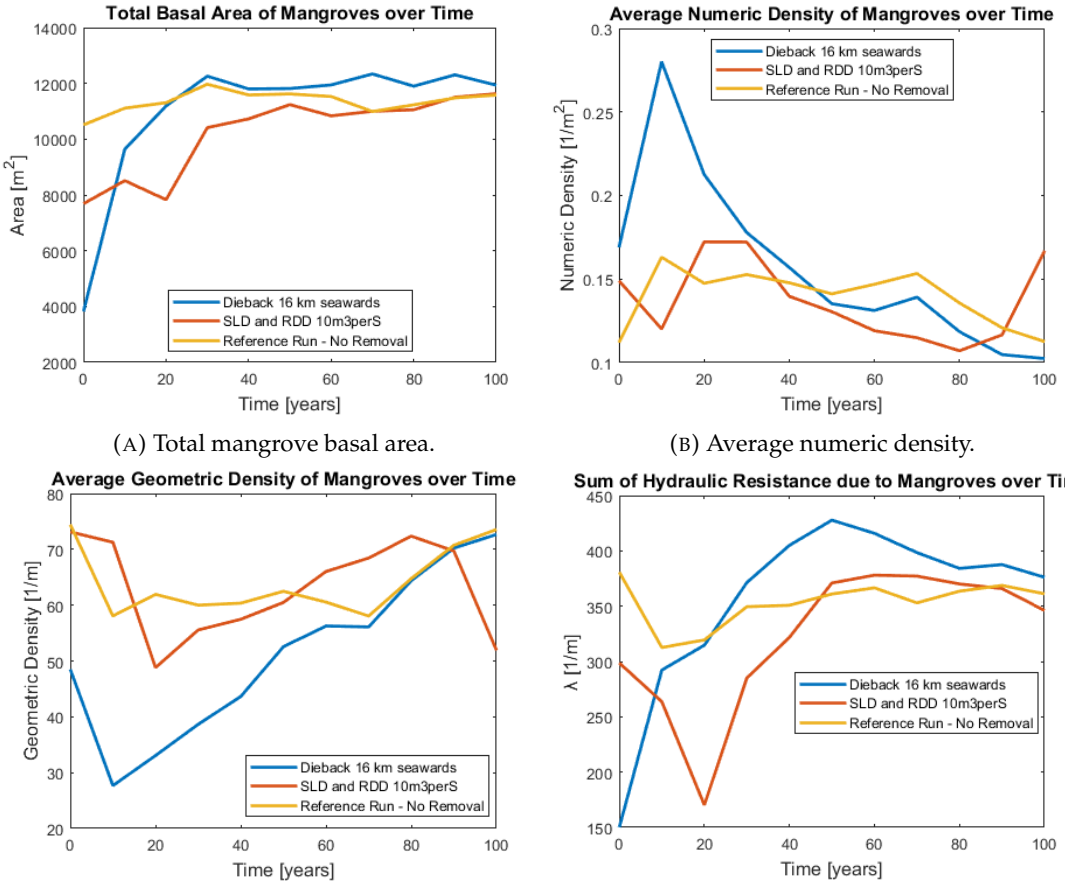

(A) Total mangrove basal area.

(B) Average numeric density.

(C) Average geometric density.

(D) Sum of the hydraulic resistance.

FIGURE 6.23: Mangrove characteristics over the 100 years of recovery over the whole domain including (A) Mangrove tree total basal area, (B) average numeric density, (C) average geometric density and (B) hydraulic resistance on the basis of lamda over the 100 years recovery of the three scenarios.

that the hydraulic resistance exerted by the stems is much lower than the one exerted by the mangrove trees including their roots. This indicates that the roots have a high effect on the hydraulic resistance.

The above illustrated results (Fig. 6.23) show a similarity of vegetation characteristics between mangrove dieback scenarios and the reference run after the 100 years of recovery, indicating a complete recovery of the mangrove characteristics. However, when only regarding the areas where the dieback occurs, a different result is emerging. Figure 6.25 shows the stem diameters of the mangrove trees in a boxplot diagram over the 100 years of recovery. For both scenarios, the stem diameters are increasing, for the 16 km seawards dieback with a higher rate (Fig. 6.25a, green). However, at the end of the 100 years, the median value and variance does not reach the values for the stem diameters seen in the reference run (red boxes). The median values lie below the ones of the reference run even after the 100 years of recovery and the variety of stem diameters is lower than what is observed in the reference run for both dieback scenarios. This indicates that the mangrove stem diameter in the affected areas do not recover to the values seen in the undisturbed reference. In order to quantify the difference in recovery of the two scenarios further, the recovery rate was calculated. The recovery rate is based on the average stem diameter in the area where the dieback

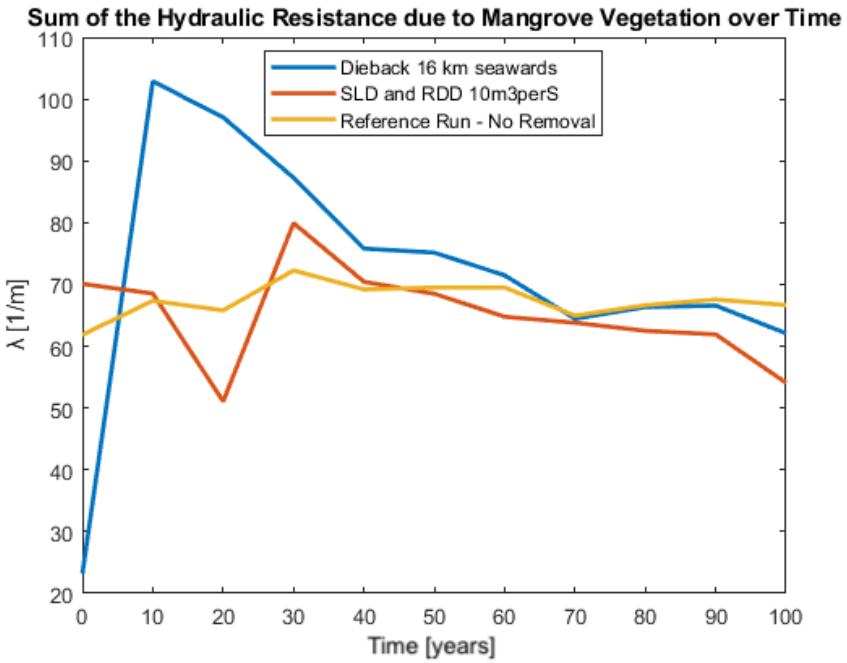

FIGURE 6.24: Mangrove stems hydraulic resistance over the 100 years of recovery.

occurred and is calculated over the 100 years of recovery. For the SLD & RDD scenario, a recovery rate of 0.7472 per year and for the 16 km seawards manual removal, a rate of 0.9952 per year was calculated. It can be seen that the recovery rate of 16 km seawards manual removal scenario is higher suggesting a faster and more complete recovery over the 100 year period.

Therefore, it can be concluded that the mangroves do recover and the total basal area as well as the hydraulic density increase over the 100 years to reach the values seen in the reference run. However, when looking specifically at the area where the dieback occurred, the mangrove stem diameter do not recover to the level of the undisturbed reference run over the 100 years of recovery. Furthermore, different recovery rates can be observed between the two dieback scenarios.

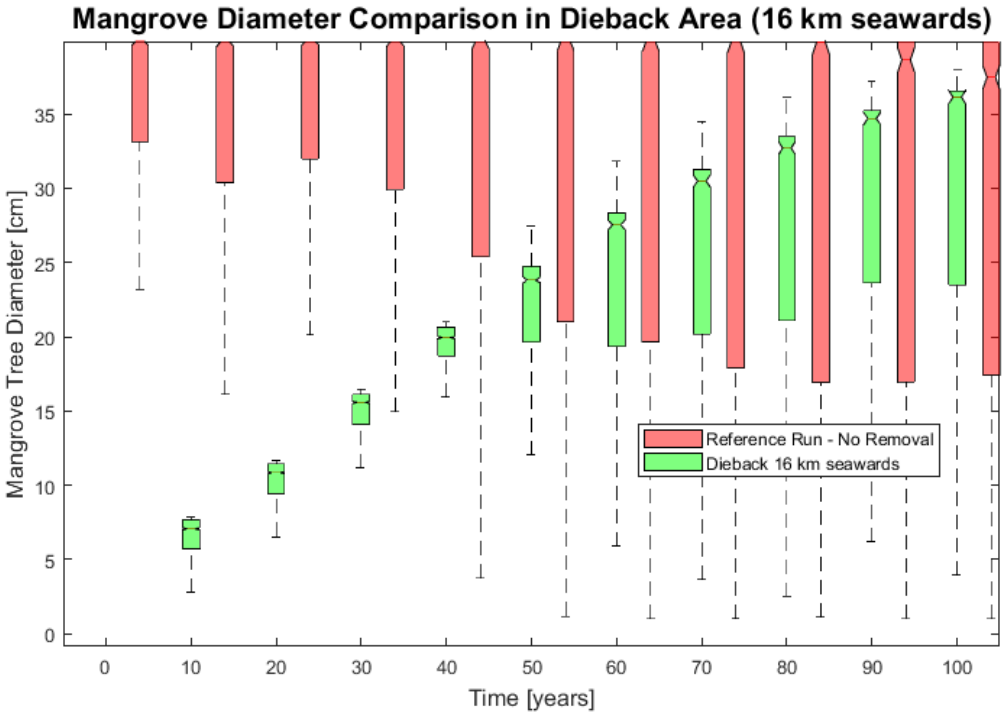

(A) Manual removal from 16 km seawards scenario, recovery.

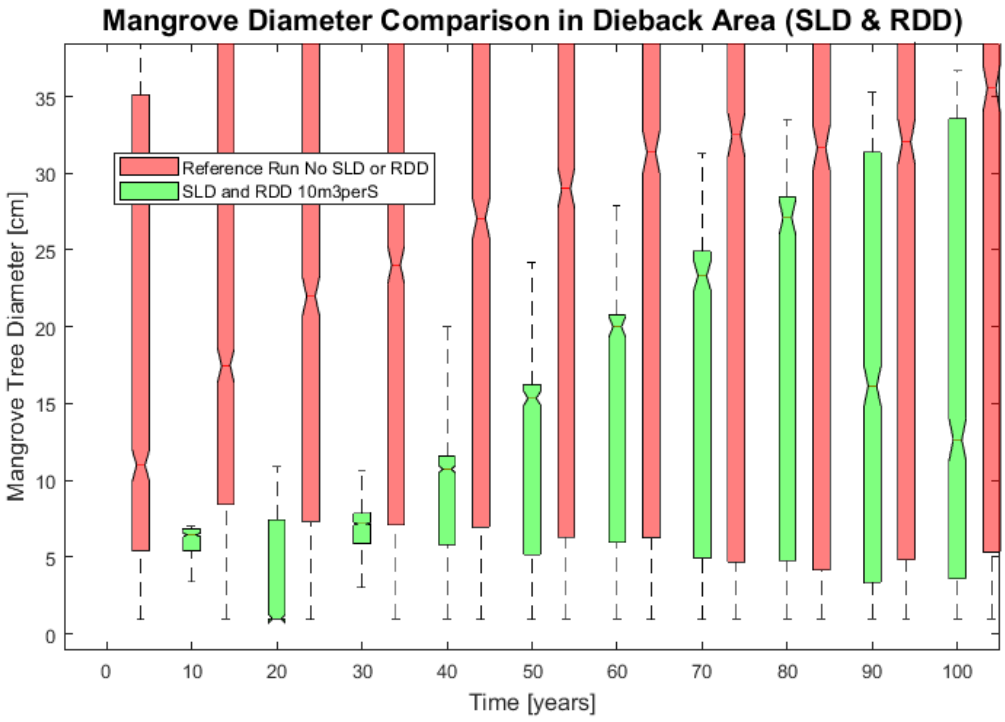

(B) SLD & RDD dieback scenario, recovery.

FIGURE 6.25: Comparison of stem diameters from the to dieback scenarios to the reference run over the 100 years of recovery.

6.5 Overall Mangrove Growth

Finally, the mangrove basal area is illustrated over the whole simulated time in Figure 6.26. This figure includes the sum of basal area during the 200 years of mangrove growth (phase 2), the 10 years of modelled dieback (SLD & RDD scenario and the undisturbed reference run) (phase 3), the sum of the basal area during the 100 years of recovery for the SLD & RDD scenario and the 16 km seawards manual removal scenario, including the respective undisturbed reference runs (phase 4). Figure 6.26

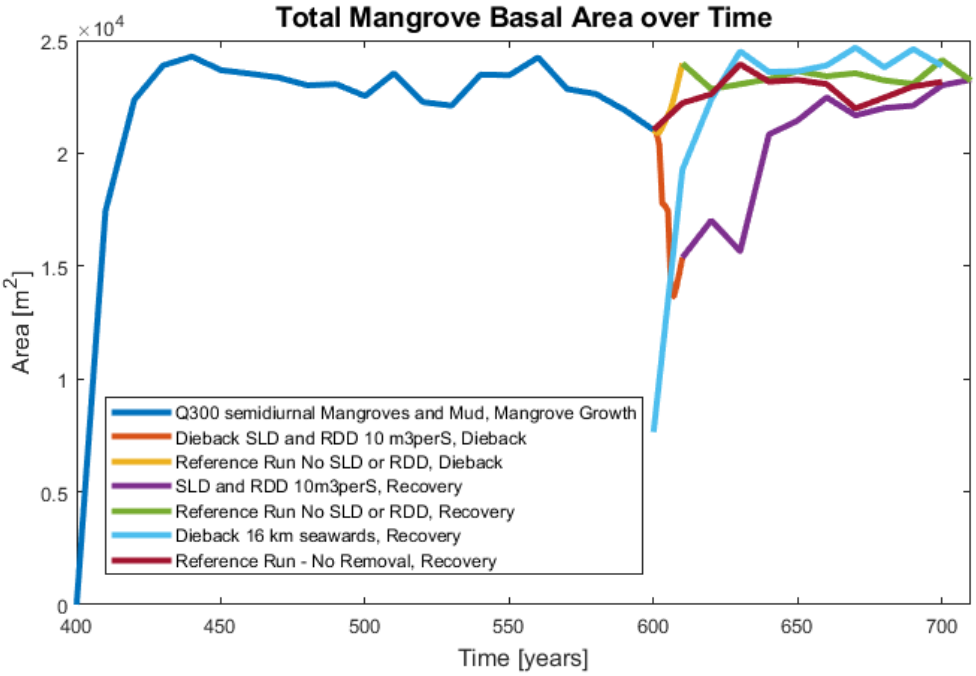

FIGURE 6.26: Mangrove total basal area for all simulations considered over the different phases of mangrove growth (year 400 - 600), mangrove dieback (year 600 - 610) and mangrove recovery (year 600/610 - 700/710).

shows the total mangrove basal area over the different model phases which contain mangroves (phases 2 - 4). Initially, the mangrove area increases rapidly, reaching about 12,000 m^2 within the first 30 years. In the following years of mangrove growth, the total basal area is relatively constant. During the last 40 years however, the basal area decreases slightly to about 10,000 m^2. Subsequently in phase 3, the mangrove dieback follows. The manual mangrove removal from 16 km seawards can be seen in the light blue graph with a sudden drop of basal areas due to the immediate removal in year 600. The model dieback is reflected in the orange graph with a decrease of basal area over a 10-year period. Comparing the basal area of the model dieback (SLD & RDD scenario) after the 10 years of dieback and the manual removal, it can be seen that less mangrove area is present for the manual removal scenario. However, in the following years (phase 4), during the recovery, the basal area of the manual removal increases up to the reference scenario (dark red) within 20 years. The recovery for the SLD & RDD scenario (violet) up to the reference run (light green) takes longer and is only reached after the 100 years of recovery. Here, it can also be seen that the recolonization in the 16 km seawards manual removal scenario (light blue graph) shows similar rates as the initial colonization of the bare domain (phase 2, dark blue graph). The recolonization in the SLD & RDD scenario (violet graph) however shows a slower rate.

In order to quantify this observation, Figure 6.27 shows the ratio of actual growth rate and the optimal growth rate (based on the change in stem diameters, according to eq.5.15) over the first 90 years of initial colonization and the recovery of the dieback area for both dieback scenarios. This therefore illustrates the ratio of growth reached, compared to optimal growth. It can be seen that the SLD & RDD scenario shows

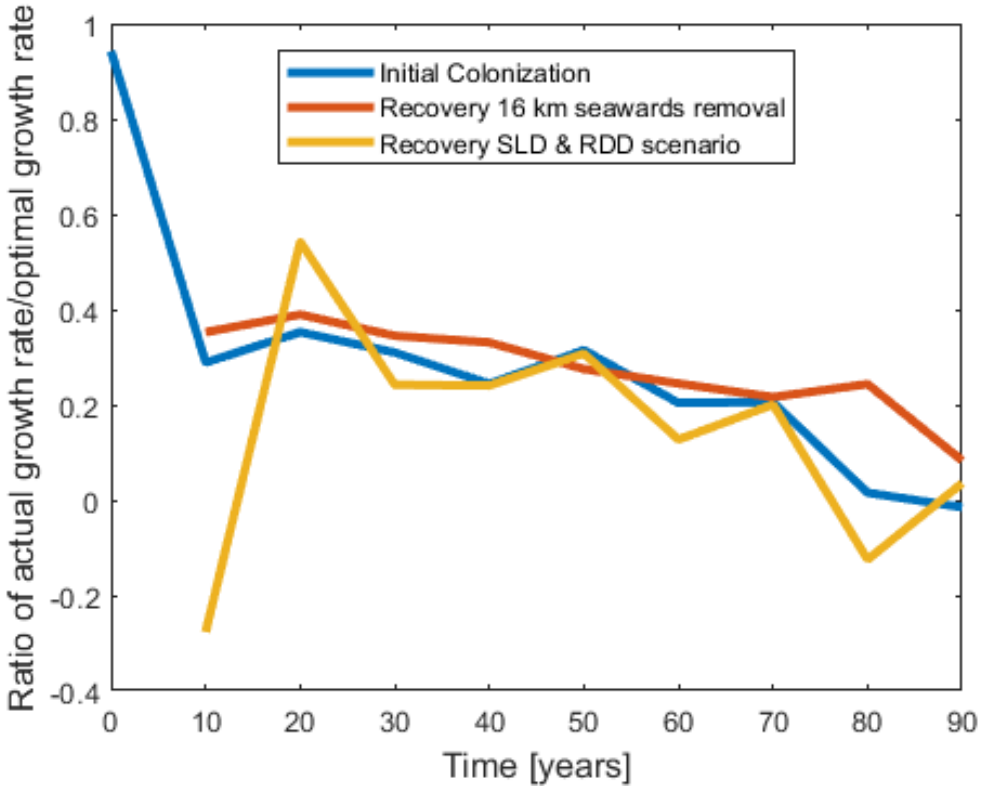

FIGURE 6.27: Ratio of the actual growth rate/optimal growth rate based on the change in average stem diameter over the first 10 years of colonization and recovery. For the dieback scenario only the dieback area is included.

an overall relatively lower ratio with drops in the ratio while the ratios for the other dieback scenario and the initial colonization are quite similar over time and more constant. All ratios are decreasing over time as the competition stress increases with increasing mangrove cover. The drops in the SLD & RDD scenario therefore originate from infrequent stresses in inundation causing a temporary lower actual growth rate. Summarized it can be seen that, the total basal area recovers more quickly when the dieback is in form of an extensive loss within the estuary mouth. However, when the dieback occurs within the channel area and stretch over a longer time period with hydrodynamic change, the recovery and colonization rate is slower.

Chapter 7

Discussion

In this thesis research, a bio-morphodynamic modelling approach is applied to study the bio-geomorphological feedback between mangrove dynamics and the estuarine morpho- and hydrodynamics. The results indicate that: (1) mud supply can lead to mud accumulation on bars, resulting in bed level increase and thereby limits the area available for mangrove colonization due to low inundation, (2) the decrease of sea level and river discharge leads to a mangrove dieback within the model with a decrease in total mangrove basal area, an increase in average tree density, decrease in hydraulic density and thereby a decrease in total hydraulic resistance, (3) mangrove dieback leads to long-term morphological changes such as channel shifting, channel infilling, increase of flow velocity on previously vegetated flats and the decreased sedimentation in those areas, (4) mangrove cover is increasing during mangrove recovery, reaching the initial mangrove cover over 100 years recovery, however the stem diameters in the dieback area indicate an incomplete recovery compared to the undisturbed reference, (5) different recovery rates can be observed between the two dieback scenarios (SLD & RDD scenario and 16 km seawards manual removal scenario).

This chapter serves as a discussion of the results summarized in the previous chapter. In particular, the most significant results are discussed and justified on the basis of literature and field data from the case study. Firstly, the influence of mud inflow on the mangrove colonization within the domain is discussed. Secondly, the modelled dieback and the dieback which occurred within the case study of the Leichhardt estuary are compared and the differences and similarities are discussed. Thirdly, the influence of the dieback on the estuary morphology is evaluated. Subsequently, the recovery of the different dieback scenarios is discussed and compared to the reference run. Finally, the feasibility and limitations of the modelling approach are evaluated.

7.1 Impacts of Mud on Mangrove Colonization

Mangrove species in the natural system colonize within species-specific characteristic hydroperiods (Chapman, 1976, Krauss et al., 2008). The appropriate inundation regime as well as limited hydrodynamic forces are needed for mangrove establishment (Balke et al., 2011). This is included within the model by including inundation stress, with optimal mangrove growth at 50 percent inundation (Fig. 5.8) (Xie et al., 2020) and by including the establishment in a initially bare cell, with a probability of establishment of five percent and under limited bed shear stress.

During the initial colonization of the mangroves within the model domain, differences between the mangrove colonization within the domain with only sand (non-cohesive

sediment) and the domain containing a mud inflow can be observed. The model results show that mud sedimentation enhances bed elevation (Fig. 6.5). This affects the hydroperiods in those areas, as an increase in bed level means that some areas are not inundated any longer. Therefore, less mangroves can colonize due no water availability. This behaviour has also been observed a previous numerical model study, where excessive mud supply led to reduced inundation and vegetation disappearance (Kleinhans et al., 2018). Therefore a correlation was seen between an increase in mud supply and a decrease in vegetation cover (Kleinhans et al., 2018). Comparing those results to the limited data available for the case study shows that the mangrove colonization within the domain which contains mud has more similarities with the case study than the one containing only sand. In both the model and the case study, mangrove colonization occurs close to the channels and on the bars between channels. Additionally, the mangrove colonization in the 'mud scenario' shows a high mangrove coverage within the delta, reflecting what can be seen in the Leichhardt estuary prior to the dieback (Asbridge et al., 2016).

7.2 Model Dieback and Differences to Case Study

Recent studies have shown different possible factors causing the large-scale mangrove dieback in the Gulf in 2015-2016. These factors include unusually hot water temperatures, prolonged severe drought and a temporary drop in sea level by 20 cm (Duke et al., 2017, Duke et al., 2021). It was concluded by Duke et al. (2021) that the temporary sea level drop is very likely related to the dieback event, while the prolonged drought and the high temperatures are likely to be related, but direct evidence is limited. Therefore, Duke et al. (2021) posed the question if the sea level drop alone was sufficient to trigger the dieback event, or if it had been enhanced by the extreme climatic conditions (e.g. drought) during the El Niño event.

Firstly, it was observed that mangrove dieback in the model occurred based on sea level drop and river discharge decrease. Both changes led to a dieback (Fig. 6.9). Therefore, the dieback due to the physical processes of decreased river discharge and sea level are simulated and align with the observations made within the Gulf (Duke et al., 2017, Duke et al., 2021). It was further seen that the highest dieback of mangrove trees occurs when both sea level drop and river discharge decrease are implemented simultaneously, which concurs with the assumption by Duke et al.(2021) that the severe dieback in the Gulf was likely caused by a combination of drivers. Additionally, the results in the SLD & RDD scenario indicate a dieback of more mature, larger trees as concluded due to the changes in numeric and geometric density. This observation was also made within the Gulf when assessing the dieback on the basis of surveys as the smaller, younger trees were found to have the greatest survivorship (Duke et al., 2020).

However, the results show a different dieback pattern along the channel for the model dieback compared to the case study. In the modelled dieback, nearly all mangroves along the channel die during 10 years under the conditions of sea level drop and river discharge decrease (Figure 6.6). While the mangroves along the channel within the case study stay intact during the natural dieback event (Fig. 3.5). This observation can be explained by the differences in bed elevation and channel slope within the model compared to the Leichhardt estuary. The model has more defined channels with a higher slope. Even though limited field data is available for the Leichhardt estuary, the observations made from satellite imagery indicate that the channels are wider and

have a more gradient slope at the inside of the bends. This could not be reflected in the model even though several attempts were made by modifying the bed slope effect (Section 5.5). A potential reason could be the assumption of a constant river discharge (Guo et al., 2015). Thus, the differences in the mangrove death along the main channel can be attributed to the differences of the channel cross-section in those areas. This can be potentially adopted in future research based on the mentioned considerations, e.g. by including more extensive meandering.

Further dieback occurs within the delta of the estuary. When looking at the Leichhardt estuary (Fig. 3.5), all dieback occurs within the backwards lying mangroves of the delta. Within the modelled dieback, this pattern can be seen as mangroves in the back of the delta die (Figure 6.6). However, the dieback area within the delta is smaller than seen in the case study, where a majority of the mangroves within the delta die. There are different potential causes for this divergence. When comparing the dieback area within the model to Figure 7.1, which describes the dieback schematically, the dieback of the mangroves at the seaward side of the saltmarsh-saltpan are reflected within the model run. The mangroves death at the back of the saltpan however is not

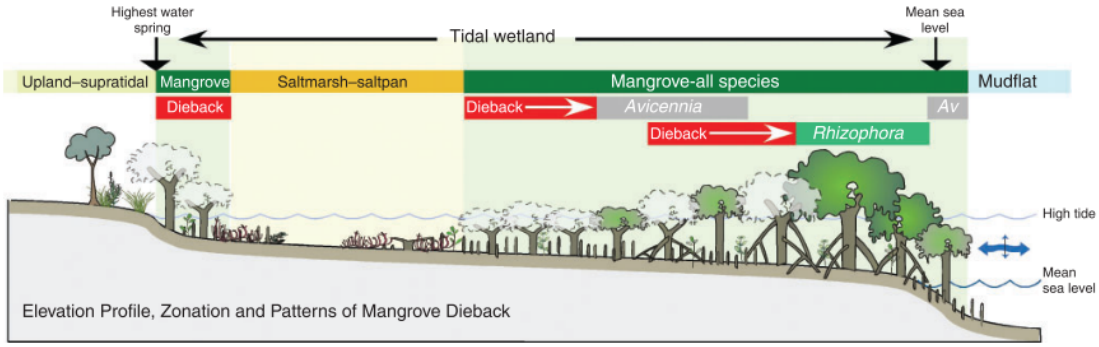

FIGURE 7.1: Cross - section of the Dieback characteristics observed in the Gulf of Carpentaria (Duke et al., 2017).

reflected in the model. On the on hand, this could be due to the facts that the salt flats area is not included within the elevation profile of the model. On the other hand, it could be an indication for the effects of salinity on the dieback. Salinity is not included in the model, meaning that the effect of high salinity due to low freshwater availability within the saltpan is not reflected. Previous literature found an influence of salinity on mangrove growth (Wimmler et al., 2021). In saline and hyper-saline environments mangrove trees can adapt to those conditions, with species-specific strategies due to different salt tolerances (Liang et al., 2008). It was seen that the species A. marina, with increasing salinity, can take up more water from other sources such as fog, dew or rainfall (Nguyen et al., 2017). However, during the dieback in the Gulf, the combined effects of drought and thereby increased soil salinity, increased temperature and dry atmosphere could have lead to the death of mangroves in the hyper-saline soils of the Gulf as no alternative water sources were available (e.g. from fog or rainfall)(Nguyen et al., 2017). Salinity could have therefore played a role in the dieback of the mangroves lining the saltpan areas of the Leichhardt estuary, which would explain differences seen in the dieback area within the delta of the model and case study.

Overall, it can be summarized that despite some differences to the case study, the model dieback showed a dieback as response to sea level drop and river discharge decrease. The comparison of the modelled dieback due to these factors and the dieback

within the case study indicate that the low inundation can be considered responsible for the dieback in certain areas. However, the results further indicate that complex biological and physiological interactions of the mangrove trees could have played a role in the dieback of the mangrove colonizing the hyper-saline soils at the landward fringe of the delta. These complex interactions with soil and surface water salinity and the availability of other water sources are not reflected in the current modelling approach. However, if the causes of the difference seen from the model to the natural system in this study, are based on bed level differences, or the exclusion of salinity, requires further investigation. Thus, the effect of salinity in mangrove dieback within this event and within an estuary in general could be further investigated in future modelling studies including the effects of salinity and salinity distribution. Additionally, further field data is needed to avoid difference in bed elevation and channel slopes.

7.3 Dieback Effects on Morphology and Hydrodynamics

In the years following the dieback, the effects of decrease in mangrove coverage on morphology and hydrodynamics is investigated within the disturbed state scenarios. The effects of the presence of mangrove trees was previously investigated (Section 2.2.2) (Horstman et al., 2013c, Van Maanen et al., 2015, Willemsen et al., 2016, Xie et al., 2020, Gijsman et al., 2021). However, the effects of the sudden absence of mangrove area on morphology and hydrodynamics has been barely investigated previously, in particular on long-term scales (Twilley et al., 1999, Duke et al., 2021). Due to the importance of coastal ecosystems, the ability to predict the changes which occur due to the loss of coastal ecosystems such as mangroves or tidal marshes is important. Temmerman et al. (2012) investigated the effects of the large scale die-off of tidal marsh within the Scheldt estuary (in Belgium). Due to the lack of data regarding the effects of mangrove die-off, the here obtained results from the dieback modelling are compared to the field observations by Temmerman et al. (2012). This allows for the identification of the main processes and for the comparison to the effects of the tidal marsh die-off.

The observed wider and shallower upstream channel within the SLD & RDD scenario were identified to originate from sediment deposition as seen from the increased mud content in those regions. The model results align with the findings that large scale salt marsh die-off enhances sediment infilling in the channels (Temmerman et al., 2012). The effects of the dieback on hydrodynamic parameters are that the velocities on the platform within the delta, where the mangrove dieback occurred, is increased compared to the reference run. Therefore, the absence of mangrove trees which exert a vegetation-induced friction, leads to an increase in flow velocity within the inundated dieback area (Fig. 6.15). This is directly linked to the reduced mud content seen within the delta area compared to the reference run. It can be explained by the decreased sedimentation rates within the dieback area after the die-off due to the increase in flow velocity, as is also observed in the tidal marsh dieback event (Temmerman et al., 2012). Furthermore, the main channel location in the delta area varies for all three scenario. This indicates the influence of mangrove vegetation on the channel pattern, the flow and the formation of creeks.

The physical interactions between the changes in vegetation cover, hydrodynamics, and morphology are summarized in Figure 7.2. The presence of mangrove stems and roots lead to a reduction in flow velocity in the vegetated areas due to their resistance and thereby increased sedimentation. This leads to bed elevation over time. The increased bed level can have positive as well as negative effects on the mangrove cover.

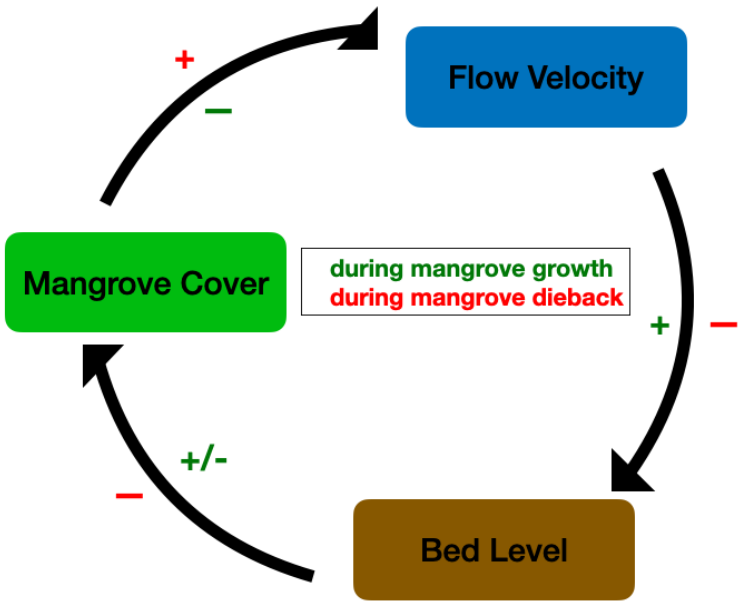

FIGURE 7.2: Overview of the interactions between mangrove cover, flow velocity and bed level elevation during mangrove colonization and mangrove dieback within an estuary.

High bed elevations lead to too low inundation for mangrove growth, while it can also elevate areas which would otherwise be inundated too much for the mangrove growth and thereby become suitable for the colonization of mangroves. The absence of mangroves after the dieback event on the other hand lead to the increase of flow velocity in the affected areas. This in turn can induce a reduced sediment deposition in those areas, leading to a constant or even decreasing bed level in the inundated areas. The bed level reduction in those areas can lead to the area being inundated more frequently which potentially could make the area uninhabitable for the mangroves.

This show clear pattern for areas of mangrove growth and dieback. However, as seen from the difference in channel pattern and sedimentation, this feedback has effects on the whole estuary, changing hydro- and morphodynamics and thereby influencing channel locations. Different influences were observed throughout the estuary indicating a complex interactions on an estuary scale. These processes can potentially increase the vulnerability of coastal wetland in the context of sea level rise due to lower sediment accumulation and increased flow velocities.

7.4 Mangrove Recovery

Following the dieback, the recovery of the mangrove characteristics was modelled by restoring the boundary conditions. It was discussed in the previous section how the absence of mangrove area influences the morphology. These processes have effects on the mangrove recovery. This will be discussed in the following.

Firstly, it has to be noted that before the recovery, the hydrodynamics and mud distribution in the SLD & RDD scenario differ from the reference run and the 16 km seawards removal scenario (Fig. 6.10). The SLD & RDD scenario was simulated over 10 years. Even though morphological change was not allowed during this simulation, the system changed and developed during this time (regarding the mud distribution and

flow velocities) (Fig. 6.10), due to the changes in boundary conditions with a decreased sea level and river discharge. While in the 16 km seawards scenario, the mangroves were removed manually, without any simulation being conducted, meaning that the conditions within the model are the same as before the dieback. After the recovery, it was found that the location of the main channel after the recovery differs between the different simulations (16 km seawards manual removal, SLD & RDD model dieback and the reference run) (Fig. 6.18), indicating the effect of the mangrove vegetation on the channel velocity. This is interpreted to result from the flow focus by the vegetation, leading to higher flow velocities in cross-channel direction and enhancing erosion. Thus, the confinement of the channel between the vegetated bars (Fig. 6.18) leads to an increase in the vertical flow velocity and thereby erosion and shifts the channel further northwards. This observation is in accordance with the observations made by Kleinhans et al. (2018) regarding rivers confined by vegetated bars. Further differences in hydromorphodynamics were observed between the three scenarios, namely differences in bed elevation and flood/ebb velocity ratios on the tidal flats. This show that during the recovery and resettlement of the mangroves, hydro-morphodynamic changes occur due to the difference in mangrove area in the estuary. This shows the two different time scales of the hydromorphodynamic processes and mangrove resettlement, where the hydromorphodynamic changes due to reduced mangrove cover occur faster than the mangrove resettlement.

These processes however exert a feedback on the mangrove vegetation leading to differences in mangrove resettlement and recovery rate between the scenarios. Regarding the mangrove characteristics, it was observed that during the recovery run, the hydraulic resistance is increasing over the 100 years of recovery and with the maturation of the trees (Fig. 6.23b). Thereby, the two dieback scenarios showed different rates of increase in hydraulic resistance. The hydraulic resistance in the SLD & RDD scenario first decreased and then increased more slowly towards the values of the undisturbed reference scenario. As the hydraulic resistance exerted by the mangrove trees is equally related to both the mangrove tree density (trees per m2) and the stem diameter (eq. 5.4, 5.4), the increased hydraulic resistance of more mature trees must be linked to the increased number of root associated with an increased stem diameter (eq. 5.24, 5.7c). Previous field and modelling studies have shown similar observations of a significant contribution of the mangrove roots systems to the imposed friction (Mazda et al., 1997, Horstman et al., 2013b, Kazemi et al., 2021). For the dieback within the natural system that means, that during the recovery when mangroves are resettling and growing again, it takes decades to reach the initial state again in terms of hydraulic resistance and therefore flow velocity attenuation the mangroves offer. Thus, even though there might be a high number of small trees recolonizing after the dieback, the resistance exerted by these trees is smaller than the one exerted by the grown, mature mangroves and their higher number of roots, which dominated the area prior to the dieback. This in turn causes differences in the hydrodynamics and sedimentation processes.

Furthermore, when looking at the sum of the basal area over all runs (Fig. 6.26), it can be seen that the recovery rates are different for the SLD & RDD dieback scenario compared to the 16 km seawards manual removal scenario. The manual removal scenario recovers faster even though the amount of mangrove area removed was almost twice as much as from the model dieback scenario. The same pattern can be seen when looking at the recovery rates[1] according to the average stem diameters in the

[1]Recovery rate is here defined according to equation 5.28, following the previous research by Jones et al. (2018). The recovery rate describes the average percentage of recovery per year measured on the

dieback area of the two dieback scenario. The recovery rate of the average stem diameter for the 16 km seawards scenario (0.9952) exceeds the one of the SLD & RDD dieback scenario (0.7472). This indicates a faster and more complete recovery of the area where the dieback occurred within the 16 km seawards scenario. Furthermore, the average stem diameters in the dieback areas of the two dieback scenarios show an incomplete recovery on the basis of median and varianz in diameter as compared to the undisturbed reference. When looking at the ratio of the actual growth to the optimal growth, it was seen that especially for the SLD & RDD scenario, the ratio is more varying and shows lower values than seen during the colonization, indicating a slower growth and higher stresses in the dieback areas as compared to the initial colonization (Fig. 6.27).

The differences in hydromorphodynamics over the system therefore lead to differences in the recovery time in the dieback scenarios. Three main factors of difference can thereby be identified. Firstly, the difference in hydromorphodynamics prior to the recovery as the different methods of mangrove dieback lead to a different recovery of the SLD & RDD scenario. Secondly, as mangrove recovery was previously found to be site-dependent (Twilley et al., 1999, Field, 2007, Ketelaars et al., 2013), the differences in the recovery rates of the two dieback scenarios can also be connected to the location where the recovery occurred. The recovery within the delta therefore would be faster than the recovery in the back of the delta and along the channel. This side dependence here originated from difference in the local hydromorphodynamics in the different sides, making some sides more and other less suitable for mangrove recovery. Thirdly, the difference in mangrove cover during the recovery leading to differences in hydromorphodynamics. This is caused by the differences in time scales of the hydromorphodynamic processes and the resettlement, as shown above. Thus, it can be said that due to mangrove dieback, unfavorable conditions in terms of morpho- and hydrodynamics can develop, slowing down recovery. This further indicates a hysteresis during the recovery, as the previous morphodynamic change during the dieback influences the recovery of the mangrove characteristics even though the driving force (changed boundary condition) is restored. This is seen here with the slower recovery for the SLD & RDD model dieback due to morphological and hydrodynamic changes during the dieback. This process was previously observed in mangrove forests, showing that the relationship between mangrove wetland cover and average annual rainfall existing in a state of hysteresis (Duke et al., 2019).

For the natural system this suggests that there are different rates of recovery which depend on the duration of the disturbance and the severity of the dieback in terms of change of the hydrodynamic and morphology. This is in accordance with observations made by Twilley et al. (1999), indicating that trajectories of restoration efforts are dependent on conditions of the initial disturbance, site modifications, the recruitment of new individuals, and environmental constraints of ecogeomorphic settings. Therefore, regarding the recovery projections seen in the model, it has to be considered that in nature, additional constraints hinder mangrove growth, such as salinity and availability of propagules leading to many failures in mangrove restoration (Twilley et al., 1999, Winterwerp et al., 2013). This could lead to potential differences in the recovery in the natural system as compared to the projections from the model. In addition, there are external influences. It needs to be considered that in nature a period of 100 years without disturbances is unlikely. Considering the average sea level rise of 8-9

basis of the average stem diameter. Thus, when the recovery rate equals to 1, 1 percent of recovery is reached per years and full recovery will be reached after 100 years.

mm/year in the southern Gulf, the increasing severity of tropical cyclones in the Gulf and the high potential for flooding (Duke et al., 2020, Duke et al., 2021), rather increasing disturbances and stresses are exerted on the mangrove forest. In fact, during a monitoring trip in 2019, Duke et al. (2020) found that the two cyclones which occurred in December 2018 and March 2019 caused serious further damage to the vulnerable remaining mangrove forests in the Gulf, hindering the recovery process.

Therefore, it can be said that the recovery even under optimal conditions, as simulated within this study, is slow compared to the initial colonization, while further disturbances and limiting factors would hinder mangrove recovery in the natural system further. In accordance with Duke et al. (2020) and Duke et al. (2021), it can thus be concludes that this modelling study and the observation of the recent events demonstrate that a full recovery of the mangroves is unlikely to be reaches as disturbances re-occur too frequently for the observed recovery rates. This rather suggest the development of an alternative stable state over the full recovery after this large-scale dieback event. In order to link these observations further, future studies could include disturbances during the mangrove recovery, such as sea level rise or effect of cyclones. Of importance for mangrove restoration could also be a process previously observed for the recovery of a tidal marsh system (van Belzen et al., 2017). It was concluded from time series of remotely sensed imagery, that the recovery rate of the system from inundation stress decreased with increasing inundation stress. This process is called "critical slowing down" and was proposed to be a useful tool in ecosystem management to identify tipping points of disturbance on the basic of recovery rates (van Belzen et al., 2017, van de Leemput et al., 2018). The differences in recovery rates in this model were seen to originate from the differences of the hydromorphodynamics causing unfavorable conditions for mangrove resettlement in the dieback areas. An increased change in hydromorphodynamics during the recovery was shown here (SLD & RDD scenario), leads to a slower recovery. Therefore, the difference in mangrove characteristics recovery rate in this study raises the question whether the process of "critical slowing down" may also apply to mangrove vegetation recovery.

7.5 Evaluation of the Modelling Approach

During this discussion different aspects regarding the modelling approach became apparent. In the following, the model approach will be discussed and evaluated regarding the ability to reflect the patterns of mangrove coverage and the bathymetry seen within the case study of the Leichhardt estuary before and after the dieback event.

Regarding the morphology, it was found when comparing the bathymetry of the model domain and the Leichhardt estuary, that the model is not able to reflect the extend of meandering seen in the case study (Fig.5.6 & 5.2). Furthermore, the channel slopes do not fully resemble the case study. In the case study mangrove growth occurs also within the slip-off slope of the meanders (Figure 3.5). Within the inside of the bend, a gradual slope provides the conditions for mangrove growth (Lymburner et al., 2020). In the model, these conditions are not reflected, as the meanders are less formed out compared to the case study and the bed slopes are therefore steeper. This results in a smaller area within the bend suitable for mangrove growth, leading to different pattern in mangrove colonization. Additionally, this leads to differences in the mangrove dieback as discussed previously. A further factor to consider when looking at the mud accumulation within the model is that in the natural system wash events occur,

redistributing the accumulated sediment due to high flow events (e.g. high river discharge during the wet season). This process is not considered within the model as the discharge is constant over time, potentially causing different patterns in mud accumulation and distribution in the model. According to Choi et al. (2013), temporally varying discharge and the occurrence of flood events in the real system can further lead to erosion of mud on bars and mudflat, and thereby cause bed level decrease. This would lead to more suitable area for mangrove colonization. However, detailed field data is required to realize this. Furthermore, the bed levels of the delta might be different from the case study (e.g. missing saltpan) as the dieback pattern observed in the back of the delta differ from the real system.

The difference seen in the dieback pattern could also be attributed to limitations in the mangrove vegetation model. Mangrove growth is a complex process. It depends on many factors such as salinity, nutrient availability, temperature, inter- and intra-species interaction and below ground processes such as the water uptake from the soil and the feedback of the vegetation on the availability of that water (Van Maanen et al., 2015, Peters et al., 2020, Wimmler et al., 2021). So can varying salinity and inter-species competition for example have an effect on mangrove growth (Burchett et al., 1989, Ye et al., 2005, Jiang et al., 2015, Kodikara et al., 2018, Barik et al., 2018). In this model solely intra-species competition and inundation stress was considered as growth limiting factors, to reduce the complexity of the model and to test the hypothesis of the main influencing factors (sea level drop and river discharge decrease) causing the dieback. On the Western Australian coast however, it was found that the 2015-2016 ENSO event, and the associated sea level drop has led to an enhanced soil salinity, potentially responsible for mangrove cover loss and slow recovery (Lovelock et al., 2017). Furthermore, it has to be considered that inter-species competition as well as the competition between mangroves and terrestrial plants and salt marshes is not included. That means, when the inundation reaches zero, unfavorable conditions for mangrove growth are present. However, in the natural system, this area could be occupied by another mangrove species, salt marsh or a terrestrial species which outcompetes the mangrove forest under the changed conditions (Ball, 1980, Feller et al., 2010). Research regarding these processes of competition and bistability at the interface of these ecotones is currently undertaken (Sternberg et al., 2007, Jiang et al., 2015). This therefore raises two questions for future investigations and studies. Firstly, the question arises whether salinity has an important influence on the dieback and the mangrove recovery and how inter-species competition could affect the mangrove recovery. And secondly, the question is whether there is a likelihood of an ecotone shift after a large-scale dieback event.

Additionally, in the coupling of the two models, simplifications were adopted to reduce the complexity of the model. The morphodynamic effects such as the settling and sediment capture on the trees and pneumatophores or roots are not included (Van Maanen et al., 2015). Furthermore, the organic matter accretion and the associated morphodynamic changes within the mangrove forest is a complex process. While biotic processes such as root production were previously found to contribute to soil volume increase in mangrove forests, other processes such as subsidence, decomposition and compaction can cause elevation deficit (Mckee et al., 2007, McKee, 2011). These counterbalancing processes are simultaneously occurring in nature, but they are highly site-dependent. Therefore, the below-ground process including organic matter accretion, subsidence and sediment compaction is neglected in this study based on the assumption that they counterbalance each other to a large extend. Regarding the

hydrodynamic processes considered here, the effect of the trees and roots on the hydrodynamics are included by decreasing the drag coefficient. Further effects such as the influence on the turbulent field are not considered. Additionally, the effects of waves are not included in the model which could potentially lead to over estimation of mangrove resilience as mangrove do not need to dissipate the wave energy within this model. Therefore, the implications of this on the recovery projections have to be considered. The inclusion of only the two stress factors and the idealised boundary conditions (tide and river) could lead to a higher likelihood of mangrove recovery as compared to the natural case. In nature, in addition to these two constraints specified in the model, there are more limiting factors for natural mangrove recovery processes, such as salinity, available seeds or propagules, and frequent extreme weather events, impeding mangrove colonization. This might also be the reason why there are still many failures for mangrove restoration projects (Winterwerp et al., 2013).

In summary, the main processes of mangrove development, such as the self-thinning process and the growth limitation due to inundation stress (too much and not enough inundation) are reflected in this modelling approach. The approach taken here, is sufficient to reflect the main feedback and processes occurring in the estuaries mangrove forest in order to model the dieback event and the subsequent recovery. Insights were gained in the processes and interactions of mangrove forest, morphology and hydrodynamics within an estuarine system. Even though some questions remain for further research, the overall results show a good indication of the feedback driving the estuaries ecosystem and the dieback event. Furthermore, insights were gained in the recovery processes of the mangroves. These insights offer valuable information for conservation of mangroves in future dieback events and for restoration projects. Additionally, within this discussion it became clear, that the results from a modelling study are sensitive on the choices made within the model. Therefore, a need for further complementary field data becomes evident to calibrate and further validate the model.

Chapter 8

Conclusion

The research conducted in this study leads to four main conclusion, which will be pointed out in the following.

Firstly, the results from the dieback modelling (in phase 3) have shown that the model shows mangrove area dieback due to sea level drop and river discharge decrease. It was seen that both effects separately cause dieback, but the combined effect of both factors leads to most severe mangrove dieback. Comparing the dieback pattern to the natural system has indicated that similar pattern can be observed, while the dieback in the delta area has a smaller extend in the model. This suggests that the dieback adjacent to the saltmarsh-saltpan area in the natural case was influences by factors not considered in the model. Therefore, the hypothesis from field observations identifying drought conditions and especially sea level drop as the main factors causing the dieback event could be validated within this model, while as the same time suggesting that further factors played a role in the dieback in certain areas.

Secondly, during phase 4, it was seen that the mangrove area dieback leads to long-term morphological changes of channel shifting, channel infilling, increase in flow velocity in the previously vegetated area, decrease of flow velocity in the channel area and decreased sedimentation in the affected areas. Similar effect were previously observed in a tidal marsh die-off study. The hydromorphodynamic change also occurs during the recovery, due to the differences in mangrove cover. This shows the two timescales of faster hydrodynamic change and slower mangrove resettlement. Therefore, a full recovery regarding the stem diameter in the affected areas is not occurring and the recovery rate for the SLD & RDD scenario is slower than for the 16 km manual removal scenario, due to the differences in hydromorphodynamics in the affected areas. This indicates a hysteresis in the feedback between the changes in morphology and hydrodynamics and the recovery of the mangrove characteristics. In summary, the mangrove area dieback leads to morphological and hydrodynamic change within the estuary which in turn can a negative effect in the resettlement of mangroves in the dieback area, as it can slow down recovery. This can potentially lead to development of alternative stable states over a recovery to previous conditions.

Thirdly, the study has shown that the model produces similar patterns of mangrove coverage and mangrove dieback as occurred in the Leichhardt estuary. This similarity thus, leads to the conclusion that aspects of the natural system can be simulated in the model. Therefore, the model offers insights into the processes governing the mangrove forest structure and tree cover within the estuary. Furthermore, during the comparison with the dieback event in case study, the model gave indication to the extend of dieback that can be attributed to the drop in sea level and decrease in river

discharge. Overall, the model has shown the complexity of the feedback between mangrove vegetation and the hydrmorphodynamic process in an estuary.

Lastly, the model application has shown a need for further field data, such as hydrodynamic parameters, flow currents and river discharge, morphodynamic sediment conditions, characteristic bed level outline of the estuary and vegetation dimensions, to calibrate and design and validate the model. Additionally, it was shown that the changes in hydrodynamics and morphodynamics due to the mangrove dieback lead to the loss of the coastal protection services. This combined with the slow recovery rates and the uncertainty in recovery due to the high dependence on the local hydrodynamic conditions, stresses the importance of mitigating such events in the future and conserve mangrove forests. The future effects of climate change such as sea level rise and an increase in extreme weather events (e.g. storms and droughts) puts mangrove forests at risk of dieback and adds stresses to those valuable ecosystems. Apart from climate change mitigation, it is therefore important to manage mangroves forests in conservation efforts, promoting further research and establish guidelines to protect mangroves. In that, models can represent a valuable tool to understand the processes governing the the mangrove coverage.

Appendix A

Appendix

A.1 Model Design Runs

During the model design different simulations were conducted for the choice of the initial domain. In the following the bathymetries are illustrated for those simulations after 200 or 400 of initial estuary formation within Delft3D (5, Modelling Overview, Phase 0). The initial bathymetry varies in initial channel outline between a straight channel, a sinus channel and an idealized meandering channel (Section 5.1.2). Furthermore, the simulations vary in the Ashld and Islope values, as well as in the tidal signal (diurnal and semidiurnal). Additionally, different river discharges of 50, 100 and 300 m3/s were simulated.

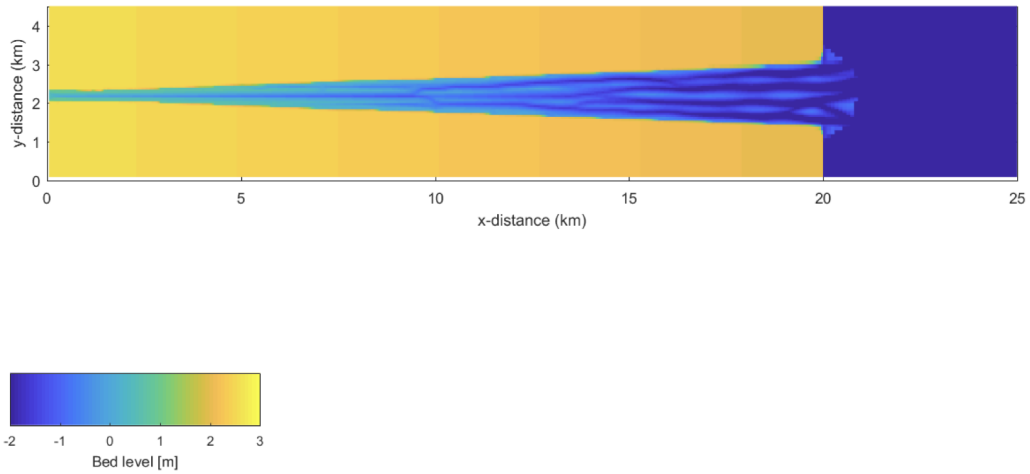

FIGURE A.1: Straight Q50 Y200

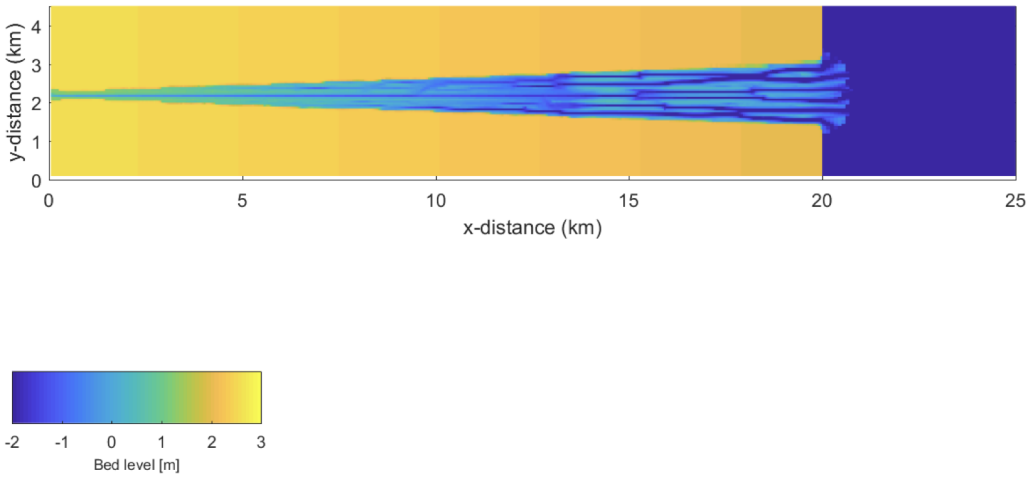

FIGURE A.2: Straight Q50 IK A10 Y200

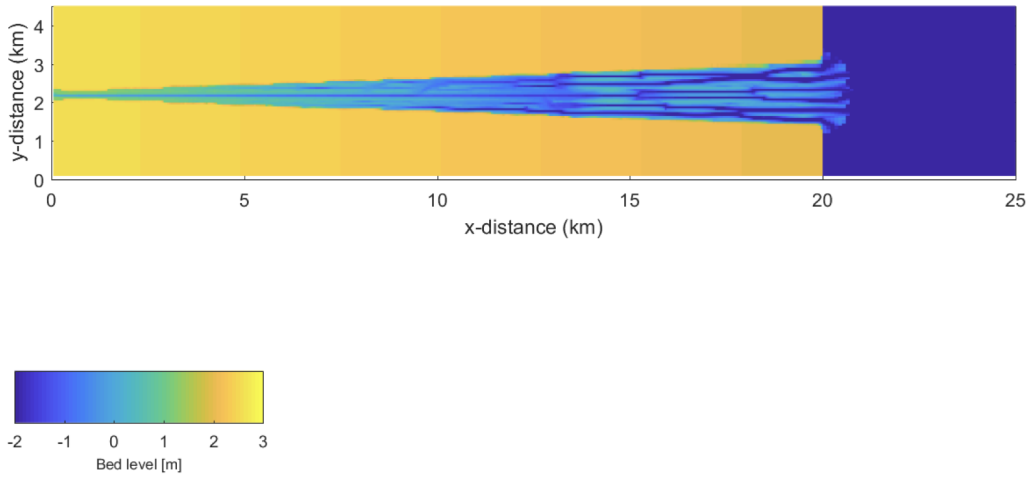

FIGURE A.3: Straight Q50 IK A100 Y200

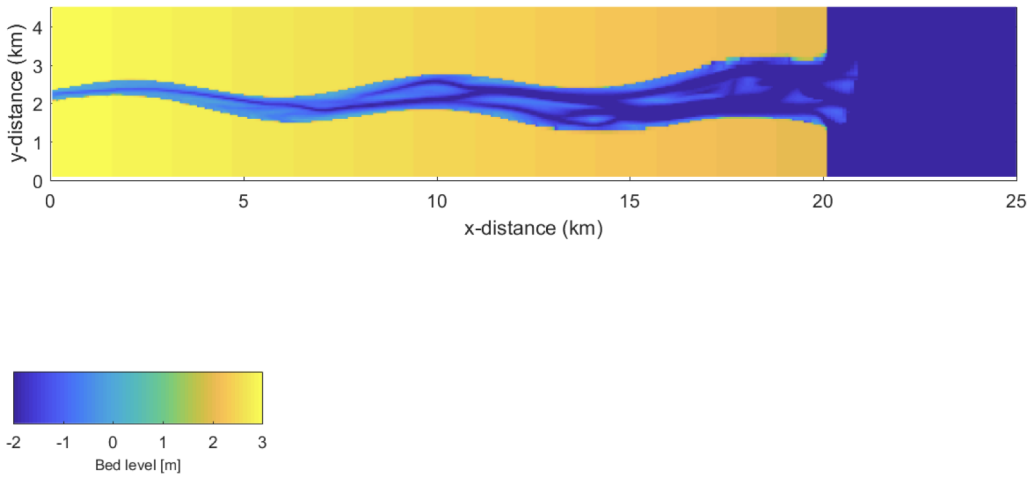

FIGURE A.4: Sinus shallower Q50 Y200

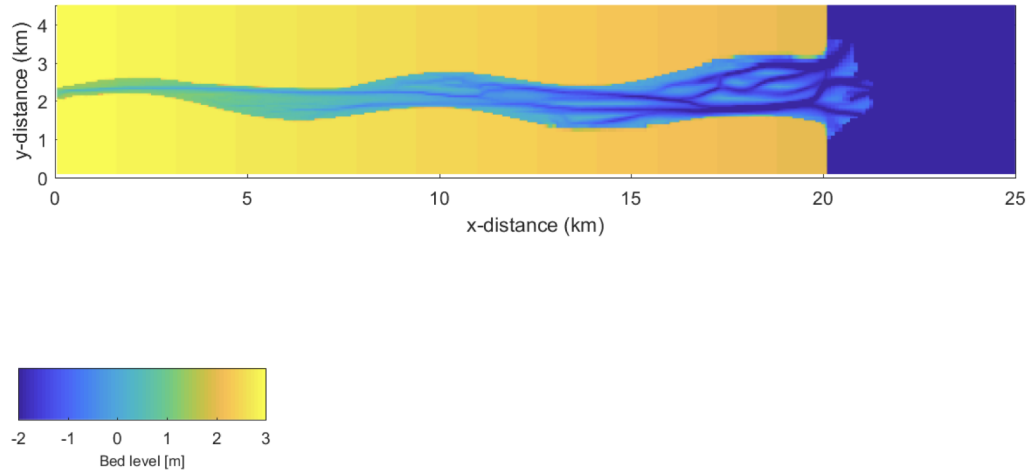

FIGURE A.5: Sinus Q50 shallower2 Y200

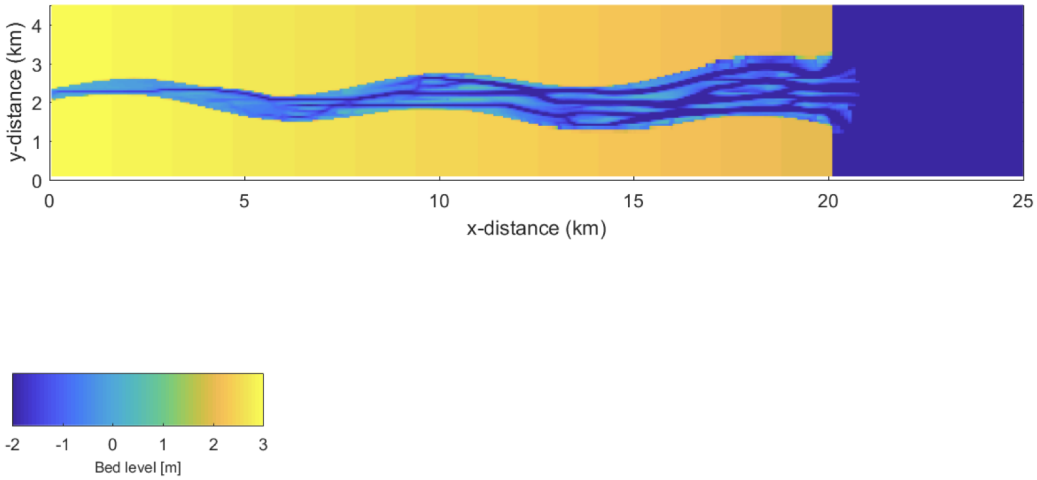

FIGURE A.6: Sinus Q50 shallower IK A10 Y200

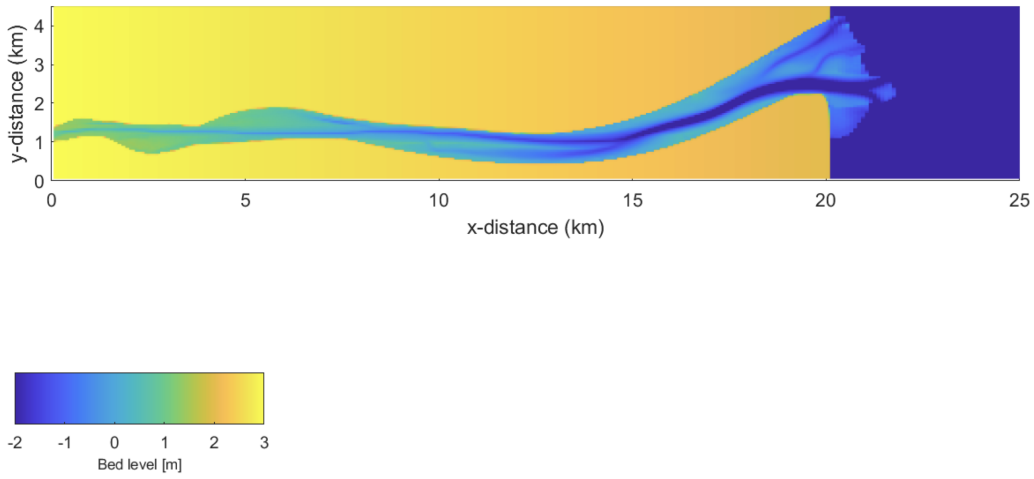

FIGURE A.7: Q50 FK A0.1 Y400 diurnal

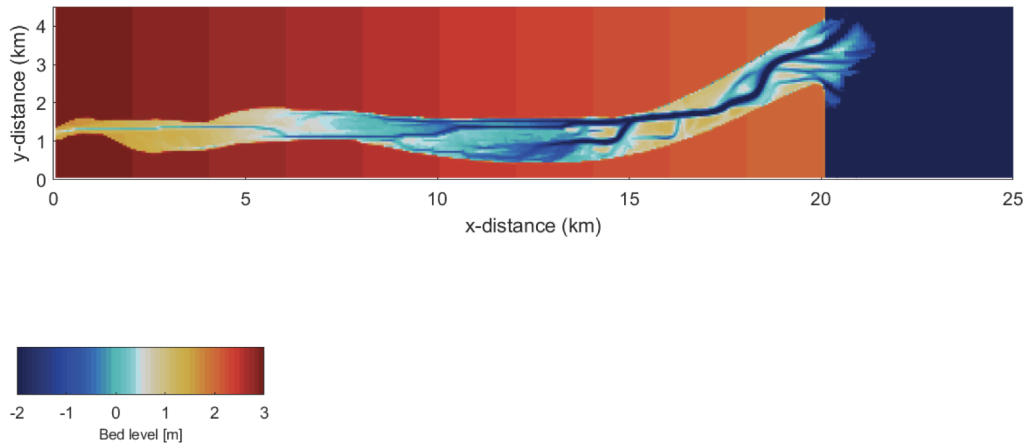

FIGURE A.8: Q50 IK A100 diurnal Y400

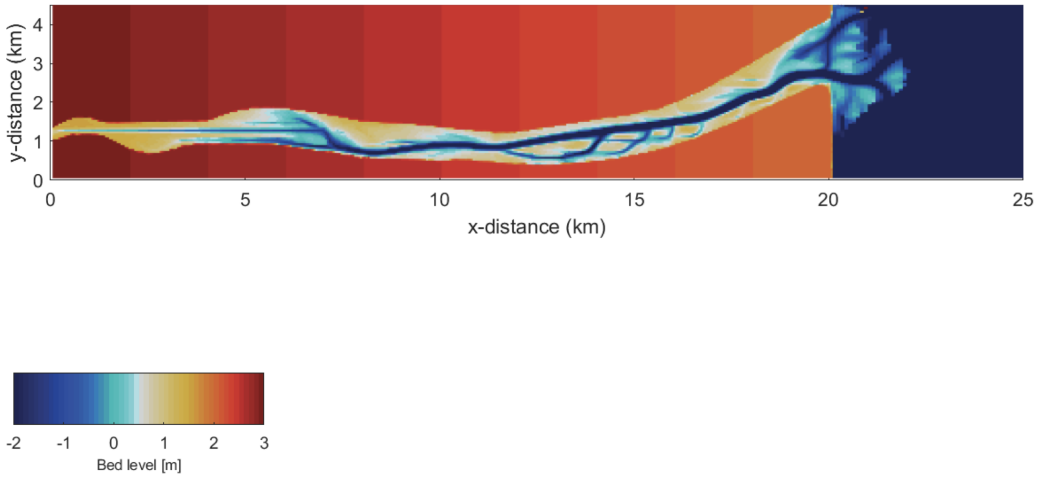

FIGURE A.9: Q50 IK A100 semidiurnal Y400

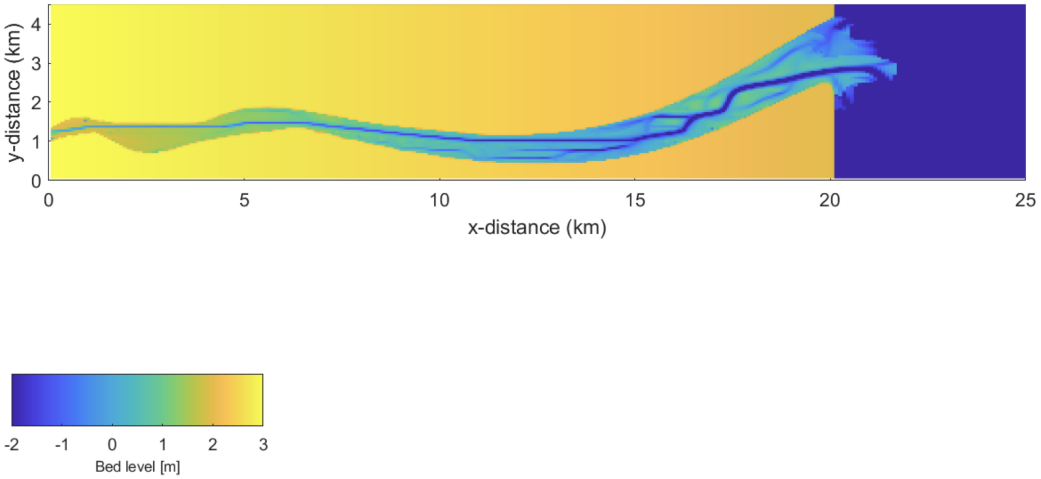

FIGURE A.10: Q100 IK A100 diurnal Y400

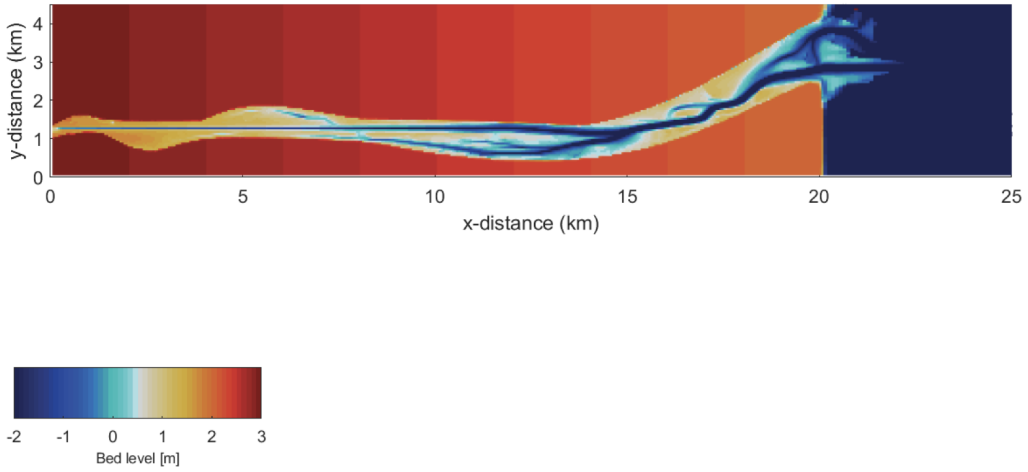

FIGURE A.11: Q100 IK A100 semidiurnal Y200

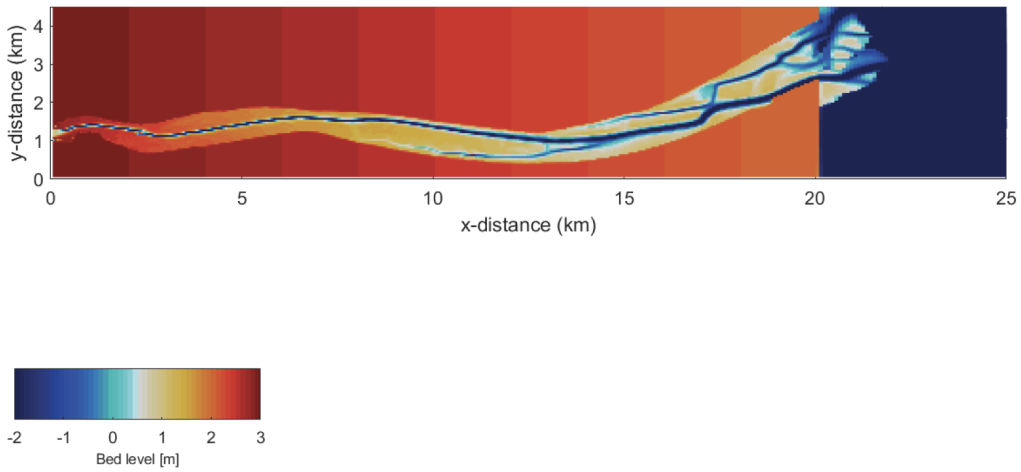

FIGURE A.12: Q300 IK A100 semidiurnal Y400

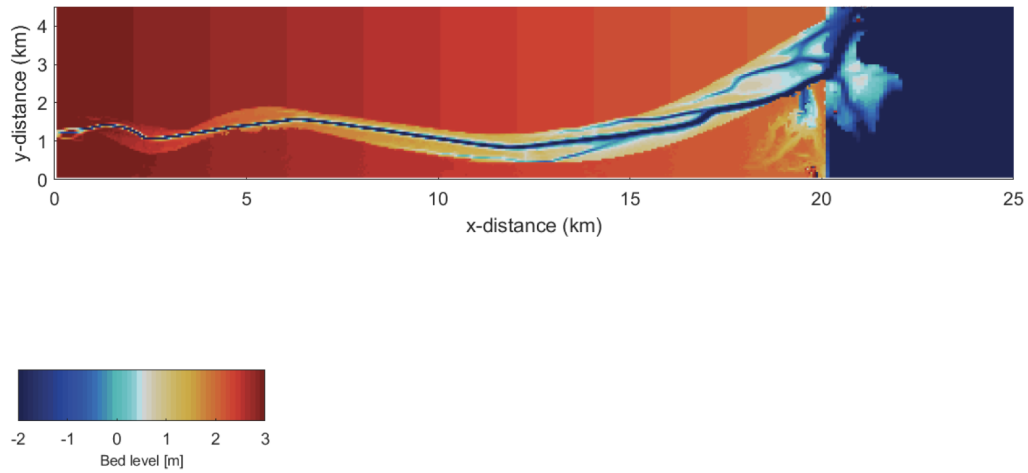

FIGURE A.13: Q400 IK A100 semidiurnal Y200

Bibliography

Abhik, S., Hope, P., Hendon, H. H., Hutley, L. B., Johnson, S., Drosdowsky, W., Brown, J. R., & Duke, N. C. (2021). Influence of the 2015–2016 El Niño on the record-breaking mangrove dieback along northern Australia coast. *Scientific Reports*, *11*(1), 1–12. https://doi.org/10.1038/s41598-021-99313-w

Accad, A., Li, J., Dowling, R., Neldner, V. J., & Turpin, G. (2019). *Mangrove dieback in the Gulf of Carpentaria: baseline for monitoring future trajectory in Queensland* (tech. rep.). Queensland Herbarium, Queensland Department of Environment and Science. Brisbane.

Akter, R., Asik, T. Z., Sakib, M., Akter, M., Sakib, M. N., Al Azad, A. S., Maruf, M., Haque, A., & Rahman, M. M. (2019). The Dominant Climate Change Event for Salinity Intrusion in the GBM Delta. *Climate*, *7*(5), 1–23. https://doi.org/10.3390/cli7050069

Alongi, D. M. (2014). Carbon cycling and storage in mangrove forests. *Annual Review of Marine Science*, *6*, 195–219. https://doi.org/10.1146/annurev-marine-010213-135020

Amma, P. K. G., & Bhaskaran, P. K. (2020). Role of mangroves in wind-wave climate modeling – A review. *Journal of Coastal Conservation*, *24*(2). https://doi.org/10.1007/s11852-020-00740-0

Amrit, C., van Rees, F., de Lucas Pardo, M., & van Wesenbeeck, B. (2021). *Ecological mangrove restoration with permeable structures: monitoring report* (tech. rep.). EcoShape.

Asbridge, E., Lucas, R., Rogers, K., & Accad, A. (2018). The extent of mangrove change and potential for recovery following severe Tropical Cyclone Yasi, Hinchinbrook Island, Queensland, Australia. *Ecology and Evolution*, *8*(21), 10416–10434. https://doi.org/10.1002/ece3.4485

Asbridge, E., Lucas, R., Ticehurst, C., & Bunting, P. (2016). Mangrove response to environmental change in Australia's Gulf of Carpentaria. *Ecology and Evolution*, *6*(11), 3523–3539. https://doi.org/10.1002/ece3.2140

Ashworth, P. J., Best, J. L., & Parsons, D. R. (2015). *Fluvial-Tidal Sedimentology*.

Baar, A. W., Boechat Albernaz, M., van Dijk, W. M., & Kleinhans, M. G. (2019). Critical dependence of morphodynamic models of fluvial and tidal systems on empirical downslope sediment transport. *Nature Communications*, *10*(1). https://doi.org/10.1038/s41467-019-12753-x
Use to reason why the parameters in Delft3D were chosen.

Balke, T., Bouma, T. J., Horstman, E. M., Webb, E. L., Erftemeijer, P. L., & Herman, P. M. (2011). Windows of opportunity: Thresholds to mangrove seedling establishment on tidal flats. *Marine Ecology Progress Series*, *440*, 1–9. https://doi.org/10.3354/meps09364

Ball, M. C. (1980). Patterns of secondary succession in a mangrove forest of Southern Florida. *Oecologia*, *44*(2), 226–235. https://doi.org/10.1007/BF00572684

Baptist, M. J., Babovic, V., Uthurburu, J. R., Keijzer, M., Uittenbogaard, R. E., Mynett, A., & Verwey, A. (2007). On inducing equations for vegetation resistance. *Journal of Hydraulic Research*, *45*(4), 435–450. https://doi.org/10.1080/00221686.2007.9521778

Barik, J., Mukhopadhyay, A., Ghosh, T., Mukhopadhyay, S. K., Chowdhury, S. M., & Hazra, S. (2018). Mangrove species distribution and water salinity: an indicator species approach to Sundarban. *Journal of Coastal Conservation*, *22*(2), 361–368. https://doi.org/10.1007/s11852-017-0584-7

Bathmann, J., Peters, R., Naumov, D., Fischer, T., Berger, U., & Walther, M. (2020). The MANgrove–GroundwAter feedback model (MANGA) – Describing belowground competition based on first principles. *Ecological Modelling*, *420*(February), 108973. https://doi.org/10.1016/j.ecolmodel.2020.108973

Berger, U., & Hildenbrandt, H. (2000). A new approach to spatially explicit modelling of forest dynamics: Spacing, ageing and neighbourhood competition of mangrove trees. *Ecological Modelling*, *132*(3), 287–302. https://doi.org/10.1016/S0304-3800(00)00298-2
Papers to include other parameters (drought, temp, ...)

Berger, U., Rivera-Monroy, V. H., Doyle, T. W., Dahdouh-Guebas, F., Duke, N. C., Fontalvo-Herazo, M. L., Hildenbrandt, H., Koedam, N., Mehlig, U., Piou, C., & Twilley, R. R. (2008). Advances and limitations of individual-based models to analyze and predict dynamics of mangrove forests: A review. *Aquatic Botany*, *89*(2), 260–274. https://doi.org/10.1016/j.aquabot.2007.12.015
Review of IBM for Mangroves out there!!

Boechat Albernaz, M., Roelofs, L., Pierik, H. J., & Kleinhans, M. G. (2020). Natural levee evolution in vegetated fluvial-tidal environments. *Earth Surface Processes and Landforms*, *45*(15), 3824–3841. https://doi.org/10.1002/esp.5003
Use to reason why the parameters in Delft3D were chosen.

Botkin, D. B., Janak, J. F., & Wallis, J. R. (1972). Some Ecological Consequences of a Computer Model of Forest Growth. *Journal of Ecology*, *60*(3), 849–872. https://doi.org/https://doi.org/10.2307/2258570

Braat, L., Van Kessel, T., Leuven, J. R., & Kleinhans, M. G. (2017). Effects of mud supply on large-scale estuary morphology and development over centuries to millennia. *Earth Surface Dynamics*, *5*(4), 617–652. https://doi.org/10.5194/esurf-5-617-2017

Broekema, Y. (2013). Hydrodynamic modelling of a mangrove system in Singapore.

Brown, S., & Nicholls, R. J. (2015). Subsidence and human influences in mega deltas: The case of the Ganges-Brahmaputra-Meghna. *Science of the Total Environment*, *527-528*, 362–374. https://doi.org/10.1016/j.scitotenv.2015.04.124

Brückner, M. Z., Braat, L., Schwarz, C., & Kleinhans, M. G. (2020). What Came First, Mud or Biostabilizers? Elucidating Interacting Effects in a Coupled Model of Mud, Saltmarsh, Microphytobenthos, and Estuarine Morphology. *Water Resources Research*, *56*(9). https://doi.org/10.1029/2019WR026945

Brückner, M. Z., Schwarz, C., Coco, G., Baar, A., Boechat Albernaz, M., & Kleinhans, M. G. (2021). Benthic species as mud patrol - modelled effects of bioturbators and biofilms on large-scale estuarine mud and morphology. *Earth Surface Processes and Landforms*, *46*(6), 1128–1144. https://doi.org/10.1002/esp.5080
Use to create Delft3D hydrdynamic Domain!

Burchett, M. D., Clarke, C. J., Field, C. D., & Pulkownik, A. (1989). Growth and respiration in two mangrove species at a range of salinities. *Physiologia Plantarum*, *75*(2), 299–303. https://doi.org/10.1111/j.1399-3054.1989.tb06185.x

Burns, B. R., & Ogden, J. (1985). The demography of the temperate mangrove [Avicennia marina (Forsk.) Vierh.] at its southern limit in New Zealand. *Australian Journal of Ecology*, *10*(2), 125 –133.

Chapman, P. C. (1976). *Mangrove Vegetation* (J. Cramer, Ed.).

Chen, Q., Li, Y., Kelly, D. M., Zhang, K., Zachry, B., & Rhome, J. (2021). Improved modeling of the role of mangroves in storm surge attenuation. *Estuarine, Coastal and Shelf Science*, *260*(February), 107515. https://doi.org/10.1016/j.ecss.2021.107515

Chen, R., & Twilley, R. R. (1998). A gap dynamic model of mangrove forest development along gradients of soil salinity and nutrient resources. *Journal of Ecology*, *86*(1), 37–51. https://doi.org/10.1046/j.1365-2745.1998.00233.x
First Mangrove Model (gab model), basis for Danghans model! formulas to include salinity and temperature! GROWTH FUNCTION!

Choi, K., Hong, C. M., Kim, M. H., Oh, C. R., & Jung, J. H. (2013). Morphologic evolution of macrotidal estuarine channels in Gomso Bay, west coast of Korea: Implications for the architectural development of inclined heterolithic stratification. *Marine Geology*, *346*, 343–354. https://doi.org/10.1016/j.margeo.2013.10.005

Clarke, P. J. The population dynamics of the mangrove Avicennia marina; demographic synthesis and predictive modelling (Y.-S. Wong & N. F. Y. Tam, Eds.). In: In *Asia-pacific symposium on mangrove ecosystems* (Y.-S. Wong & N. F. Y. Tam, Eds.). Ed. by Wong, Y.-S., & Tam, N. F. Y. Dordrecht: Springer Netherlands, 1995, 83–88. ISBN: 978-94-011-0289-6.

Comley, B. W., & McGuinness, K. A. (2005). Above- and below-ground biomass, and allometry, of four common northern Australian mangroves. *Australian Journal of Botany*, *53*(5), 431–436. https://doi.org/10.1071/BT04162
Use to validate why mangrove model parameters choosen (max stem diameter).

Costanza, R., de Groot, R., Sutton, P., van der Ploeg, S., Anderson, S. J., Kubiszewski, I., Farber, S., & Turner, R. K. (2014). Changes in the global value of ecosystem services. *Global Environmental Change*, *26*(1), 152–158. https://doi.org/10.1016/j.gloenvcha.2014.04.002

Dalrymple, R. W., & Choi, K. (2007). Morphologic and facies trends through the fluvial-marine transition in tide-dominated depositional systems: A schematic framework for environmental and sequence-stratigraphic interpretation. *Earth-Science Reviews*, *81*(3-4), 135–174. https://doi.org/10.1016/j.earscirev.2006.10.002

de Mutsert, K., Lewis, K., Milroy, S., Buszowski, J., & Steenbeek, J. (2017). Using ecosystem modeling to evaluate trade-offs in coastal management: Effects of large-scale river diversions on fish and fisheries. *Ecological Modelling*, *360*, 14–26. https://doi.org/10.1016/j.ecolmodel.2017.06.029

de Vriend, H. J., Zyserman, J., Nicholson, J., Roelvink, J. A., Péchon, P., & Southgate, H. N. (1993). Medium-term 2DH coastal area modelling. *Coastal Engineering*, *21*(1-3), 193–224. https://doi.org/10.1016/0378-3839(93)90050-I

Deltares. (2021). *Delft3D-FLOW, User Manual* (tech. rep.). Deltares. Delft, The Netherlands.

Doyle, T. W., Girod, G. F., & Books, M. A. (2003). *Modeling Mangrove Forest Migration Along the Southwest Coast of Florida Under Climate Change* (tech. rep.). Louisiana State University Graphic Services, Gulf Coast Climate Change Assessment Council (GCRCC).

Doyle, T. W., & Girod, G. F. The Frequency and Intensity of Atlantic Hurricanes and Their Influence on the Structure of South Florida Mangrove Communities (H. F. Diaz & R. S. Pulwarty, Eds.). In: In *Hurricanes* (H. F. Diaz & R. S. Pulwarty,

Eds.). Ed. by Diaz, H. F., & Pulwarty, R. S. Springer, 1997. Chap. 6, pp. 109–120. https://doi.org/10.1007/978-3-642-60672-4_6.

Duke, N., Mackenzie, J., Kovacs, J., Staben, G., Coles, R., Wood, A., & Castle, Y. (2020). *Assessing the Gulf of Carpentaria mangrove dieback 2017 – 2019 Volume 1 : Aerial surveys* (Vol. Vol. 1).

Duke, N. C., Field, C., Mackenzie, J. R., Meynecke, J. O., & Wood, A. L. (2019). Rainfall and its possible hysteresis effect on the proportional cover of tropical tidal-wetland mangroves and saltmarsh-saltpans. *Marine and Freshwater Research*, *70*(8), 1047–1055. https://doi.org/10.1071/MF18321

Duke, N. C., Hutley, L. B., Mackenzie, J. R., & Burrows, D. Processes and Factors Driving Change in Mangrove Forests: An Evaluation Based on the Mass Dieback Event in Australia's Gulf of Carpentaria (J. Canadell & R. Jackson, Eds.). In: In *Ecosystem collapse and climate change* (J. Canadell & R. Jackson, Eds.). Ed. by Canadell, J., & Jackson, R. Springer, 2021, pp. 221–264. https://doi.org/10.1007/978-3-030-71330-0_9.

Duke, N. C., Kovacs, J. M., Griffiths, A. D., Preece, L., Hill, D. J., Van Oosterzee, P., Mackenzie, J., Morning, H. S., & Burrows, D. (2017). Large-scale dieback of mangroves in Australia's Gulf of Carpentaria: A severe ecosystem response, coincidental with an unusually extreme weather event. *Marine and Freshwater Research*, *68*(10), 1816–1829. https://doi.org/10.1071/MF16322

Duong, T. M., Ranasinghe, R., Thatcher, M., Mahanama, S., Wang, Z. B., Dissanayake, P. K., Hemer, M., Luijendijk, A., Bamunawala, J., Roelvink, D., & Walstra, D. (2018). Assessing climate change impacts on the stability of small tidal inlets: Part 2 - Data rich environments. *Marine Geology*, *395*(April 2016), 65–81. https://doi.org/10.1016/j.margeo.2017.09.007

Elahi, M. W., Jalón-Rojas, I., Wang, X. H., & Ritchie, E. A. (2020). Influence of Seasonal River Discharge on Tidal Propagation in the Ganges-Brahmaputra-Meghna Delta, Bangladesh. *Journal of Geophysical Research: Oceans*, *125*(11), 1–19. https://doi.org/10.1029/2020JC016417

Elmilady, H., van der Wegen, M., Roelvink, D., & van der Spek, A. (2020). Morphodynamic Evolution of a Fringing Sandy Shoal: From Tidal Levees to Sea Level Rise. *Journal of Geophysical Research: Earth Surface*, *125*(6), 1–21. https://doi.org/10.1029/2019JF005397

Fagherazzi, S., Bryan, K. R., & Nardin, W. (2017). Buried Alive or Washed Away. *Oceanography*, *30*(3), 48–59. https://tos.org/oceanography/assets/docs/30-3_fagherazzi.pdf

FAO. (2007). *The world's mangroves 1980-2005* (tech. rep.).

Feller, I. C., Lovelock, C. E., Berger, U., McKee, K. L., Joye, S. B., & Ball, M. C. (2010). Biocomplexity in mangrove ecosystems. *Annual Review of Marine Science*, *2*(1), 395–417. https://doi.org/10.1146/annurev.marine.010908.163809

Field, C. (2007). Local management and rehabilitation of mangroves: present and future, 293–308.

Gijsman, R., Horstman, E. M., van der Wal, D., Friess, D. A., Swales, A., & Wijnberg, K. M. (2021). Nature-Based Engineering: A Review on Reducing Coastal Flood Risk With Mangroves. *Frontiers in Marine Science*, *8*(July). https://doi.org/10.3389/fmars.2021.702412

Giri, C., Ochieng, E., Tieszen, L. L., Zhu, Z., Singh, A., Loveland, T., Masek, J., & Duke, N. (2011). Status and distribution of mangrove forests of the world using earth observation satellite data. *Global Ecology and Biogeography*, *20*(1), 154–159. https://doi.org/10.1111/j.1466-8238.2010.00584.x

Goldberg, L., Lagomasino, D., Thomas, N., & Fatoyinbo, T. (2020). Global declines in human-driven mangrove loss. *Global Change Biology*, *26*(10), 5844–5855. https://doi.org/10.1111/gcb.15275

Goswami, S. (2021). *Clearing the Coast - How aquaculture and construction threaten the pristine coast of West Bengal* (tech. rep.). Legal Initiative for Forest and Environment.

Grueters, U., Seltmann, T., Schmidt, H., Horn, H., Pranchai, A., Vovides, A. G., Peters, R., Vogt, J., Dahdouh-Guebas, F., & Berger, U. (2014). The mangrove forest dynamics model mesoFON. *Ecological Modelling*, *291*, 28–41. https://doi.org/10.1016/j.ecolmodel.2014.07.014
An IB mangrove model that includes crown plasticity of mangrove tree (can grow "away" from competition/ trunk bending).

Guo, L., van der Wegen, M., Roelvink, D., & He, Q. (2015). Exploration of the impact of seasonal river discharge variations on long-term estuarine morphodynamic behavior. *Coastal Engineering*, *95*, 105–116. https://doi.org/10.1016/j.coastaleng.2014.10.006
Using Hydrograph for varying river discharge (1D Model)!

Harris, T., Hope, P., Oliver, E., Smalley, R., Arblaster, J., Holbrook, N., Duke, N., Pearce, K., Braganza, K., & Bindoff, N. (2017). Climate drivers of the 2015 Gulf of Carpentaria mangrove dieback. *Earth Systems and Climate Change Hub Report No. 2*, (2), 34 pages. http://nespclimate.com.au/wp-content/uploads/2018/05/ESCC-R002-Mangrove-dieback-1711.pdf

Heap, A., Harris, P., Passlow, V., Wassenberg, T., Sbaffi, L., Mathews, E., Fellows, M., Fountain, L., Porter-smith, R., Daniell, J., Buchanan, C., & Robertson, L. (2006). Sources and sinks of terrigenous sediments in the Southern Gulf of Carpentaria. *Geoscience Australia Record 2006/11*, *11*(June 2003). https://doi.org/ISSN/ISBN:1920871837

Hickey, S. M., Radford, B., Callow, J. N., Phinn, S. R., Duarte, C. M., & Lovelock, C. E. (2021). ENSO feedback drives variations in dieback at a marginal mangrove site. *Scientific Reports*, *11*(1), 1–9. https://doi.org/10.1038/s41598-021-87341-5

Horstman, E. M., Dohmen-Janssen, C. M., Narra, P. M., van den Berg, N. J., Siemerink, M., & Hulscher, S. J. (2014). Wave attenuation in mangroves: A quantitative approach to field observations. *Coastal Engineering*, *94*, 47–62. https://doi.org/10.1016/j.coastaleng.2014.08.005

Horstman, E., Dohmen-Janssen, C. M., & Hulscher, S. J. (2013a). Modeling tidal dynamics in a mangrove creek catchment in Delft3D. *International Conference on Coastal Dynamics*, *12*(2), 833–844. https://research.utwente.nl/en/publications/modeling-tidal-dynamics-in-a-mangrove-creek-catchment-in-delft3d

Horstman, E. M., Dohmen-Janssen, C. M., & Hulscher, S. J. (2013b). Flow routing in mangrove forests: A field study in Trang province, Thailand. *Continental Shelf Research*, *71*, 52–67. https://doi.org/10.1016/j.csr.2013.10.002

Horstman, E. M., Dohmen-Janssen, C. M., & Hulscher, S. J. (2013c). Flow routing in mangrove forests: A field study in Trang province, Thailand. *Continental Shelf Research*, *71*, 52–67. https://doi.org/10.1016/j.csr.2013.10.002

Hu, K., Ding, P., Wang, Z., & Yang, S. (2009). A 2D/3D hydrodynamic and sediment transport model for the Yangtze Estuary, China. *Journal of Marine Systems*, *77*(1-2), 114–136. https://doi.org/10.1016/j.jmarsys.2008.11.014

Ikeda, S. (1982). Incipient Motion of Sand Particles on Side Slopes. *Journal of the Hydraulics Division, ASCE*, *108*(1), 95–114.

IPCC. (2021). Assessment Report 6 Climate Change 2021: The Physical Science Basis. https://www.ipcc.ch/report/ar6/wg1/

Jaensch, R., & George, P. (2019). *South-East Gulf of Carpentaria: Leichhardt River to Gore Point (Wernadinga coast)* (tech. rep.). East Asian-Australasian Flyway Network Sites.

Jiang, J., DeAngelis, D. L., Smith, T. J., Teh, S. Y., & Koh, H. L. (2012). Spatial pattern formation of coastal vegetation in response to external gradients and positive feedbacks affecting soil porewater salinity: A model study. *Landscape Ecology*, *27*(1), 109–119. https://doi.org/10.1007/s10980-011-9689-9
SEHM model A spatially explicit individual-based model of vegetation, coupled with a model of soil hydrology and salinity dynamics is presented here to simulate mangrove/hammock ecotones in the coastal margin habitats of South Florida.

Jiang, J., Fuller, D. O., Teh, S. Y., Zhai, L., Koh, H. L., DeAngelis, D. L., & Sternberg, L. d. S. L. (2015). Bistability of mangrove forests and competition with freshwater plants. *Agricultural and Forest Meteorology*, *213*, 283–290. https://doi.org/10.1016/j.agrformet.2014.10.004

Jones, H. P., Jones, P. C., Barbier, E. B., Blackburn, R. C., Rey Benayas, J. M., Holl, K. D., McCrackin, M., Meli, P., Montoya, D., & Mateos, D. M. (2018). Restoration and repair of Earth's damaged ecosystems. *Proceedings of the Royal Society B: Biological Sciences*, *285*(1873). https://doi.org/10.1098/rspb.2017.2577

Joshi, H., & Ghose, M. (2003). Forest structure and species distribution along soil salinity and pH gradient in mangrove swamps of the Sundarbans. *Tropical Ecology*, *44*(2), 197–206.

Juliandri, M. R., Radjawane, I. M., Tarya, A. (2020). Modeling the distribution of floating marine debris movement in tourism area in pelabuhan Ratu bay, West Java. *AACL Bioflux*, *13*(5), 3105–3116.

Kazemi, A., Castillo, L., & Curet, O. M. (2021). Mangrove roots model suggest an optimal porosity to prevent erosion. *Scientific Reports*, *11*(1), 1–14. https://doi.org/10.1038/s41598-021-88119-5

Ketelaars, M., Franken, J., Janssen, S., & Maarse, M. (2013). Deltafact: Mangrove restoration. *STOWA (Stichting Toegepast Onderzoek Waterbeheer)*, 15.

Kirwan, M. L., & Megonigal, J. P. (2013). Tidal wetland stability in the face of human impacts and sea-level rise. *Nature*, *504*(7478), 53–60. https://doi.org/10.1038/nature12856

Kleinhans, M. G., de Vries, B., Braat, L., & van Oorschot, M. (2018). Living landscapes: Muddy and vegetated floodplain effects on fluvial pattern in an incised river. *Earth Surface Processes and Landforms*, *43*(14), 2948–2963. https://doi.org/10.1002/esp.4437

Kodikara, K. A. S., Jayatissa, L. P., Huxham, M., Dahdouh-Guebas, F., & Koedam, N. (2018). The effects of salinity on growth and survival of mangrove seedlings changes with age. *Acta Botanica Brasilica*, *32*(1), 37–46. https://doi.org/10.1590/0102-33062017abb0100

Krauss, K. W., Lovelock, C. E., McKee, K. L., López-Hoffman, L., Ewe, S. M., & Sousa, W. P. (2008). Environmental drivers in mangrove establishment and early development: A review. *Aquatic Botany*, *89*(2), 105–127. https://doi.org/10.1016/j.aquabot.2007.12.014

Kumar, P., Debele, S. E., Sahani, J., Rawat, N., Marti-Cardona, B., Alfieri, S. M., Basu, B., Basu, A. S., Bowyer, P., Charizopoulos, N., Gallotti, G., Jaakko, J., Leo, L. S., Loupis, M., Menenti, M., Mickovski, S. B., Mun, S. J., Gonzalez-Ollauri, A., Pfeiffer, J., … Zieher, T. (2021). Nature-based solutions efficiency evaluation

against natural hazards: Modelling methods, advantages and limitations. *Science of the Total Environment*, *784*. https://doi.org/10.1016/j.scitotenv.2021.147058

Le Minor, M., Bartzke, G., Zimmer, M., Gillis, L., Helfer, V., & Huhn, K. (2019). Numerical modelling of hydraulics and sediment dynamics around mangrove seedlings: Implications for mangrove establishment and reforestation. *Estuarine, Coastal and Shelf Science*, *217*(November 2018), 81–95. https://doi.org/10.1016/j.ecss.2018.10.019

Leonardi, N., Canestrelli, A., Sun, T., & Fagherazzi, S. (2013). Effect of tides on mouth bar morphology and hydrodynamics. *Journal of Geophysical Research: Oceans*, *118*(9), 4169–4183. https://doi.org/10.1002/jgrc.20302

Lesser, G. R., Roelvink, J. A., van Kester, J. A., & Stelling, G. S. (2004). Development and validation of a three-dimensional morphological model. *Coastal Engineering*, *51*(8-9), 883–915. https://doi.org/10.1016/j.coastaleng.2004.07.014
The thing to cite for DELFT3D references! When explainig what delft3D is!

Lesser, G. (2009). *An Approach to Medium-term Coastal Morphological Modelling* (Doctoral dissertation). http://www.narcis.nl/publication/RecordID/oai:tudelft.nl:uuid:62caa573-4fc0-428e-8768-0aa47ab612a9

Leuven, J. R., Kleinhans, M. G., Weisscher, S. A., & van der Vegt, M. (2016). Tidal sand bar dimensions and shapes in estuaries. *Earth-Science Reviews*, *161*, 204–223. https://doi.org/10.1016/j.earscirev.2016.08.004

Leuven, J. R., Pierik, H. J., van der Vegt, M., Bouma, T. J., & Kleinhans, M. G. (2019). Sea-level-rise-induced threats depend on the size of tide-influenced estuaries worldwide. *Nature Climate Change*, *9*(12), 986–992. https://doi.org/10.1038/s41558-019-0608-4

Leuven, J. R., van Maanen, B., Lexmond, B. R., van der Hoek, B. V., Spruijt, M. J., & Kleinhans, M. G. (2018). Dimensions of fluvial-tidal meanders: Are they disproportionally large? *Geology*, *46*(10), 923–926. https://doi.org/10.1130/G45144.1

Liang, S., Zhou, R. C., Dong, S. S., & Shi, S. H. (2008). Adaptation to salinity in mangroves: Implication on the evolution of salt-tolerance. *Chinese Science Bulletin*, *53*(11), 1708–1715. https://doi.org/10.1007/s11434-008-0221-9

Lokhorst, I. R., Braat, L., Leuven, J. R., Baar, A. W., Van Oorschot, M., Selaković, S., & Kleinhans, M. G. (2018). Morphological effects of vegetation on the tidal-fluvial transition in Holocene estuaries. *Earth Surface Dynamics*, *6*(4), 883–901. https://doi.org/10.5194/esurf-6-883-2018

Lovelock, C. E., Cahoon, D. R., Friess, D. A., Guntenspergen, G. R., Krauss, K. W., Reef, R., Rogers, K., Saunders, M. L., Sidik, F., Swales, A., Saintilan, N., Thuyen, L. X., & Triet, T. (2015). The vulnerability of Indo-Pacific mangrove forests to sea-level rise. *Nature*, *526*(7574), 559–563. https://doi.org/10.1038/nature15538

Lovelock, C. E., Feller, I. C., Reef, R., Hickey, S., & Ball, M. C. (2017). Mangrove dieback during fluctuating sea levels. *Scientific Reports*, *7*(1), 1–8. https://doi.org/10.1038/s41598-017-01927-6

Lu, S., Tong, C., Lee, D.-Y., Zheng, J., Shen, J., Zhang, W., & Yan, Y. (2015). Propagation of tidal waves up in Yangtze Estuary during the dry season. *Journal of Geophysical Research: Oceans*, *120*, 6445–6473. https://doi.org/10.1002/2014JC010414

Luan, H. L., Ding, P. X., Wang, Z. B., & Ge, J. Z. (2017). Process-based morphodynamic modeling of the Yangtze Estuary at a decadal timescale: Controls on estuarine evolution and future trends. *Geomorphology*, *290*(September 2016), 347–364. https://doi.org/10.1016/j.geomorph.2017.04.016

Luan, H., Liu, T., Yao, S., & Lu, J. (2019). Effects of high river discharge on decadal morphological evolution of the inner Yangtze Estuary. *IOP Conference Series: Earth and Environmental Science*, *304*(2), 0–14. https://doi.org/10.1088/1755-1315/304/2/022081

Lugo, A., Sell, M., & Snedaker, S. Mangrove ecosystem analysis. In: *Pattern, b.c. (ed.), system analysis and simulation in ecology*. New York: Academic Press, Inc., 1976, pp. 113–145.

Lymburner, L., Bunting, P., Lucas, R., Scarth, P., Alam, I., Phillips, C., Ticehurst, C., & Held, A. (2020). Mapping the multi-decadal mangrove dynamics of the Australian coastline. *Remote Sensing of Environment*, *238*(April 2018), 111185. https://doi.org/10.1016/j.rse.2019.05.004

Malvin, N., Pudjaprasetya, S. R., & Adytia, D. Neural Network Modelling on Wave Dissipation Due to Mangrove Forest. In: *2020 international conference on data science and its applications (icodsa)*. 2020, 1–7. https://doi.org/10.1109/ICoDSA50139.2020.9212826.

Marchand, M. (2008). Mangrove restoration in Vietnam Key considerations and a practical guide. (December), 34.

Mazda, Y., Wolanski, E., King, B., Sase, A., Ohtsuka, D., & Magi, M. (1997). Drag force due to vegetation in mangrove swamps. *Mangroves and Salt Marshes*, *1*(3), 193–199. https://doi.org/10.1023/A:1009949411068

Mcivor, A., Spencer, T., Möller, I., & Spalding, M. D. (2013). The response of mangrove soil surface elevation to sea level rise Natural Coastal Protection Series: Report 3. *Natural Coastal Protection Series*, 2050–7941.

McKee, K. L. (2011). Biophysical controls on accretion and elevation change in Caribbean mangrove ecosystems. *Estuarine, Coastal and Shelf Science*, *91*(4), 475–483. https://doi.org/10.1016/j.ecss.2010.05.001

Mckee, K. L., Cahoon, D. R., & Feller, I. C. (2007). Caribbean mangroves adjust to rising sea level through biotic controls on change in soil elevation. *Global Ecology and Biogeography*, *16*(5), 545–556. https://doi.org/10.1111/j.1466-8238.2007.00317.x

Mehvar, S., Filatova, T., Sarker, M. H., Dastgheib, A., & Ranasinghe, R. (2019). Climate change-driven losses in ecosystem services of coastal wetlands: A case study in the West coast of Bangladesh. *Ocean and Coastal Management*, *169*(July 2018), 273–283. https://doi.org/10.1016/j.ocecoaman.2018.12.009

Mullarney, J. C., & Henderson, S. M. Flows within marine vegetation canopies. In: *Advances in coastal hydraulics*. WORLD SCIENTIFIC, 2018, pp. 1–46. ISBN: 9789813231283. https://doi.org/10.1142/9789813231283_0001.

Murray, A. B. (2003). Contrasting the goals, strategies, and predictions associated with simplified numerical models and detailed simulations. *Geophysical Monograph Series*, *135*, 151–165. https://doi.org/10.1029/135GM11

Nardin, W., & Edmonds, D. A. (2014). Optimum vegetation height and density for inorganic sedimentation in deltaic marshes. *Nature Geoscience*, *7*(10), 722–726. https://doi.org/10.1038/NGEO2233

Naskar, S., & Palit, P. K. (2015). Anatomical and physiological adaptations of mangroves. *Wetlands Ecology and Management*, *23*(3), 357–370. https://doi.org/10.1007/s11273-014-9385-z

National Geographic Society. (2012, October 9). *Estuary*. Retrieved January 8, 2022, from https://www.nationalgeographic.org/encyclopedia/estuary/

Nguyen, H. T., Meir, P., Sack, L., Evans, J. R., Oliveira, R. S., & Ball, M. C. (2017). Leaf water storage increases with salinity and aridity in the mangrove Avicennia marina: integration of leaf structure, osmotic adjustment and access to multiple

water sources. *Plant Cell and Environment*, *40*(8), 1576–1591. https://doi.org/10.1111/pce.12962

Oh, R. R., Friess, D. A., & Brown, B. M. (2017). The role of surface elevation in the rehabilitation of abandoned aquaculture ponds to mangrove forests, Sulawesi, Indonesia. *Ecological Engineering*, *100*, 325–334. https://doi.org/10.1016/j.ecoleng.2016.12.021

Pannozzo, N., Leonardi, N., Carnacina, I., & Smedley, R. (2021). Salt marsh resilience to sea-level rise and increased storm intensity. *Geomorphology*, *389*, 107825. https://doi.org/10.1016/j.geomorph.2021.107825

Parida, B. R., & Kumari, A. (2021). Mapping and modeling mangrove biophysical and biochemical parameters using Sentinel-2A satellite data in Bhitarkanika National Park, Odisha. *Modeling Earth Systems and Environment*, *7*(4), 2463–2474. https://doi.org/10.1007/s40808-020-01005-3

Peters, R., Olagoke, A., & Berger, U. (2018). A new mechanistic theory of self-thinning: Adaptive behaviour of plants explains the shape and slope of self-thinning trajectories. *Ecological Modelling*, *390*(June), 1–9. https://doi.org/10.1016/j.ecolmodel.2018.10.005

Peters, R., Vovides, A. G., Luna, S., Grüters, U., & Berger, U. (2014). Changes in allometric relations of mangrove trees due to resource availability - A new mechanistic modelling approach. *Ecological Modelling*, *283*, 53–61. https://doi.org/10.1016/j.ecolmodel.2014.04.001

Peters, R., Walther, M., Lovelock, C., Jiang, J., & Berger, U. (2020). The interplay between vegetation and water in mangroves: new perspectives for mangrove stand modelling and ecological research. *Wetlands Ecology and Management*, *28*(4), 697–712. https://doi.org/10.1007/s11273-020-09733-0
Description of state of art mangrove modelling, explanation of different models that are out there! (USE INTRODUCTION and Methods as intro in mangrove modelling)

Prandle, D. (2009). *Estuaries: Dynamics, mixing, sedimentation and morphology*. Cambridge University Press. https://doi.org/10.1017/CBO9780511576096

Samiksha, S. V., Vethamony, P., Bhaskaran, P. K., Pednekar, P., Jishad, M., & James, R. A. (2019). Attenuation of Wave Energy Due to Mangrove Vegetation off Mumbai, India. *Energies*, *12*(22). https://doi.org/doi:10.3390/en12224286

Sandbach, S. D., Nicholas, A. P., Ashworth, P. J., Best, J. L., Keevil, C. E., Parsons, D. R., Prokocki, E. W., & Simpson, C. J. (2018). Hydrodynamic modelling of tidal-fluvial flows in a large river estuary. *Estuarine, Coastal and Shelf Science*, *212*(November 2017), 176–188. https://doi.org/10.1016/j.ecss.2018.06.023

Schuerch, M., Spencer, T., Temmerman, S., Kirwan, M. L., Wolff, C., Lincke, D., McOwen, C. J., Pickering, M. D., Reef, R., Vafeidis, A. T., Hinkel, J., Nicholls, R. J., & Brown, S. (2018). Future response of global coastal wetlands to sea-level rise. *Nature*, *561*(7722), 231–234. https://doi.org/10.1038/s41586-018-0476-5

Schuurman, F., Ta, W., Post, S., Sokolewicz, M., Busnelli, M., & Kleinhans, M. (2018). Response of braiding channel morphodynamics to peak discharge changes in the Upper Yellow River. *Earth Surface Processes and Landforms*, *43*(8), 1648–1662. https://doi.org/10.1002/esp.4344

Shing, V. H. R.-m., Lee, Y., Kristensen, E., & Twilley, R. R. (2017). *Mangrove Ecosystems: A Global Biogeographic Perspective*. https://doi.org/10.1007/978-3-319-62206-4

Short, A. D. (2020). *Australian Coastal Systems* (Vol. 32). http://link.springer.com/10.1007/978-3-030-14294-0

Sippo, J. (2019). *Causes and consequences of a massive mangrove dieback event in the Gulf of Carpentaria , Australia* (Doctoral dissertation). Southern Cross University.

Sousa, M. C., DeCastro, M., Gago, J., Ribeiro, A. S., Des, M., Gómez-Gesteira, J. L., Dias, J. M., & Gomez-Gesteira, M. (2021). Modelling the distribution of microplastics released by wastewater treatment plants in Ria de Vigo (NW Iberian Peninsula). *Marine Pollution Bulletin*, *166*(November 2020). https://doi.org/10.1016/j.marpolbul.2021.112227

Spalding, M. D., & Leal, M. e. (2021). *The State of the World's Mangroves 2021* (tech. rep.). Global Mangrove Alliance. https://ejournal.unisba.ac.id/index.php/kajian_akuntansi/article/view/2615%0Ahttp://scholar.unand.ac.id/60566/

Sternberg, L. D. S. L., Teh, S. Y., Ewe, S. M., Miralles-Wilhelm, F., & DeAngelis, D. L. (2007). Competition between hardwood hammocks and mangroves. *Ecosystems*, *10*(4), 648–660. https://doi.org/10.1007/s10021-007-9050-y

Stive, M. J., & de Vriend, H. J. (1995). Modelling shoreface profile evolution. *Marine Geology*, *126*(1-4), 235–248. https://doi.org/10.1016/0025-3227(95)00080-I

Teh, S. Y., Koh, H. L., DeAngelis, D. L., & Turtora, M. (2013). Interaction between salinity intrusion and vegetation succession: A modeling approach. *Theoretical and Applied Mechanics Letters*, *3*(3), 032001. https://doi.org/10.1063/2.1303201

Temmerman, S., Moonen, P., Schoelynck, J., Govers, G., & Bouma, T. J. (2012). Impact of vegetation die-off on spatial flow patterns over a tidal marsh. *Geophysical Research Letters*, *39*(3), 1–5. https://doi.org/10.1029/2011GL050502

Twilley, R. R., Rivera-Monroy, V. H., Chen, R., & Botero, L. (1999). Adapting an ecological mangrove model to simulate trajectories in restoration ecology. *Marine Pollution Bulletin*, *37*(8-12), 404–419. https://doi.org/10.1016/S0025-326X(99)00137-X

van Belzen, J., van de Koppel, J., Kirwan, M. L., van der Wal, D., Herman, P. M., Dakos, V., Kéfi, S., Scheffer, M., Guntenspergen, G. R., & Bouma, T. J. (2017). Vegetation recovery in tidal marshes reveals critical slowing down under increased inundation. *Nature Communications*, *8*(1). https://doi.org/10.1038/ncomms15811

van Dijk, W. M., Hiatt, M. R., van der Werf, J. J., & Kleinhans, M. G. (2019). Effects of Shoal Margin Collapses on the Morphodynamics of a Sandy Estuary. *Journal of Geophysical Research: Earth Surface*, *124*(1), 195–215. https://doi.org/10.1029/2018JF004763

van Veelen, T. J., Karunarathna, H., & Reeve, D. E. (2021). Modelling wave attenuation by quasi-flexible coastal vegetation. *Coastal Engineering*, *164*(November 2020), 103820. https://doi.org/10.1016/j.coastaleng.2020.103820

van Zelst, V. T. M., Dijkstra, J. T., van Wesenbeeck, B. K., Eilander, D., Morris, E. P., Winsemius, H. C., Ward, P. J., & de Vries, M. B. (2021). Cutting the costs of coastal protection by integrating vegetation in flood defences. *Nature Communications*, *12*(1), 1–11. https://doi.org/10.1038/s41467-021-26887-4

Van Coppenolle, R., Schwarz, C., & Temmerman, S. (2018). Contribution of Mangroves and Salt Marshes to Nature-Based Mitigation of Coastal Flood Risks in Major Deltas of the World. *Estuaries and Coasts*, *41*(6), 1699–1711. https://doi.org/10.1007/s12237-018-0394-7

van de Leemput, I. A., Dakos, V., Scheffer, M., & van Nes, E. H. (2018). Slow Recovery from Local Disturbances as an Indicator for Loss of Ecosystem Resilience. *Ecosystems*, *21*(1), 141–152. https://doi.org/10.1007/s10021-017-0154-8

van der Wegen, M., & Roelvink, J. A. (2012). Reproduction of estuarine bathymetry by means of a process-based model: Western Scheldt case study, the Netherlands. *Geomorphology*, *179*, 152–167. https://doi.org/10.1016/j.geomorph.2012.08.007

Van Der Wegen, M., Jaffe, B. E., & Roelvink, J. A. (2011a). Process-based, morphodynamic hindcast of decadal deposition patterns in San Pablo Bay, California, 1856-1887. *Journal of Geophysical Research: Earth Surface*, *116*(2), 1–22. https://doi.org/10.1029/2009JF001614

Van Der Wegen, M., & Roelvink, J. A. (2008). Long-term morphodynamic evolution of a tidal embayment using a two-dimensional, process-based model. *Journal of Geophysical Research: Oceans*, *113*(3), 1–23. https://doi.org/10.1029/2006JC003983

Van Der Wegen, M., Dastgheib, A., Jaffe, B. E., & Roelvink, D. (2011b). Bed composition generation for morphodynamic modeling: Case study of San Pablo Bay in California, USA. *Ocean Dynamics*, *61*(2-3), 173–186. https://doi.org/10.1007/s10236-010-0314-2

Van Maanen, B., Coco, G., & Bryan, K. R. (2015). On the ecogeomorphological feedbacks that control tidal channel network evolution in a sandy mangrove setting. *Proceedings of the Royal Society A: Mathematical, Physical and Engineering Sciences*, *471*(2180). https://doi.org/10.1098/rspa.2015.0115

Van Rijn, L. C. (1993). *Principles of sediment transport in rivers, estuaries, and coastal seas*. Aqua Publication.

Van Santen, P., Augustinus, P. G., Janssen-Stelder, B. M., Quartel, S., & Tri, N. H. (2007). Sedimentation in an estuarine mangrove system. *Journal of Asian Earth Sciences*, *29*(4), 566–575. https://doi.org/10.1016/j.jseaes.2006.05.011

Willemsen, P. W., Horstman, E. M., Borsje, B. W., Friess, D. A., & Dohmen-Janssen, C. M. (2016). Sensitivity of the sediment trapping capacity of an estuarine mangrove forest. *Geomorphology*, *273*, 189–201. https://doi.org/10.1016/j.geomorph.2016.07.038

Wimmler, M. C., Bathmann, J., Peters, R., Jiang, J., Walther, M., Lovelock, C. E., & Berger, U. (2021). Plant–soil feedbacks in mangrove ecosystems: establishing links between empirical and modelling studies. *Trees - Structure and Function*, *35*(5), 1423–1438. https://doi.org/10.1007/s00468-021-02182-z

Winterwerp, J. C., Erftemeijer, P. L., Suryadiputra, N., Van Eijk, P., & Zhang, L. (2013). Defining eco-morphodynamic requirements for rehabilitating eroding mangrove-mud coasts. *Wetlands*, *33*(3), 515–526. https://doi.org/10.1007/s13157-013-0409-x

Xie, D., Schwarz, C., Brückner, M. Z., Kleinhans, M. G., Urrego, D. H., Zhou, Z., & van Maanen, B. (2020). Mangrove diversity loss under sea-level rise triggered by bio-morphodynamic feedbacks and anthropogenic pressures. *Environmental Research Letters*, *15*(11). https://doi.org/10.1088/1748-9326/abc122

Xie, D., Schwarz, C., Kleinhans, M. G., Zhou, Z., & Maanen, B. (2022). Implications of Coastal Conditions and Sea-Level Rise on Mangrove Vulnerability: a Bio-morphodynamic Modelling Study. *Journal of Geophysical Research: Earth Surface*. https://doi.org/10.1029/2021jf006301

Xu, C., Zhang, J., Bi, X., Xu, Z., He, Y., & Gin, K. Y. H. (2017). Developing an integrated 3D-hydrodynamic and emerging contaminant model for assessing water quality in a Yangtze Estuary Reservoir. *Chemosphere*, *188*, 218–230. https://doi.org/10.1016/j.chemosphere.2017.08.121

Ye, Y., Tam, N. F. Y., Lu, C. Y., & Wong, Y. S. (2005). Effects of salinity on germination, seedling growth and physiology of three salt-secreting mangrove species. *Aquatic Botany*, *83*(3), 193–205. https://doi.org/10.1016/j.aquabot.2005.06.006

Younes, N., Northfield, T. D., Joyce, K. E., Maier, S. W., Duke, N. C., & Lymburner, L. (2020). A novel approach to modelling mangrove phenology from satellite

images: A case study from Northern Australia. *Remote Sensing*, *12*(24), 1–24. https://doi.org/10.3390/rs12244008

Zheng, J., Elmilady, H., Röbke, B. R., Taal, M., Wang, Z. B., van Prooijen, B. C., de Vet, P. L., & van der Wegen, M. (2021). The impact of wind-waves and sea level rise on the morphodynamics of a sandy estuarine shoal. *Earth Surface Processes and Landforms*, (November 2020), 1–18. https://doi.org/10.1002/esp.5207

zu Ermgassen, P. S., Mukherjee, N., Worthington, T. A., Acosta, A., da Rocha Araujo, A. R., Beitl, C. M., Castellanos-Galindo, G. A., Cunha-Lignon, M., Dahdouh-Guebas, F., Diele, K., Parrett, C. L., Dwyer, P. G., Gair, J. R., Johnson, A. F., Kuguru, B., Savio Lobo, A., Loneragan, N. R., Longley-Wood, K., Mendonça, J. T., … Spalding, M. (2021). Fishers who rely on mangroves: Modelling and mapping the global intensity of mangrove-associated fisheries. *Estuarine, Coastal and Shelf Science*, *248*(January). https://doi.org/10.1016/j.ecss.2020.107159